Neuroimaging of binocular vision in human amblyopia

Freya Alexandria Lygo

Doctor of Philosophy

University of York
Psychology

September 2019

Abstract

Amblyopia is a visual developmental condition that usually occurs when one eye receives abnormal input. For many years amblyopia was thought to be untreatable beyond 8 years old, after which the visual system would become functionally monocular. Recent research has shown that binocular mechanisms do remain intact in amblyopia and therefore investigating the nature of the deficit is crucial for understanding where neural problems arise and how they can be treated. Chapter 3 used population receptive field (pRF) modelling to further understand the cortical problems caused by amblyopia. Findings suggest that neurons responding to the amblyopic eye have reduced spatial resolution within striate and extrastriate areas. Chapters 4 and 5 aimed to test the predictions of different computational models of amblyopia using functional magnetic resonance imaging (fMRI) and electroencephalography (EEG), within the same group of participants. This is the first study to use a model driven approach to directly compare both neuroimaging methods within the same participants. The pattern of fMRI responses from the amblyopic eye showed evidence of a response gain effect and unbalanced interocular suppression, whereas EEG responses showed evidence of a contrast gain shift. Finally, Chapter 6 used EEG to objectively measure visual improvements, following treatment for amblyopia in children and adults. Measurable steady-state EEG responses were found for both groups; however, there was no convincing evidence of improvements in amblyopic eye responses throughout treatment. The studies undertaken in this thesis contribute to the wider understanding of the neural basis of amblyopia. Two different neuroimaging methods are compared, which has enabled insight into how current computational models of amblyopia could be improved. It is hoped that this research will further the development of treatments for amblyopia, by providing more insight into how binocular visual processes break down between the eyes.

Contents

Abstract 2

Contents 3

List of Figures 7

List of Tables 8

List of Equations 9

Acknowledgements 10

Author's Declaration 11

Chapter 1: Introduction 12

1.1 Overview 12

1.2 Mechanisms of binocular vision 13

1.3 The neural basis of amblyopia 19

1.4 Treatment for amblyopia 25

1.5 Methodological considerations for neuroimaging studies 29

1.6 Summary 30

1.7 Thesis overview 32

Chapter 2: General Methods 35

2.1 Neuroimaging methods 35

2.2 Participants 37

2.3 Materials 41

2.3.1 Measuring Contrast responses 41

2.3.2 MRI 43

2.3.3 EEG 44

2.3.4 Dry-electrode EEG 45

2.4 Procedure 46

Chapter 3: Binocular population receptive field mapping in human amblyopia 47

3.1 Introduction 47

3.1.1 Background 47

3.1.2 Retinotopic and population receptive field mapping methods 48

3.1.3 Aims and hypotheses 49

3.2 Methods 50

3.2.1 Participants 50

3.2.2 Materials 50

3.2.3 Procedure 52

3.2.4 Data Processing 52

3.3 Results 53

3.3.1 Retinotopic maps and ROIs 53

3.3.2 pRF size verses eccentricity 55

3.3.2.1 Comparisons within visual areas 57

3.3.2.2 Comparisons between visual areas 58

3.4 Discussion 60

3.5 Conclusion 62

Chapter 4: Interocular fMRI responses in human amblyopia 63

4.1 Introduction 63

4.2 Methods 65

4.2.1 Participants 65

4.2.2 Materials 65

4.2.3 Procedure 66

4.2.4 Data Processing 68

4.2.4.1 Defining regions of interest 68

4.2.4.2 Response time course 69
4.2.4.3 Models 70
4.3 Results 74
4.3.1 Comparisons between monocular and binocular responses 74
4.3.2 Interocular contrast responses and model comparisons 76
4.3.3 Measuring interocular suppression 78
4.4 Discussion 79
4.5 Conclusion 83

Chapter 5: Interocular steady-state EEG responses in human amblyopia 84
5.1 Introduction 84
5.2 Methods 85
5.2.1 Participants 85
5.2.2 Materials 85
5.2.3 Procedure 85
5.2.4 Data Processing 86
5.3 Results 87
5.3.1 Comparisons between monocular and binocular responses 87
5.3.2 Interocular contrast responses and model comparisons 91
5.3.3 Measuring interocular suppression 93
5.4 Discussion 94
5.5 Conclusion 96

Chapter 6: Objective measures of visual improvement following amblyopia therapy in children and adults 97
6.1 Introduction 97
Experiment 1: Visual improvement following amblyopia treatment in children
6.2 Methods 99

6.2.1 Participants 99
6.2.2 Materials 101
6.2.3 Procedure 101
6.2.4 Data Processing 102
6.3 Results 104
6.4 Discussion 109
Experiment 2: Visual improvement following amblyopia treatment in adults
6.5 Methods 111
6.5.1 Participants 111
6.5.2 Materials 112
6.5.2.1 Experimental equipment and stimuli 112
6.5.2.1 Game treatment 112
6.5.3 Procedure 114
6.5.4 Data Processing 115
6.6 Results 115
6.7 Discussion 118
6.8 Overall conclusion 120

Chapter 7: General discussion 121
7.1 Summary of findings 121
7.2 Multimodal neuroimaging 124
7.3 Future directions 125
7.4 Overall conclusion 128

Appendices 129
References 130

List of Figures

1.1 Schematic diagrams demonstrating the model architecture for binocular interactions 18

1.2 Example of pRF estimates on a flattened cortical surface 24

1.3 Schematic diagram of a dichoptic game paradigm (adapted from To et al., 2011). 28

1.4 Summary of thesis chapter layout 32

2.1 Example of the stimulus used to measure contrast responses in Chapters 4-6 42

3.1 Example of pRF and retinotopic mapping stimuli 51

3.2 Retinotopic maps for a control participant 54

3.3 Retinotopic maps for an amblyopic participant 55

3.4 Average pRF sizes from amblyopic and fellow eyes for areas V1-V3 56

3.5 pRF sizes averaged across eccentricities for each eye in areas V1-V3 59

4.1 All possible stimulus combinations when combined across each eye 66

4.2 An example of the stimulus display 67

4.3 An example of the phase-encoded localiser stimulus 68

4.4 An example fMRI timecourse 69

4.5 Model predictions for contrast response functions of the amblyopic and fellow eye 73

4.6 Contrast response functions for monocular and binocular responses 74

4.7 Contrast responses plotted as function of increasing target and mask contrast 77

4.8 Comparisons of fMRI suppression ratios. 79

5.1 Fourier spectra and head plots for SSVEP responses 87

5.2 Contrast response functions for monocular and binocular responses 90

5.3 Contrast responses plotted as function of increasing target and mask contrast 92

5.4 Comparisons of steady-state suppression ratios. 94

6.1 Fourier spectra and head plots for dry-electrode SSVEP responses. 103

6.2 Improvements in visual acuity between sessions 1-3 in experiment 1 105

6.3 SNRs for both eyes at each stimulus contrast and across sessions. 107

6.4 Ratios between both eyes across sessions 108

6.5 Example of the 'Dig Rush' game treatment 114

6.6 Monocular, binocular and dichoptic SNRs at each stimulus contrast and across session 116

Appendix 1 – Photograph of the dry-electrode EEG equipment set up 129

List of Tables

2.1 Summary of which participants took part in each experiment 38

2.2 Demographic and clinical details for amblyopic participants in Chapters 3-6 40

2.3 Demographic and clinical details for control participants in Chapters 3-5 41

3.1 Mean ROI size for visual areas V1, V2 and V3 53

3.2 Percentage of cases that were included and excluded in the GLMM analysis 57

3.3 Results of GLMM analysis in Chapter 2 58

4.1 Mean ROI size for localiser scans 69

6.1 Demographic and visual acuity measurements across sessions 100

6.2 Results of a GLMM analysis to explore changes in visual acuity for experiment 1 104

6.3 Results of a GLMM analysis to explore changes in SNR in experiment 1. 106

6.4 Demographic and visual acuity measurements across sessions 112

List of Equations

1.1 Binocular summation ratio (Legge, 1948) 15

4.1 Model of binocular summation (Legge, 1948) 70

4.2 Two-state model of binocular gain control (Meese et al., 2006) 71

4.3 Attenuator model (Baker et al., 2008) 71

4.4 Contrast gain shift model 72

4.5 Interocular suppression model 72

Acknowledgements

There are many people I would like to thank for providing support and guidance throughout my PhD. Firstly, a huge thank you must go to my supervisor Dr Daniel Baker for giving me this opportunity and for working patiently with me during every stage of my PhD. His enthusiasm and expertise in vision research has been immensely helpful, especially at times when my confidence has wavered. I believe that under his mentorship I have developed considerably as a researcher and it has encouraged me to continue a career in academia.

I would also like to thank my thesis advisory panel, Professor Antony Morland, Dr Silke Goebel and Dr Catherine Preston for their insightful comments and advice throughout my research. Also, my sincere thanks goes to Dr Bruno Richard for his help in setting up my experiments, teaching me how to code and keeping me company during many hours of traveling to Hull. Furthermore, I am grateful to the staff at the Eye Clinic at Hull Royal Infirmary, particularly Mr Usman Mahmood and Dr Aftab Maqsud, for their collaboration. Also my thanks must go to my very loyal group of participants who completed many hours of testing, especially those that contributed to the results in every experimental chapter!

My friends and family have shown me an endless amount of love and support over the years. Thank you to Alex, Charlotte, Hannah and Pippa for the thousands of hugs and motivational chats, as well as my little dog Lily for being a relentlessly happy presence in my life. A special thanks goes to my wonderful family, especially my parents, without whom I would never have had the opportunity to embark on this journey. They have provided an infinite amount of encouragement, home cooked meals and helped me recover from broken limbs on more than one occasion! I would not have enjoyed this experience half as much without these people and so I am eternally grateful for all their support over the years.

Finally, I would like to dedicate my thesis to my amazing husband, Joshua. His love, generosity, feedback and pep talks have motivated me throughout every stage of my PhD, especially during the months writing this thesis. Thank you for everything.

Author's declarations

I declare that this thesis is a presentation of original work and I am the sole author. This work has not previously been presented for an award at this, or any other University. All sources are acknowledged as References. Each of the studies contained in this thesis were conducted in accordance with the ethical standards of the University of York, Department of Psychology. Chapters 3 and 4 were also conducted in accordance with the ethical standards of York Neuroimaging centre. Chapter 6 also gained ethical approval from Leeds East Research Ethics Committee (Yorkshire & The Humber - reference number: 15/YH/0532).

Data from Chapters 3-5 were presented in a preliminary incomplete form in a poster presentation at the following conferences:

ECVP, Trieste (Italy) August 2018

Lygo, F. A., Richard, B., & Baker, D. H., (2018) Multimodal neuroimaging of interocular contrast responses in human amblyopia

SFN, San Diego (USA) November 2016

Richard, B., Lygo, F. A., & Baker, D. H. (2016) Inter-ocular contrast normalization in the amblyopic visual cortex

CHAPTER 1

Introduction

1.1 Overview

Binocular vision and how the brain integrates binocular signals have been the subject of much clinical, psychophysical and neuroscientific research. Binocular vision occurs in humans and animals that have two eyes with overlapping images of the world. In a healthy visual system these overlapping images are pooled into a single percept in the visual cortex, to enable the viewer to develop a meaningful interpretation of the world. A primary advantage of this system is that it enables the viewer to see in depth and develop a three-dimensional view of the world (stereopsis). This would not be possible with only one eye, or if the two eyes fail to work together.

Amblyopia, commonly referred to as lazy eye, is a disorder of binocular vision. It typically occurs when one eye is disturbed during development, commonly through a strabismus (squint) or anisometropia (difference in refractive power of the two eyes) and in some cases both types can co-occur. Additionally, an infant can develop amblyopia if one eye experiences deprivation at birth through for example, a unilateral cataract or ptsosis (drooping of the upper eye lid). All of these types of amblyopia result in the patient having one weaker eye and rarely developing normal stereopsis (Scheiman et al., 2005; Taylor & Elliott, 2014) forcing the viewer to rely on other depth cues such as texture, perspective and size (Gibson & Flock, 1962). The input from the amblyopic (weaker) eye is not always correctable using refractive lenses alone, as it is thought to be suppressed by the brain to avoid conflicting visual inputs (e.g. diplopia) and confusion for the viewer. Therefore, amblyopia is caused not by a problem with the eyes but a problem with how the brain processes this information. This abnormal visual experience is thought to modify the functional properties and architecture of visual cortical neurons. Consequently, although the amblyopic visual system appears to be

structurally binocular, it remains functionally monocular by mainly using the fellow (stronger) eye (Baker, Meese, & Hess, 2008; Hess et al., 2010). These changes in the visual cortex are associated with many changes in visual performance, which will be reviewed throughout this chapter.

The prevalence of amblyopia is high, affecting around 3% of the population (Hess et al., 2010). There is thought to be a critical period, up to around 7 years old, before which treatment will be useful in correcting the deficit (Assaf, 1982; Epelbaum, Milleret, Buisseret, & Duffer, 1993; Scott & Dickey, 1988). If the underlying problem is treated after this period, such as through surgery for the squint, the visual deficit will still remain (Vaegan & Taylor, 1979). Studying amblyopia enables some insight into the neural and computational mechanisms involved in processing binocular vision, as it allows us to investigate the changes that occur in these mechanisms when the normal processes break down. Therefore, researching this condition is crucial in order to understand more about how binocular vision works, as well as develop new and more effective forms of treatment for people suffering from amblyopia.

This chapter will outline some of the key findings in the computational processes and neural mechanisms that are involved in binocular vision. It will focus on research from psychophysical, neuroimaging and treatment studies of amblyopia and will discuss how this early abnormal visual experience can affect brain organisation and binocular visual function.

1.2 Mechanisms for binocular vision

Over the years, studies have characterized individuals with amblyopia has having a reduction in visual acuity and contrast sensitivity in the amblyopic eye. Contrast sensitivity is the minimum amount of contrast needed to detect the presence of a barely visible stimulus. Psychophysical studies characterise contrast sensitivity using stimuli comprised of flickering gratings varying in contrast level (expressed as a percentage), spatial frequency (measured in

cycles per degree) and temporal frequency (measured in Hz) (Campbell & Robson, 1968). In order to investigate how the brain combines information from each eye to form a single binocular percept, studies have manipulated the properties of the stimuli presented to each eye. In doing so, inferences can be made regarding the neural processes used to combine information across the eyes.

Many studies have measured how contrast sensitivity differs in the amblyopic eye, compared to the fellow eye and healthy controls. Findings typically reveal reduced contrast sensitivity at high spatial frequencies in the impaired eye (Hess & Howell, 1977; Levi & Harwerth, 1977) and particularly in the central visual field (Hess & Pointer, 1987). Studies have also shown that amblyopes show errors in spatial discrimination, such as target localisation and contour integration (Wiesel & Hubel, 1963) and problems with higher-level tasks, such as reduced sensitivity for motion and form (Aaen-Stockdale, Ledgeway, & Hess, 2007). For many years these deficits were interpreted within a framework that assumed amblyopes lacked any binocular visual function (Holopigian, Blake, & Greenwald, 1986; Lema & Blake, 1977; Levi, Harwerth, & Smith, 1980). More recent research has since suggested that binocularity in the amblyopic visual system is not as compromised as once thought (Baker, Meese, Mansouri, & Hess, 2007).

One common method of assessing binocular function is by measuring the improved visual sensitivity when viewing with two eyes compared to one eye. The advantage of binocular vision is defined as the binocular summation ratio (BSR); the ratio of binocular contrast sensitivity to monocular contrast sensitivity (Campbell & Green, 1965; Legge, 1984). Campbell and Green (1965) found that in a normal visual system the mean sensitivity improvement was a factor of $\sqrt{2}$, meaning that a monocular stimulus needs to be presented at a contrast 1.4 times higher than a binocular stimulus to be equally detectable. One of the most widely accepted models of binocular summation states that the signals from the two eyes are

subject to nonlinear neural processing and are squared before being summed together (Legge, 1984b). Therefore the output would be the square root of the summed value:

$$CB = \sqrt{({C_L}^2) + ({C_R}^2)} \qquad (1.1)$$

In this quadratic summation *C* is contrast and *L* and *R* corresponds to the left and right eyes. If *L* is replaced with 0 and *R* replaced with 1, the response equals 1. If the binocular inputs are both 1, the response is 1.4 ($\sqrt{2}$) (Fig. 1.1A).

Other research has since reported BSRs that are much higher, ranging between 1.7 – 1.9, which indicates weaker nonlinearity (Medina & Mullen, 2007; Meese, Georgeson, & Baker, 2006; Valberg & Fosse, 2002). However, a recent meta-analysis of 65 studies revealed that summation estimates are greatly influenced by methodological factors, including the spatial and temporal frequency of the stimulus, and individual differences in monocular sensitivities (Baker, Lygo, Meese, & Georgeson, 2018). Therefore, in a healthy visual system binocular summation should typically lie between $\sqrt{2}$ and 2, depending on the participants, methods and stimuli used.

Early studies measuring BSRs in amblyopic observers suggested that binocular mechanisms are not present or show much smaller summation ratios, compared to control observers (Harwerth, Smith, & Levi, 1980; Lema & Blake, 1977; Pardhan & Gilchrist, 1992). This supports data from single-unit recordings, where fewer binocular neurons were found in cats with an artificial strabismus (Hubel & Wiesel, 1965; Schröder, Fries, Roelfsema, Singer, & Engel, 2002). However, greater levels of summation have been measured in amblyopic observers when contrast sensitivity is normalised across the eyes. This is achieved by adjusting the monocular contrasts to compensate for the difference in sensitivity between the amblyopic and fellow eyes, allowing normal BSRs (exceeding $\sqrt{2}$) to be measured (Baker, Meese, Mansouri, & Hess, 2007). This indicates that the visual systems in some amblyopic

observers are not structurally monocular but any residual binocular function is suppressed under binocular viewing conditions. Moreover, this effect can be simulated in viewers with normal binocular vision by using neutral density (ND) filters to reduce the luminance presented to one eye (Richard, Chadnova, & Baker, 2018). Equally, this effect can be resolved by increasing the contrast level presented to the filtered eye (Baker, Meese, Mansouri & Hess, 2007). This absence of binocular summation in healthy observers with an ND filter before one eye, further demonstrates how reduced sensitivity in one eye can reduce binocular summation levels. In amblyopia, a similar process might occur where the contrast energy from the amblyopic eye is too low to improve binocular sensitivity. This suggests that in amblyopia, both amblyopic and fellow eyes can drive binocular cortical neurons, contrary to earlier findings that found a complete loss of binocularity these cells (Hubel & Wiesel, 1965).

Although this suggests that binocular inputs *are* combined in neurotypical and amblyopic observers, it does not provide an explanation for *how* the underlying mechanisms or systems architecture work to combine binocular inputs in human visual cortex. In a series of psychophysical masking and detection experiments Meese, Georgeson and Baker (2006) examined binocular interactions for patterns differing in contrast across the two eyes for neurotypical observers. They developed a two-stage model of binocular contrast gain control to provide an account of discrimination and detection thresholds (Fig. 1.1B). At the first stage, the left (L) and right (R) channels pass through a gain control nonlinearity which involves suppression from the opposite eye. At the second stage, the channels are summed and pass through a further binocular gain control nonlinearity (Fig. 1.1B). This model has been shown to account for many aspects of binocular vision, including contrast matching, contrast detection and contrast discrimination (Baker, Meese, & Georgeson, 2007; Meese et al., 2006).

The two-stage model of contrast gain control was later extended to account for the binocular deficits in amblyopia. Baker, Meese and Hess (2008) measured psychophysical responses using a contrast discrimination paradigm, for monocular, binocular and dichoptic (different stimuli presented to each eye) pedestals, in strabismic amblyopes. The amblyopic eye showed increased detection thresholds for all the full range of pedestal contrasts (from 0-32%). The two-stage model was 'lesioned' to account for the pattern of responses observed in the amblyope data (Fig. 1.1C). This demonstrated that the responses from the amblyopic eye could be explained by two changes to the model: firstly through attenuation of the response from the amblyopic eye before binocular summation and inhibition, and secondly through an increase in internal noise in the pathways relaying the information from the amblyopic eye. Strikingly, binocular combination still occurs in this model, and suppression between the eyes remains unaffected. This 'attenuator model' suggests that binocular interactions remain intact in amblyopia, and therefore provides strong support for studies reporting normal BSRs (Baker et al., 2007).

As well as psychophysical studies, human studies using electroencephalography (EEG) have provided support for the attenuator model by comparing differences in the neural signal from the amblyopic and fellow eyes (more information on this technique in Chapter 2). Baker et al. (2008) used steady-state visual evoked potentials (SSVEPs) (Norcia, Appelbaum, Ales, Cottereau, & Rossion, 2015) to measure contrast response functions of amblyopic observers, to flickering stimuli. Their results showed a monocular response that increases monotonically with increasing contrast level. Findings also showed a significant reduction in response amplitude for the amblyopic eye compared to the fellow eye, supporting the predictions made by the attenuator model (Fig. 1.1C). However, researchers have failed to observe strong interocular suppression from the fellow eye onto the amblyopic eye. This could suggest that the sensitivity to inputs in the amblyopic eye are attenuated permanently during disease progression, rather than being supressed moment-by-moment through a dynamic process of interocular suppression (Baker et al., 2015).

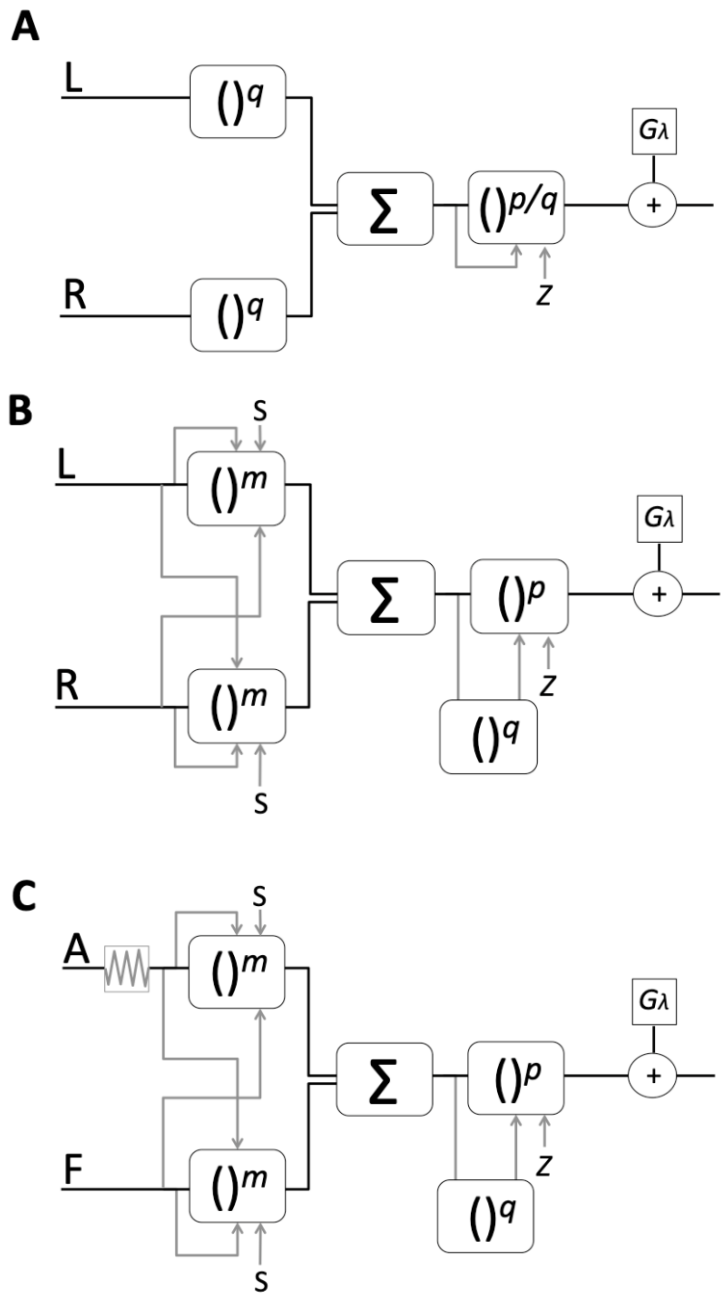

Figure 1.1. Schematic diagrams demonstrating the model architecture for binocular interactions. The original model of binocular summation is shown in (A) (Legge, 1984). In (B), the two-stage model of binocular contrast gain control (Meese et al., 2006). In (C), the attenuator model to account for the pattern of responses observed in amblyopia (Baker et al., 2008). In (A) and (B) the L and R refer to the left and right eyes. In (C) the A is the amblyopic eye where the attenuator occurs before the first stage. F is the Fellow eye. Black pathways are excitatory and grey pathways are inhibitory. Arrows indicate division, and brackets raised to a power denote exponentiation of inputs. Σ represents summation of inputs. Exponents (*m*, *p*, *q*) and saturation constants (*S*, *Z*) are free parameters. Gλ indicates Gaussian noise generators.

This evidence suggests that neural mechanisms that combine information from both eyes remain intact in amblyopia and that the lack of binocular function could be due to unbalanced inputs from each eye in binocular viewing conditions. To examine this, Mansouri, Thompson and Hess (2008) quantified the influence of interocular suppression when measuring the extent to which the stimuli presented to each eye need to differ for binocular combination to occur. They used suprathreshold motion and spatial tasks to quantify the suppressive effects between the eyes. Their findings showed that information from the two eyes interacts anomalously but by changing the relative information presented to each eye, balanced interocular performance can be observed (Mansouri et al., 2008). This understanding supports evidence that binocular cortical mechanisms do remain intact in amblyopia. This finding has also enabled potential advances in clinical treatments for amblyopia (Hess, Mansouri, & Thompson, 2010; To et al., 2011), which treat both eyes together (rather than just the weaker eye) and is discussed in more detail the final section of this chapter (section 1.4).

1.3 The neural basis of amblyopia

Despite many studies investigating amblyopia and suggestions of how binocular inputs are combined, it is still not clearly understood where in the brain the functional connections are altered. As well as psychophysical studies in humans, researchers have studied the characteristics of amblyopia using animal models, such as cats or non-human primates (e.g. macaques), raised with an artificial strabismus (Kiorpes, Kiper, O'Keefe, 1998), anisometropia (Crawford & Harwerth, 2004) or through deprivation produced by suturing the eyelid closed (Smith, Harwerth, & Crawford, 1985; Wiesel & Hubel, 1963). Psychophysical studies from these animal models of amblyopia have revealed similar effects to those measured in humans, such as reduced visual acuity and contrast sensitivity from the amblyopic eye (Kiorpes, Kiper, O'Keefe, Cavanaugh, & Movshon, 1998; Movshon et al., 1987). This suggests that the neural basis of human amblyopia is likely to have a similar foundation to that found in animal studies. Therefore, these animal models provide a good

basis from which to explore amblyopia by using more invasive techniques then can be ethically used in humans, such as single-unit recording.

Electrophysiology in non-human primates and non-invasive neuroimaging techniques in both humans and animals have enabled researchers to consider how the visual areas of the brain respond differently in amblyopia. Both methods have enabled detailed exploration of the early visual cortex and show comparable findings to psychophysical data in both species (Orban, Van Essen, & Vanduffel, 2004). Homologous retinotopic organisation can be mapped across species in primary visual cortex (V1) and other early visual areas (V2 and V3), with functional and structural differences only arising further up the visual hierarchy (e.g. V4, V5/MT) (Orban et al., 2004; Wandell & Winawer, 2011). This is important, as studies using both electrophysiology and neuroimaging techniques have implicated early visual areas, such as V1 and V2, as the location of the deficit seen in amblyopia.

Animal models of amblyopia typically show that visual information from both eyes is relayed normally from the retina to the lateral geniculate nucleus (LGN), suggesting that normal visual inputs reach the cortex (Levitt, Schumer, Sherman, Spear, & Movshon, 2001; Movshon et al., 1987). Therefore, the deficit is thought to occur in V1 as the first level of the visual system where monocular signals are combined (Smith et al., 1997). Some animal models using the deprivation technique appear to show a loss of binocularity in V1 cells, arising from neurons developing a preference for inputs predominantly from the non-dominant eye (Hubel & Wiesel, 1965; Shooner et al., 2015). This is supported by other electrophysiology studies that found single neurons in V1 exhibit lower sensitivity and altered spatial resolution for stimuli presented to the amblyopic eye (Kiorpes, Kiper, O'Keefe, 1998). Another study measured V1 neuronal activity in non-human primates with strabismus or anisometropia and again found reduced sensitivity when the amblyopic eye was stimulated (Shooner et al., 2015). However, the authors suggest that these interocular differences in V1 are too small to explain the behavioural deficits and suggest that subsequent processing in extrastriate regions

like V2 must amplify the effects (Kiorpes et al., 1998; Shooner et al., 2015). These findings have led to much debate as to whether the amblyopic deficit is confined to area V1 or whether the deficit extends to extrastriate areas (Barnes, Hess, Dumoulin, Achtman, & Pike, 2001; Clavagnier, Dumoulin, & Hess, 2015; Conner, Odom, Schwartz, & Mendola, 2007; Tao et al., 2014).

It is plausible that the deficit in amblyopia extends beyond V1, as the majority of extrastriate neurons are known to process information from both eyes, so the connections from either eye are equally vulnerable to abnormal visual experience in the early stages of development. For example, ocular misalignment for as little as two weeks has been shown to disrupt the binocularity of neurons in both V1 and V2 (Kumagami, Zhang, Smith, & Chino, 2000; Mori, Matsuura, Zhang, Smith, & Chino, 2002). A study by Tao et al. (2014) found that V2 neurons in amblyopic (anisometropic) monkeys were severely disorganised and contained robust binocular suppression compared to healthy monkeys. They also showed that the level of suppression positively correlated with the severity of the amblyopia and suggest that the disorganised V2 structure might affect higher cortical processing by causing difficulties in decoding incoming signals (Tao et al., 2014). This could go someway in explaining perceptual difficulties that amblyopes commonly have, e.g. stimulus position uncertainty or image distortion. Additionally, ocular dominance bias has been observed in both V1 and V2, but V1 was found to correlate more strongly with behavioural deficits (Shooner et al., 2015). Although this evidence presents a strong case that some deficits reside beyond V1, it should not be ruled out that V1 is a major locus for the deficits in amblyopia.

Whilst animal studies have been critical in learning more about the neural mechanisms of amblyopia, due to the structural differences between species and artificially inducing the condition, it cannot be expected to exactly parallel that of human amblyopia. Non-invasive techniques, such as functional magnetic resonance imaging (fMRI), have been fundamental in enabling researchers to look carefully at where the deficit in binocular visual function may

occur in amblyopic humans (see Chapter 2 for more details on fMRI). Some studies using fMRI have reported the amblyopic deficit to be localised to V1, which has been demonstrated by reduced signal strength and diminished activation (Algaze, Roberts, Leguire, Schmalbrock, & Rogers, 2002; Barnes et al., 2001; Goodyear, Nicolle, Humphrey, & Menon, 2000; Mendola et al., 2005). Contradictory to this, other studies such as that by Imamura et al. (1997) using positron emission tomography (PET), report normal V1 function for amblyopes and suggest that the problems lie beyond V1 in extrastriate areas (Imamura et al., 1997). Discrepancies among these studies in the locus of deficits from amblyopia could be due to many different methodological factors, including: the type of neuroimaging technique and scanning procedure (PET and fMRI); the type of stimulus presented during scanning (whether it is optimised to activate striate and extrastriate cortex) and measuring baseline activity; and individual differences between patients, including different forms and severity of the condition (Wong, 2012).

It is now generally agreed that the visual deficit in amblyopia could be a caused by a combination of problems arising from V1 and extrastriate cortex. Li, Dumoulin, Mansouri, & Hess (2007) conducted an fMRI study that measured blood oxygen level dependent (BOLD) responses within retinotopically defined visual areas, in amblyopic and control observers. They used a spatially broadband stimulus and compared responses between the amblyopic and fellow eyes, and the left and right eye for the control participants. Their results showed that in most cases there were consistent reductions in the activation in V1 when the stimulus is shown to the amblyopic eye, compared to the response derived from the fellow eye. They also found that areas V2, V3 and V3a, showed significantly reduced responses across the amblyopic group, which correlated with the reduced response found in V1. These findings are supported by Conner, Odom, Schwartz & Mendola (2007), who used monocular stimulation in fMRI to compare activation in V1 and V2, in amblyopes and controls. They reported reduced BOLD responses in V1 and V2 for amblyopic eyes compared to the fellow eye, and

controls. These findings suggest that both V1 and extrastriate visual areas are affected in human amblyopia, supporting physiological research conducted in animals (Tao et al., 2014).

Whilst it is crucial to understand where in the human visual cortex the deficit occurs it is also important to understand what might be causing the deficit in these regions. Possibilities include that there are fewer cortical neurons that respond to a stimulus when presented to the amblyopic eye (Goodyear et al., 2000), or that the proportion of cortex that responds to inputs from the amblyopic eye is reduced (Baker et al., 2015). Other studies suggest that visual cortical neurons are still able to respond to inputs from the amblyopic eye but a lack of synchronised firing causes the signals to be cancelled out (Roelfsema, König, Engel, Sireteanu, & Singer, 1994). Other explanations suggest that there are fewer connections between the input and output layers of V1 or feedback effects from other visual regions actively inhibit V1 neurons from responding (Goodyear et al., 2000; Kiorpes & McKee, 1999). Alternative theories include reduced cortical magnification, reduced spatial resolution, or a topographic disarray in the cellular map in individuals with amblyopia (Clavagnier et al., 2015; Hussain et al., 2015). These suggestions provide a useful baseline for studies to investigate the neural causes of amblyopia.

One method that has been used to tackle these questions is population receptive field (pRF) mapping (Dumoulin & Wandell, 2008). This is a forward modelling fMRI technique that estimates properties of neurons within each voxel in the visual cortex. It not only enables the visual field to be retinotopically mapped, but other neuronal properties such as receptive field sizes to be explored. Traditional pRF stimuli are made up of high contrast black and white drifting bar stimuli. This enables the activity from populations of neurons responding to high contrast achromatic stimuli to be pooled together and used to approximate the size parameters for the pRF. Stimuli must be rich enough to evoke a range of responses in each voxel so that accurate fitting can occur. The predicted BOLD timeseries for a range of pRF sizes (and positions) are compared to the actual BOLD response produced by different voxels in

response to the pRF stimuli. As demonstrated in Figure 1.2, pRF size in early visual areas increases as a function of eccentricity (larger pRF sizes in the periphery compared to the fovea) and progressing through the visual processing hierarchy (V1- V3), as higher visual areas tend to be less modality specific (Dumoulin & Wandell, 2008). Studies have shown that pRF size estimates agree well with electrophysiological measurements obtained from a range of eccentricities in corresponding locations in both monkey and human visual cortex (Logothetis, Pauls, Augath, Trinath, & Oeltermann, 2001). Therefore, this technique is useful as it improves on other phase-encoded mapping techniques (retinotopic mapping), by coupling fMRI signals measured at the millimetre scale with receptive field sizes measured at the micron scale.

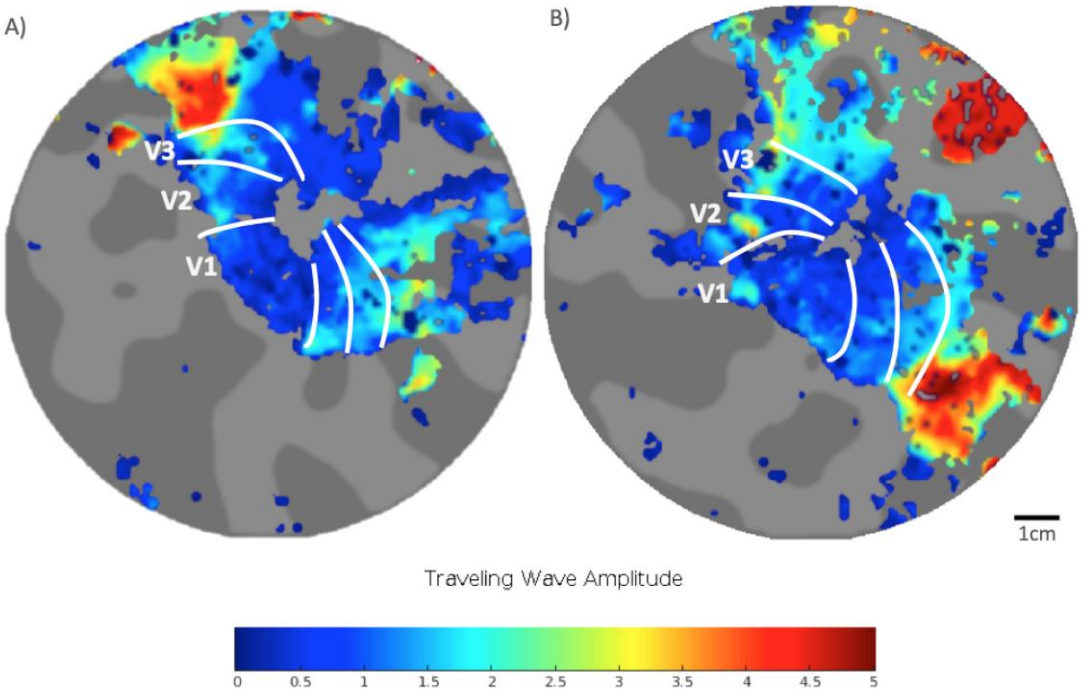

Figure 1.2. Example of pRF size estimates shown on a flattened cortical surface of the left hemisphere (A) and right hemisphere (B) (taken from control participant FL from Chapter 3). Dark blue areas show small pRF sizes and red areas show large pRF sizes. Boundaries between areas V1, V2 and V3 are overlaid, showing pRF sizes increase with distance from the fovea and between visual areas.

Studies have used pRF modelling to compare the projections from the amblyopic and fellow eyes in early visual areas. Clavagnier et al. (2015) measured the responses from each eye independently by covering the eye not being tested with a black patch. Results for the amblyopic eye showed that cortical magnification was normal but revealed much larger pRF sizes in V1, V2 and V3. They suggest that this increase in pRF size in the amblyopic eye reflects the neurons' reduced spatial resolution. Furthermore, they found that there was more variability in the positions of the pRFs from the amblyopic eye. The authors speculate that this could be due to increased cellular position disarray within the representation of the amblyopic eye. These findings support other research showing that the deficits in the projections from the amblyopic eye in visual cortex extend beyond V1 into extrastriate areas (Conner et al., 2007; Li et al., 2007; Tao et al., 2014).

It is reasonable to conclude from the evidence presented in this section that the main locus of amblyopia is in early visual areas, especially V1 and V2. A range of cortical deficits has been established but further studies are needed in order to ascertain the fundamental cause of amblyopia. Techniques like pRF modelling have been useful in providing further insight into the differences in projections from the amblyopic and fellow eye and further developments in neuroimaging methods and analysis techniques will help further our understanding of the root cause of amblyopia.

1.4. Treatment for Amblyopia

Amblyopia can be treated in young children using a variety of techniques directed at recovering monocular function in the amblyopic eye. One common method is through 'occlusion' therapy, where a patch is worn over the fellow eye in an effort to force the amblyopic eye to work harder. Treatments also include blurring the vision in the fellow eye using atropine drops to paralyse accommodation or the ability to focus, to encourage the use of the amblyopic eye. Another method often used for treating anisometropic amblyopes, is to provide glasses to reduce or eliminate the refractive error difference between the eyes and

enable a more balanced binocular viewing experience. Although these treatments have been shown to help improve vision in the amblyopic eye, it has rarely been shown to improve binocular function (Mitchell, Howell, & Keith, 1983; Scheiman et al., 2005). Furthermore, there is evidence to suggest that these treatments are not long-lasting and amblyopia could reoccur after the treatment has been completed (Bhola, Keech, Kutschke, Pfeifer, & Scott, 2006).

One of the reasons for this could be compliance to the treatment during the critical period (up to around 7 years old) (Searle, Norman, Harrad, & Vedhara, 2002). Studies have suggested that these treatments lack effectiveness, as it requires young children to function normally whilst partially sighted, which can impact their social, sporting and psychological development (Hess et al., 2010; Koklanis, Abel, & Aroni, 2006; Searle et al., 2002). Additionally, if the condition is left untreated into adulthood it could impact future decisions and exclude them from pursuing career choices that require good binocular vision, e.g. police work, the armed forces and driving heavy goods vehicles (Scheiman et al., 2005). Perhaps most importantly, the risk of blindness is significantly increased if sight in the fellow eye were to be lost later in life (Rahi et al., 2002). One study in Finland found that the risk of total blindness in patients with untreated amblyopia is nearly three times that of the normal population (Tommila & Tarkkanen, 1981). Therefore, amblyopia is not only clinically significant but also because of the socioeconomic impact it has on the sufferer and the potential societal cost of providing care and rehabilitation if sight is completely lost.

A major problem with these traditional methods of treating amblyopia is that they are fundamentally monocular (they only treat one of the eyes) when the condition is binocular in nature. Within the last decade, various studies have begun to overcome these traditional treatment problems by developing binocular treatments that aim to promote cooperation between the two eyes. As discussed above (section 1.2) amblyopes have been shown to

possess binocular mechanisms and normal binocular summation when the imbalance of the monocular signals is taken into account (Baker et al., 2007; Mansouri et al., 2008).
Hess et al. (2010) used dichoptic stimuli and adjusted the level of contrast presented to each eye to control for the imbalance of monocular signals. By adjusting the contrast in the amblyopic eye to be higher than the contrast presented to the fellow eye, it creates an artificial viewing condition where the suppression of the amblyopic eye is controlled for, enabling binocular viewing. Their results found that over time the difference in contrast sensitivity between the eyes can be reduced, as the binocular combination and suppression improved.

The findings from this study have enabled a new treatment, known as dichoptic perceptual learning, to be developed using a game platform (Hess, Thompson, & Baker, 2014; To et al., 2011). This treatment involves giving patients a hand held device, e.g. a phone or tablet, with a game that presents a dichoptic stimulus. To et al. (2011) designed a version of a 'Tetris' game, where some content was presented to one eye (e.g. the falling blocks) and another set of content was presented to the other (e.g. the landing blocks) (Fig. 1.3). Therefore, in order to play the game successfully the participant has to use both eyes to see the full content of the game. As described in the paradigm used by Hess et al. (2010), initially the contrast of this stimulus is stronger in the amblyopic eye than the fellow eye and over time the difficulty of the game is increased by raising the contrast of the stimulus presented to the fellow eye. After some time this should reach equal contrast levels in each eye, resulting in progressive strengthening of their binocular vision (Hess et al., 2010). This dichoptic paradigm is different to traditional amblyopia treatments by encouraging binocular cooperation through contrast imbalance. It also avoids the psychosocial side effects of traditional occlusion therapies that can cause children especially to avoid treatment. Moreover, it has been shown to significantly improve both visual acuity and stereo acuity and to be effective in adults as well as children within the critical period, providing evidence for wide clinical application (Epelbaum, Milleret, Buisseret, & Duffer, 1993; Hess et al., 2010). Insight into neural changes that occur over time during these treatments could reveal more about the primary

location of the deficit and the capability of the brain to recover binocular visual function. This should inevitably influence the design of this treatment so it can have the maximum benefit for as many people as possible.

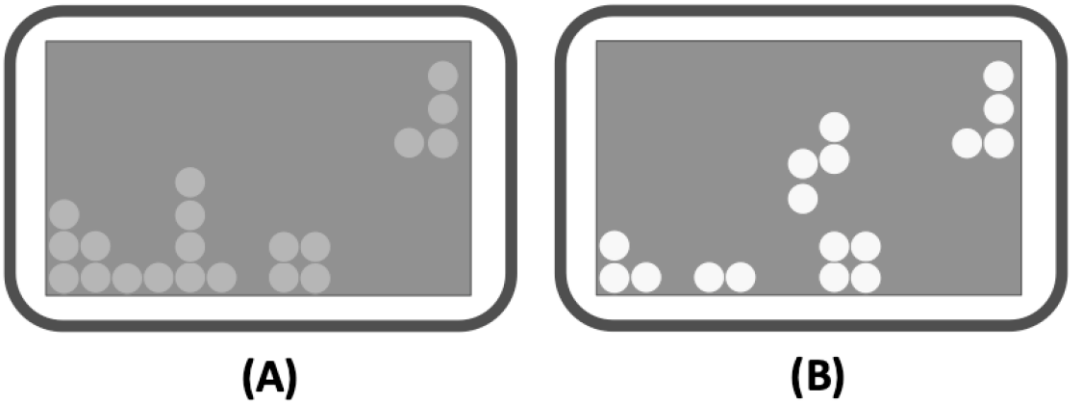

Figure 1.3. Schematic adapted from To et al. (2011) to help illustrate the game paradigm. The Tetris game is displayed on a handheld device, such as tablet or phone (with an overlay lenticular lens that enables information to be presented to each eye separately). Images in (A) and (B) are presented simultaneously. (A) displays the information being shown to the fellow eye in low contrast. (B) displays the information being shown to the amblyopic eye in high contrast.

Another treatment method that has been developed in recent years is using transcranial magnetic stimulation (TMS) - a non-invasive technique that can be used to stimulate regions on the lateral surface of the brain. The mechanisms of how TMS works is still relatively unknown, however its therapeutic use has been widely documented and has been used to help treat many clinical disorders, such as: strokes (Talelli, Greenwood, & Rothwell, 2007); Parkinson's disease (Koch, Brusa, Caltagirone, Peppe, Oliveri, Stanzione, & Centonze, 2005); addiction (Camprodon, Martínez-Raga, Alonso-Alonso, Shih, & Pascual-Leone, 2007); and depression (Klein et al., 1999), to name just a few. A study by Thompson, Mansouri, Koski, and Hess (2008) used repetitive TMS (rTMS) to stimulate the visual cortex of amblyopes to see whether it could improve their contrast sensitivity. Their findings showed that just 10 minutes of rTMS applied to V1 improved their performance on a subsequent

contrast sensitivity task. One explanation for this effect could be that the rTMS is modulating the inhibitory interactions in the visual cortex and therefore reducing the suppression of the amblyopic eye (Thompson et al., 2008). These findings provide further evidence that amblyopes do have binocular neural connections but in binocular viewing conditions the suppressive mechanisms result in a functionally monocular response from the visual cortex. This further indicates the plasticity of the amblyopic visual system and provides evidence for the use of rTMS as a therapy for treating amblyopia. However, because the location of the neural deficit of amblyopia remains unclear and there is not a clear target where this stimulation therapy should be applied to achieve the maximum effect. Therefore, it remains important for future studies to continue to explore where the neural deficit lies in amblyopia in order to develop further treatments.

1.5. Methodological considerations for neuroimaging studies

Based on the evidence studies presented in this chapter, there are a few key methodological considerations to address. Firstly, there appears to be some inconsistency between the response amplitude recorded between the amblyopic and fellow eyes in different neuroimaging techniques. For example, fMRI studies have reported much smaller differences between the amblyopic eye and the fellow eye compared to studies measuring SSVEPs, even for severely amblyopic participants (Baker et al., 2015; Conner et al., 2007; Li, Dumoulin, Mansouri, & Hess, 2007). It is unclear whether this difference is due to the inherent advantages and disadvantages of the different measurement techniques, or because of methodological design differences, such as the stimulus or the heterogeneous nature of amblyopia as a disorder. Chapters 4 and 5 of this thesis address this issue by conducting the same experiment in both fMRI and EEG using exactly the same participants, stimuli and experimental procedure.

Another point for consideration concerns disparities in the neural deficit between different forms of amblyopia. Studies comparing the differences in fMRI activation in early visual

areas in human strabismic and anisometropic amblyopes have found significantly fewer voxels that respond to binocular stimuli in strabismic amblyopes, suggesting that binocularity is more impaired in strabismic amblyopes (Lee et al., 2001). Moreover, anisometropic amblyopes have shown a reduced response for stimuli at high spatial frequencies, whereas strabismic amblyopes did not (Choi et al., 2001). These findings agree well with electrophysiology studies that have shown binocularity is more impaired in strabismic monkeys (Kiorpes et al., 1998), whereas anisometropic monkeys show a loss of high spatial frequency channels (Movshon et al., 1987). These results have important implications for future studies to be careful in participant recruitment and to distinguish between different types of amblyopia. As the focus of this thesis is on understanding binocular vision the experimental chapters here have aimed to recruit strabismic amblyopes, as they show a stronger binocular deficit.

Finally, another methodological issue can occur when testing monocular visual function. Many studies measure monocular visual function in an unnatural viewing situation by leaving one eye open and the other eye closed or covered, meaning one eye is always in darkness. This is the case for animal studies that involve one eye being sutured closed (Smith et al., 1985; Wiesel & Hubel, 1963) and human studies where one eye is occluded using a patch (Clavagnier et al., 2015). The studies undertaken here use a stereoscopic computer monitor or projector system that enables both eyes to be open and stimuli to be carefully presented to one eye at a time. This has enabled much more realistic viewing conditions for measuring accurate monocular, binocular and dichoptic visual responses.

1.6. Summary

Many studies have been conducted to understand more about the computational processes and neural mechanisms behind binocular vision in amblyopia. It is clear from this evidence that binocular neural mechanisms do remain intact in amblyopia, which has been demonstrated in studies measuring binocular summation (Baker et al., 2007) and interocular suppression

(Mansouri et al., 2008). This research has enabled models to be developed to explain how the inputs from the amblyopic and fellow eyes are processed (Baker et al., 2008). Furthermore, electrophysiology and neuroimaging techniques have given an insight into where these problems may arise in the brain. Although the specific location is still somewhat debated, the majority of evidence suggests that the deficit in amblyopia occurs in V1 and extends into extrastriate areas, such as V2 and possibly V3 (Clavagnier et al., 2015; Conner et al., 2007; X. Li et al., 2007; Tao et al., 2014). Studies have also begun to investigate what might be causing these deficits in amblyopia, such as fewer cortical cells and increased cellular position disarray within the representation of the amblyopic eye (Clavagnier et al., 2015; Goodyear et al., 2000). These findings have directly influenced the development of new, more effective forms of treatment for amblyopia (Thompson et al., 2008; To et al., 2011). More research into understanding the location and cause of the amblyopic deficit will provide more treatments to improve vision in amblyopia and will help towards deploying them on a larger scale.

1.7. Thesis Overview

The aim of the research undertaken in this thesis is to use EEG and fMRI to further understand how binocular visual information is processed in amblyopia. The layout of this thesis is outlined in Figure. 1.4 and includes a summary of what to expect from each chapter.

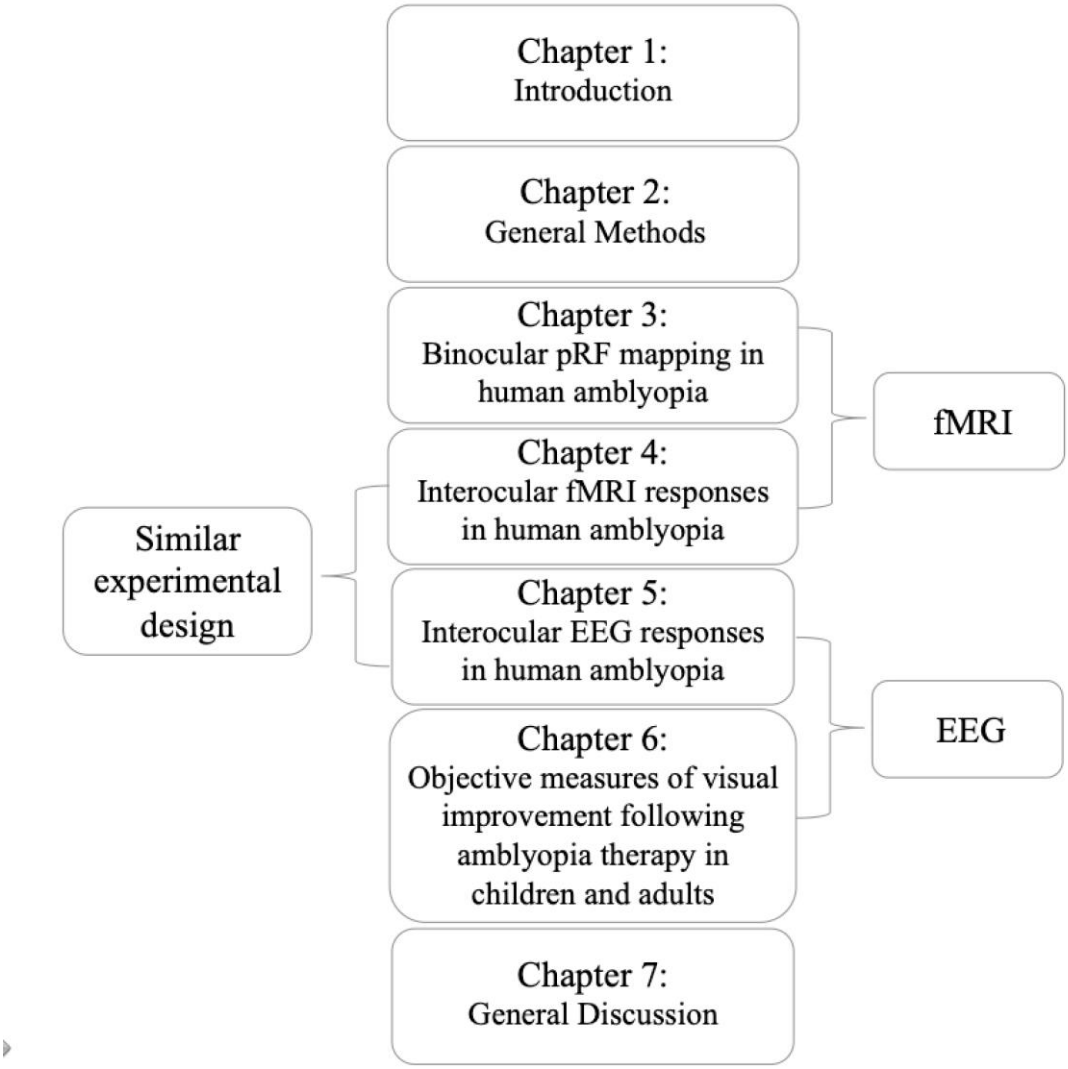

Figure 1.4. Summary of thesis layout. Experimental chapters 3-6 can be categorised by technique (EEG and fMRI) or experimental design.

Chapter 1 is this introductory chapter that includes: an overview of amblyopia; a discussion on important psychophysical and neuroscientific research in binocular vision and amblyopia; and treatments options for people with amblyopia.

Chapter 2 outlines the general methods that have been used throughout the experiments in this thesis. It contains information regarding the demographic and clinical details for the participants, stimulus design and neuroimaging techniques.

Chapter 3 reports the results from a pRF study which builds on previous research from Clavagnier et al., 2015. This study measured pRF sizes across V1-V3 from both eyes, from a group of amblyopic and control observers. In amblyopic observers, pRF sizes are shown to be larger for the amblyopic eye compared to the fellow eye across visual areas, whereas control participants showed no difference between the eyes. However, the extent of the differences between the eyes is less pronounced than previous studies have found.

Chapter 4 uses fMRI to measure interocular contrast responses in amblyopes and controls, using sinusoidal gratings, presented either monocularly, binocularly or dichoptically at a range of contrasts (Moradi & Heeger, 2009). Different computational models of binocular vision in amblyopia are explored to explain these responses measured in fMRI. Responses from amblyopic observers were best predicted by a model simulating a response gain attenuation effect and unbalanced interocular suppression.

In Chapter 5, the same participants and experimental design was used as Chapter 4, but used steady-state EEG to measure interocular contrast responses. Again, different computational models of binocular vision in amblyopia are explored and found that a model simulating a contrast gain shift was best at predicting the responses recorded using EEG. Also, no evidence of abnormal interocular suppression was found in this study.

Chapter 6 reports the results from two studies that used a dry-electrode EEG system to measure steady-state responses to contrast stimuli, to objectively measure visual improvement in children and adults whilst undertaking treatment for amblyopia. Both studies measured interocular contrast responses at three time points during amblyopia therapy. In experiment 1, responses were measured in children (ages 4-6 years old) under going traditional treatment (occlusion therapy/atropine eye drops). Improvements in visual acuity were noticed throughout treatment but EEG responses provide no convincing evidence of improvements. Experiment 2 presents the findings of a pilot study to measure visual improvements in adults, using a 3D gaming treatment. Findings reveal promising indications that improvements in steady-state responses from the amblyopic eye many be observed throughout treatment if this study were to be conducted on a larger scale.

Chapter 7 contains a general discussion of the studies mentioned above, draws conclusion and suggests avenues for future research.

CHAPTER 2

General Methods

2.1. Neuroimaging methods

The research projects in this thesis used two neuroimaging techniques to further understand contrast processing in the amblyopic brain: functional magnetic resonance imaging (fMRI) and electroencephalography (EEG). By using a combination of strong magnetic fields and radio waves, fMRI-scanning is able to measure brain activity by detecting the magnetic properties associated with blood flow and blood oxygenation (Buxton, 2013; Ogawa, Lee, Kay, & Tank, 1990). It works on the principle that when a part of the brain becomes active the neurons require more glucose to pump ions across the membrane surface. As the brain does not store glucose, it is transported to the neurons via the blood along with oxygenated haemoglobin in the red blood cells. Differences in oxygenation in the cortical tissue changes the magnetic properties of the blood and these changes are measured as blood oxygen level dependent (BOLD) contrasts. One of the main benefits of using fMRI is that it provides detailed mapping of activity throughout the brain without being invasive, unlike single-unit electrophysiology or other brain imaging techniques such as positron emission tomography (PET) (Glover, 2011). Therefore, the use of fMRI in these studies has provided an estimate of summation and suppression at multiple neural stages in amblyopia. Using fMRI to explore in detail the spatial location of where the primary deficit in amblyopia may occur, could contribute towards improving treatment options such as targeted brain stimulation (Thompson et al., 2008).

Whilst fMRI enables detailed *in vivo* images of neuronal activity, the temporal resolution is limited by slow hemodynamic response times to metabolic changes (Glover, 2011; Kim, Richter, & Ugurbil, 1997). On the other hand, EEG enables excellent temporal precision by measuring electrical activity using electrodes on the surface of the scalp. The visual evoked potential (VEP) method is an EEG technique that is frequently used to measure neural signals

in response to a light stimulus. When the retina is stimulated with light it generates a bioelectric signal in the occipital cortex, which can be recorded from electrodes at the scalp. Varying the properties of visual stimuli presented to the eyes (e.g. the spatial frequency, temporal frequency, contrast level etc.) enables changes in the VEP to be measured (Kothari, Bokariya, Singh, & Singh, 2016). The steady-state visually evoked potential (SSVEP) is another EEG method that records neural responses that occur after viewing a repetitive sensory stimulus, such as a flickering light. Viewing a flickering stimulus at certain frequencies (usually between 3-20 Hz) stimulates the visual pathway causing the neurons to oscillate at the same frequency (Norcia et al., 2015). This stimulation produces electrical signals at both the base frequency and multiples that can be measured using EEG. For example, for a visual stimulus flickering at 5 Hz the neurons will also oscillate at 5 Hz and produce harmonics at 10 Hz, 15 Hz, etc. This is technique is beneficial due to high signal-to-noise ratios, which is especially useful when measuring responses from clinical populations (such as is cases of amblyopia). However, a disadvantage of using EEG is that it provides less accurate spatial representation due to the distortion that occurs when the cortical current travels through different resistive layers such as the skull (Srinivasan, Nunez, Tucker, Silberstein, & Cadusch, 1996). EEG equipment is cost effective and some versions can be easily deployed to measure neural function during therapeutic interventions in a clinical setting. Conversely, fMRI scans are expensive and contain extremely stringent safety criteria that restrict certain participants from taking part.

Both EEG and fMRI are complementary and using them together has enabled a detailed insight into contrast processing in the amblyopic brain. Furthermore, this is the first set of studies to directly compare these two techniques within the same group of participants and using the same stimuli. Ethics committees at the York Neuroimaging Centre and the Department of Psychology at the University of York approved all experiments included in this thesis.

2.2. Participants

With the exception of the children recruited at Hull Royal Infirmary (Chapter 6), all participants were recruited via posters located around the University of York campus and on the Department of Psychology website. The posters advertised MRI and EEG studies for people who had amblyopia or had worn an eye patch as a child. All participants in these studies had undergone varying treatments for strabismic amblyopia as children (self-reported). Several participants recruited for these studies participated in all experiments, details of which can be found in Table 2.1.

Table 2.1. Summary table for all the experiments that each participant took part in at the University of York. The same participants took part in multiple studies included in this thesis, which are represented by a tick (✓) for each chapter. The top half of the table indicates the amblyopic participants and the bottom half indicates the control participants (W/D = participant withdrew from the study).

Observer	Chpt 3 (fMRI)	Chpt 4 (fMRI)	Chpt 5 (EEG)	Chpt 6 (Dry-EEG)
AJB	✓	✓	✓	
AWC	✓	✓	✓	
CHY			✓	
CL			✓	
CM	✓	✓	✓	
CWB			✓	
DGB			✓	
ECD	✓	✓	✓	✓
FD	✓	✓	✓	W/D
GJS			✓	
GR			✓	
HJW	✓	✓	✓	
IKL	✓	✓	✓	✓
JAC			✓	
JJM			✓	
LEH			✓	
LLR	✓	✓	✓	W/D
MEH			✓	
MRW	✓	✓	✓	✓
MSY			✓	
MTW	✓	✓	✓	
SA	✓	✓	✓	✓
SCC			✓	
SSR			✓	
XL	✓	✓	✓	
DHB	✓	✓	✓	-
BR	✓	✓	✓	-
FL	✓	✓	✓	-
MH	✓	✓	✓	-
ATL	✓	✓	✓	-
BM	✓	✓	✓	-
MK	✓	✓	✓	-
KWN	✓	✓	✓	-
AKS	✓	✓	✓	-
AVB	✓	✓	✓	-

Visual and stereo acuity was measured for all participants. Visual acuity was measured using a Snellen chart, which was viewed at a distance of 6 metres. For amblyopic participants, the amblyopic (weaker) eye was tested first followed by their fellow (dominant) eye. Visual acuity was defined as the lowest line where all the letters were reported correctly. Stereo acuity was measured using the 'graded circles test' on The Titmus Stereo Fly Test. The distance for this test was 40cm and the range of stereoacuities tested was 800 to 40 seconds of arc. If the participant was unable to perform any stereoscopic discrimination this was marked as 'none'. All acuity measures and clinical details for each participant can be found in Table 2.2. All control participants had normal or corrected-to-normal vision (see Table 2.3). All participants gave written informed consent and were able to withdraw from the study at any time.

It is important to note that a small number of the amblyopic participants recruited for these studies do not show large differences in visual acuity between each eye, which goes against the typical clinical definition of amblyopia (Table 2.2). It is possible that the improved visual acuity in the amblyopic eye for these participants is due to the treatment they received as a child. However, as a neural binocular deficit still remains for each of these individuals, they can still be considered to be 'amblyopic'. Therefore, the population of amblyopes recruited for these studies are considered to be a combination of amblyopes that meet the clinical definition, as well as binocularly anomalous 'treated' amblyopes.

Table 2.2. All demographic and clinical details that were provided for the 25 amblyopic participants, including details of any treatment or surgery (mo = months; y = years). Visual acuity was measured using a Snellen Chart (logMAR equivalents provided) and stereo acuity was measured using The Titmus Stereo Fly Test 'circles'.

Observer	Age/sex	Amblyopic Eye	Acuity: Right Eye	Acuity: Left Eye	Stereo Acuity	Age Detected	Patching (Age)	Surgery	Optical Correction
AJB	21/M	Left	6/6 (0)	6/9.5 (0.2)	140s	18 mo	5 y	18 mo	None
AWC	26/M	Left	6/6 (0)	6/15 (0.4)	140s	4 y	4 y	None	None
CHY	40/F	Left	6/6 (0)	6/15 (0.4)	None	5 y	5 - 6 y	None	None
CL	17/F	Left	6/7.5 (0.1)	6/9.5 (0.2)	40s	4 y	4 - 6 y	None	None
CM	22/F	Left	6/12 (0.3)	6/24	None	11 y	11 - 12 y	None	None
CWB	49/M	Left	6/4.8 (-0.1)	6/9.5 (0.2)	None	20 mo	4 y	20 mo, and 7 y	Not known
DGB	35/M	Right	6/38 (0.8)	6/7.5 (0.1)	400s	9 y	None	None	None
ECD	20/F	Left	6/4.8 (-0.1)	6/4.8 (-0.1)	400s	6 y	None	None	None
FD	22/F	Right	6/6 (0)	6/6 (0)	400s	3 y	None	3 & 4 y	None
GJS	22/M	Right	6/30 (0.7)	6/4.8 (-0.1)	None	4 y	4 y	None	None
GR	19/F	Left	6/4.8 (-0.1)	6/4.8 (-0.1)	None	7 y	7 - 10 y	None	None
HJW	22/M	Right	6/15 (0.4)	6/6 (0)	80s	9 y	9 y	None	None
IKL	21/F	Left	6/4.8 (-0.1)	6/6 (0)	None	18 mo	4 y	None	LE: +4; RE:+3.75
JAC	19/F	Left	6/6 (0)	6/60 (1.0)	None	18 mo	18 mo	None	None
JJM	19/M	Left	6/15 (0.4)	6/15 (0.4)	200s	<6 y	6 y	None	None
LEH	21/F	Right	6/6 (0)	6/4.8 (-0.1)	40s	5 y	5 y	None	LE: -1.25; RE: -1.75
LLR	21/M	Left	6/6 (0)	6/12 (0.3)	80s	4 y	4 y	None	None
MEH	21/F	Left	6/6 (0)	6/9.5 (0.2)	None	~6 y	6 - 7 y	~6 y	LE: +10.5; RE: +9.5
MRW	19/F	Left	6/6 (0)	6/12 (0.3)	40s	5 y	5 - 6 y	None	LE: -2.5; RE: + 0.75
MSY	20/M	Right	6/9.5 (0.2)	6/6 (0)	400s	5 y	5 y	16 y	None
MTW	22/M	Right	6/6 (0)	6/6 (0)	140s	5 y	5 y	None	None
SA	20/F	Right	6/9.5 (0.2)	6/7.5 (0.1)	None	18 mo	18 mo - 6 y	<18mo	None
SCC	20/F	Left	6/6 (0)	6/12 (0.3)	40s	4 y	4 - 5 y	None	None
SSR	23/M	Left	6/4.8 (-0.1)	6/6 (0)	140s	2 y	2 - 3 y	None	None
XL	35/F	Right	6/12 (0.3)	6/6 (0)	60s	~10 y	None	None	None

Table 2.3. Demographic and clinical details for the control participants. Visual acuity (logMAR equivalents provided) and stereo acuity was measured in exactly the same way as the amblyopic participants. None of the control participants had ever undergone any treatment or surgery to correct their vision.

Observer	Age/sex	Right Eye Acuity	Left eye Acuity	Stereo-Acuity	Dominant eye
DHB	35/M	6/6 (0)	6/6 (0)	40s	R
BR	29/M	6/4.8 (-0.1)	6/4.8 (-0.1)	40s	L
FL	22/F	6/6 (0)	6/6 (0)	40s	R
MH	27/M	6/3 (-0.3)	6/3 (-0.3)	40s	R
ATL	28/F	6/3 (-0.3)	6/4.8 (-0.1)	40s	R
BM	30/F	6/6 (0)	6/6 (0)	40s	R
MK	25/F	6/3 (-0.3)	6/3 (-0.3)	40s	L
KWN	23/F	6/4.8 (-0.1)	6/4.8 (-0.1)	40s	R
AKS	23/F	6/4.8 (-0.1)	6/4.8 (-0.1)	40s	R
AVB	25/F	6/6 (0)	6/6 (0)	40s	R

2.3. Materials

2.3.1 Measuring Contrast Responses

All experiments were created and operated in MATLAB (Mathworks, Natick, MA, USA) versions 2012 and 2015, using functions from the Psychophysics Toolbox (Brainard, 1997; Pelli, 1997). Stimuli used in Chapters 4, 5 and 6 were horizontal sinusoidal luminance gratings, presented in four identical circular patches (Fig. 2.1). Each grating was spatially ramped by a raised cosine envelope to a diameter of 4° of visual angle, and presented on a 10° circular grey-scale background. Following the paradigm used by Moradi and Heeger (2010), the stimuli were presented 1° out from the fixation point. The gratings had a spatial frequency of 3c/° and a temporal frequency of 4 Hz on-off flicker. These stimuli parameters were chosen as pilot testing revealed that these enabled measurable contrast responses to be recorded from both the strong eye and weaker eye of an amblyopic observer. Inside the grey-scale aperture was a central fixation point made up of 3×3 grey-scale pixels. The aperture was presented on a noise background designed to act as a binocular fusion lock, designed to help

participants fuse the images between their eyes. There were five different levels of contrast used throughout these studies: 0, 1.5, 6, 24, 96% Michelson contrast. These contrasts were presented either monocularly (presented to one eye at a time whilst the other eye saw the grey aperture with no gratings), binocularly (the same contrast presented to both eyes) or dichoptically (different contrasts presented to each eye). Binocular separation of the stimuli was different in each technique, due to the different hardware systems in fMRI and EEG (more details of these can be found below).

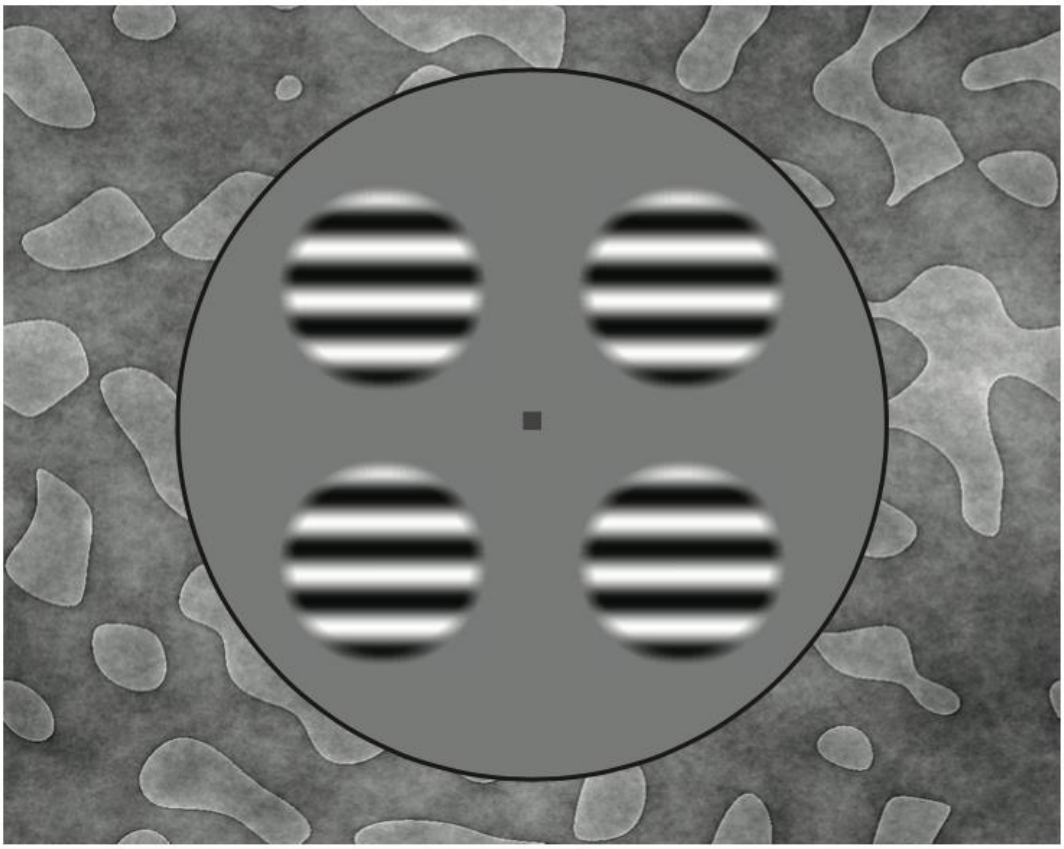

Figure 2.1. An example of the stimulus display used to measure contrast responses, in Chapters 4, 5 and 6. Stimuli consisted of horizontal sinusoidal gratings (3c/° and 4Hz flicker) presented either monocularly, binocularly or dichoptically, on a binocular fusion-lock background.

2.3.2 MRI

All fMRI data were acquired at York Neuroimaging Centre using a GE 3T HDx Excite MRI scanner. Firstly, participants carried out structural scans of the full brain using an 8-channel surface coil (Nova Medical, Wilmington, MA, USA). Two high-resolution T1-weighted structural scans (TR, 7.8ms; TE, 3ms; voxel size, 1 × 1 ×1 mm^3; flip angle, 12°; matrix size, 256 × 256; FOV, 256 mm), and two T2*-weighted fast gradient recalled echo scans (TR, 400 ms; TE, 4.2ms; voxel size 1 ×1 × 2 mm^3; flip angle, 25°; matrix size, 128 × 128; FOV, 260 × 260 mm^2) were carried out. These scans were first aligned to each other using FSL (http://fsl.fmrib.ox.ac.uk/fsl/fslwiki/) 'flirt' function (Jenkinson, Bannister, Brady, & Smith, 2002), and then averaged and divided by the T2*-weighted data using 'fslmaths'. This improved grey-white matter contrast and partially corrected for the drop-off caused by the use of a 16-channel coil for the functional scans. This average T1 was then automatically segmented into grey and white matter with manual refinements.

Functional images were acquired using a 16-channel posterior surface coil (Nova Medical, Wilmington, MA, USA) to improve signal-to-noise ratio at the occipital pole. Scan slices were aligned to cover the region containing the calcarine sulcus and occipital pole. A total of 39 EPI slices were taken within an FOV of 192 × 192 mm^2, with 2 mm^3 isotropic voxels (TR = 3000 ms, TE = 30, flip angle = 90, acquisition/reconstruction matrix = 96 × 96). Four 'dummy' TRs (12s) were included at the beginning of each scan to allow the signal to reach magnetic equilibrium. In addition to the functional scans, a proton density (PD) scan with the same spatial prescription as the EPI data was acquired at the beginning of each session – this scan was used to align the fMRI data to a high-resolution T1-weighted structural scan of the full brain.

During all scans the participant's head was placed inside the head coil and surrounded by padding to reduce movement during the scan. The participant was also given ear defenders to reduce scanner noise. The fMRI stimulus presentation was performed on a Shuttle XPC

SZ87RG high-end graphics system with an Intel Core i7-4790K processor at 40 GHz and a NVIDIA GeForce GTX970 graphics card with 4 GB DDR5 memory. Stimuli were displayed on a ProPixx DLP LED stereo projector (VPixx Technologies Inc., Saint-Bruno, QC, Canada) running at 120 Hz, with a polarizer and binocular separation was achieved by using passive stereo-glasses that were MR-compatible. Images were rear-projected onto a custom polarisation-preserving 'pale' screen placed 57 cm from the participant's eye in the bore of the magnet. Participants viewed the screen via a front-silvered mirror. Maximum luminance on the projected image (white) was 400 cd/m^2, and we confirmed using a photometer that the DLP system was entirely linear and so did not require gamma correction.

All fMRI analysis was performed in the VISTA software package (http://white.stanford.edu/software) (Vista Lab, Stanford University) for MATLAB. Anatomical scans were used to reconstruct a structural model of each participant's brain using a combination of FSL (http://fsl.fmrib.ox.ac.uk/fsl/fslwiki/) (Smith et al., 2004), Freesurfer (http://surfer.nmr.mgh.harvard.edu/) (Dale, Fischl, & Sereno, 1999; Fischl, 2012) and the VISTA software. Anatomical and functional data were co-registered and automatically aligned and the first 12 seconds of each functional scan were discarded due to start up transients. Head movement and motion artefacts within and between scans were measured and a correction algorithm applied (Nestares & Heeger, 2000). After the functional scans were aligned to the high-resolution structural scans, analyses were confined to a segmented cortical gray matter flat patch at the occipital pole (Wandell, Chial, & Backus, 2000). This enabled Regions of Interest (ROI's) to be identified on the cortical surface.

2.3.3 EEG

For the EEG data collected at the University of York (Chapter 5), stimuli were presented on a gamma corrected ViewPixx 3D display (VPixx Technologies Inc., Saint-Bruno, QC, Canada) driven by a Mac Pro (Apple Inc., Cupertino, CA, USA). Binocular separation with minimal crosstalk was achieved by synchronising the refresh rate of the display with the toggling of a

pair of Nvidia stereo shutter goggles using an infra-red signal. The monitor refresh rate was set to 120Hz (to enable each eye to be updated at 60Hz). Screen resolution was set to 1920 ×1080 pixels. At a viewing distance of 57cm a single pixel subtended 1.62 arc mins. Steady-state EEG signals were recorded from 64 electrodes across the scalp using the 5% electrode system (Chatrian, Lettich, & Nelson, 1985) in a WaveGuard cap (ANT Neuro, Netherlands). Low impedances (typically <10kΩ) were obtained by inserting conductive gel between the scalp and the electrode using a blunt tipped syringe. Eye blinks were monitored using an electroculogram – one electrode was placed above the participants left eyebrow and another was placed directly below the left eye on their cheek. Signals were amplified and digitised, before being recorded by a PC running the ASAlab software (ANT Neuro, Netherlands).

2.3.4 Dry-electrode EEG

EEG data collected in Chapter 6 at the University of York and at Hull Royal Infirmary, used a GTEC g.SAHARA active dry EEG electrode system with g.GAMMA caps and an eight channel g.USBamp (g.tec medical engineering GmbH, Schiedlberg, Austria). The dry-electrodes consisted of eight pins that had sufficient length to reach through the hair to the skin, to obtain low impedance without the need for conductive gel. Six electrodes were placed over occipital cortex (O1, O2, OZ, POZ PO1, PO2) with additional electrodes at FZ and CZ. These electrodes are connected to the cap via a clip and reference and ground electrodes were also attached. Stimuli were presented via an Oculus Rift DK2 virtual reality headset, which enabled binocular separation (Facebook Technologies, LLC., Menlo Park , CA, USA). The experiment was driven by a Dell laptop (Dell Inc., Round Rock, TX, USA). These materials were chosen as they were convenient for transportation and were quick to setup, which was especially useful when collecting data from children in a clinical setting.

2.4. Procedure

All data (with the exception of the children in Chapter 6, who were recruited and tested at Hull Royal Infirmary) were collected at the University of York in either the Department of Psychology or York Neuroimaging Centre. Participants were first asked to read an information sheet (that had previously been supplied to them electronically), MRI and EEG safety documentation, and give their consent to the study. They were asked to supply a brief history of any visual conditions they have or have been treated for (Table 2.2), and take part in a visual and stereo acuity test.

The EEG experiments took place in a darkened room, with the participants were positioned at the appropriate viewing distance. In all experiments, participants were given an opportunity to see the stimulus before the data collection begun. Participants were instructed to wear their prescribed optical correction if they required it for near work, and stereo shutter glasses were placed in front of any prescribed lenses. The experiments were split into blocks in order to give the participants the chance to have a break. Participants were instructed to stare at the fixation point and perform an attention task of pressing a key when the pixels of the fixation point changed in contrast. The pixels changed randomly throughout the duration of the experiment. After the EEG experiment, participants were given the opportunity to wash the conductive gel from their hair. Participants were paid £10 for each fMRI experiment (Chapter 3 and 4) and £20 for the EEG experiment (Chapter 5). For the treatment studies in Chapter 6, participants at the University for York were paid £100 and at Hull Royal Infirmary they were given £10 per session. All statistical analysis and modelling of the data were conducted using a combination of Microsoft Excel, SPSS and MATLAB.

CHAPTER 3

Binocular population receptive field mapping in human amblyopia

3.1. Introduction

3.1.1 Background

The nature of the cortical deficit in cases of amblyopia is still a matter of debate within the literature. Many electrophysiology studies using animal models of amblyopia have enabled a detailed insight into some of the neural problems that can arise in the brain. Such findings have suggested there to be a loss of binocularity in early visual areas, reduced spatial resolution of foveal neurons, and unbalanced excitatory and inhibitory binocular inputs (Hess & Howell, 1977; Hubel & Wiesel, 1965; Kiorpes, Kiper, O'Keefe, 1998; Levi & Harwerth, 1977; Sengpiel & Blakemore, 1996; Smith et al., 1997).

Investigating both the location and the nature of the cortical deficit of amblyopia in humans has relied on brain imaging methods, such as fMRI. A number of studies have found that both primary visual cortex (V1) and extrastriate areas (V2 and V3) are affected in human amblyopia (Barnes et al., 2001; Conner et al., 2007; Goodyear et al., 2000; Mendola et al., 2005). As detailed in Chapter 1 (section 1.3), population receptive field (pRF) mapping has been used to investigate the nature of the projections from the amblyopic eye and fellow eye in early visual areas. Clavangnier et al (2015) found that neural responses following stimulation of the amblyopic eye had much larger pRF sizes across V1, V2 and V3, compared to that of the fellow eye. These findings point towards reduced spatial resolution and increased positional disarray within the representation of the amblyopic eye. However, one shortcoming of this study is that the eye not being tested was covered with an eye patch. This presents a problem as it creates an unnatural viewing situation where one eye is kept in darkness (section 1.5).

The current study builds on the findings from Clavangnier et al (2015), by measuring pRF responses from each eye in a group of amblyopic participants and improves on the binocular separation method by using a stereoscopic projector within the scanner. This enables binocular information to be carefully presented to one eye at a time without the need to patch the other eye. A brief overview of the method for retinotopic and pRF mapping is discussed before the hypotheses for this study are outlined.

3.1.2 Retinotopic and population receptive field mapping methods

Retinotopic mapping enables visual areas to be located on the surface of the brain using a stimulus that systematically moves across the visual field. Traditionally, a rotating black and white checkerboard wedge is used to measure the polar angle of the visual field, and a ring that expands from central vision out to peripheral vision measures eccentricity (Engel, Glover, & Wandell, 1997). This produces a travelling wave of activity throughout the visual cortex representing the response from neurons (in a voxel) to the stimuli presented at the corresponding time period. This enables the boundaries between visual areas to be identified using the phase reversals from the polar angle maps.

Dumoulin and Wandell (2008) improved on this phase-encoded retinotopic mapping technique by developing a forward modeling technique, known as pRF mapping, which is able to estimate the retinotopic position and the receptive field size of neurons within each voxel in the visual cortex. The pRF stimulus typically consists of a full-field checkerboard exposed through a drifting bar aperture (Zuiderbaan, Harvey, & Dumoulin, 2012). The stimulus sweeps across the visual field with eight trajectories (four orientations and two directions) and includes 'blank' periods of mean luminance throughout that act as a baseline condition (Harvey & Dumoulin, 2011). A Gaussian model is used to estimate the receptive field sizes of populations of neurons based on the responses acquired from each voxel at the different stimulus locations. The model is fit in three stages in order to allow the best estimate of the pRF size for each voxel to be calculated. The first stage estimates the best fit for every

voxel from sets of fixed pRF parameters. Secondly, the fit is optimized for all voxels that have at least 15% of their variance explained by the model. Finally, the model applies the optimized fits from the second stage to the original voxels. Maps that represent the pRF sizes and the retinotopic boundaries between visual areas can be visualized on the cortical surface (as in standard retinotopic mapping methods).

As well as the location at which the bar is positioned in the visual field, the neural responses are also determined by the carrier within the bar aperture. Therefore, the pRF responses derived from using 100% contrast black and white checkerboard carrier stimuli are derived from specific neurons responding to high-contrast achromatic stimuli. In order to elicit responses from a wider range of neurons, studies have adapted the traditional checkerboard carrier to include dynamic white or pink (1/*f*) noise instead of a high-contrast checkerboard pattern (Himmelberg & Wade, 2019; Welbourne, Morland, & Wade, 2018). This is important as Clavangnier et al (2015) measured responses from each eye separately in amblyopic observers using the traditional checkerboard stimulus. This current study aims to improve on this method by using pink (1/*f*) noise to compare neural responses from each eye in amblyopic observers. This is a more naturalistic stimulus and should encourage more accurate pRF responses to be measured from neurons sensitive to a range of spatial frequencies.

3.1.3 Aims and hypotheses

The experiment in this chapter was designed to use pRF modeling in order to further understand the cortical problems underlying the visual deficit caused in amblyopia. The main aim was to compare the pRF sizes measured when stimulating each eye separately in a group of amblyopic observers and healthy controls, from visual areas V1, V2 and V3. It improves on the Clavangnier et al (2015) study by incorporating a more controlled method for achieving binocular separation and a dynamic pink (1/*f*) noise carrier within the bar stimulus to elicit responses from a broader range of neurons.

Based on the literature discussed above, pRF sizes measured for V1, V2 and V3 were expected to increase as a function of eccentricity and visual area hierarchy, for both the amblyopic and control groups (Alvarez et al., 2015; Binda, Thomas, Boynton, & Fine, 2013; Dumoulin & Wandell, 2008). It was predicted that pRF sizes would be larger for the amblyopic eye compared to the fellow eye but that there would be no difference between the left and right eye for control participants (Clavagnier et al., 2015). Furthermore, as receptive field sizes increase from V1 – V3 and due to the low spatial resolution of the amblyopic eye, it was hypothesized that the amblyopic eye response would reveal much larger pRF sizes with progression through the visual processing hierarchy, compared to the fellow eye and controls.

3.2. Methods

3.2.1. Participants

Participants were recruited via posters located around the University of York campus and on the Department of Psychology website. Twelve amblyopes (7 females, mean age = 22.58, standard deviation of age = 4.27) and ten controls (7 females, mean age = 26.70, standard deviation of age = 3.97) took part in this study. Demographic and clinical details for the amblyopes can be found in Chapter 2 (section 2.2). All control participants had normal or corrected to normal visual acuity. All participants gave informed consent and were screened for MRI safety.

3.2.2. Materials

Stimuli used to measure pRF sizes consisted of single drifting bars (Fig. 3.1A), similar in general form to those described in other experiments (Alvarez et al., 2015; Dumoulin & Wandell, 2008; Welbourne et al., 2018). Bar apertures displayed a dynamic pink-noise ($1/f$) carrier (RMS contrast = 0.2). The bar (width 0.5°) was presented in a circular aperture (10° radius) and moved in one of eight directions perpendicular to the bar orientation (four possible orientations: horizontal, vertical and across two diagonals) with each ‘sweep’ across the aperture lasting 24s (Fig. 3.1D). Four periods of mean luminance were included to

provide a baseline condition within each scan; these periods always occurred in the second half of a diagonal sweep and lasted 12s.

Standard phase-encoded retinotopic mapping stimuli were also presented in order to provide another estimate of the location of boundaries between visual areas (V1-V3), for each individual participant. This was undertaken as a backup measure to ensure that clear boundaries between ROIs were obtained in all participants. These phase-encoded stimuli consisted of an expanding ring stimulus (Fig. 3.1B) to measure eccentricity and a rotating wedge (Fig. 3.1C) to measure the polar angle. Stimuli were portions of a 100% contrast radial checkerboard pattern that reversed in contrast at a rate of 4 Hz. Wedges were 45° in size and rotated clockwise around a fixation point and ring stimuli expanded about fixation. Both types of stimuli were displayed on the same background as the drifting bar stimulus.

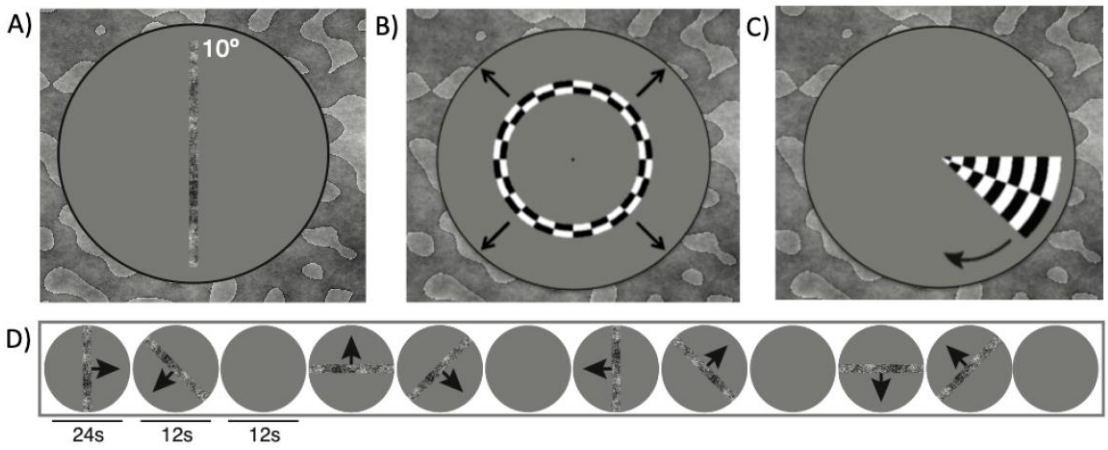

Figure 3.1. Example of the bar used as the pRF stimulus presented monocularly (A). Expanding rings (B) and rotating wedges (C) were presented binocularly and used to retinotopically map V1-V3 in each participant (arrows indicate direction of movement). (D) shows the direction of the bar movement throughout a single pRF scan. The 'blank' grey patches with no bars represent mean luminance periods (12s). Arrows indicate the direction of movement.

3.2.3. Procedure

The bar stimulus was presented to each eye separately to measure monocular pRF sizes. Stimulus runs were repeated twice for each eye and later combined to give an averaged pRF estimate for the left eye and right eye. As outlined in Chapter 2, participants were given stereo-glasses to wear in the MRI scanner and binocular separation of the stimuli was achieved using a ProPixx stereo projector with a polarizer. This enabled carefully controlled presentation of the stimuli to one eye at a time. Phase-encoded retinotopic mapping stimuli were presented binocularly and consisted of four cycles (alternating between two wedges and two rings) with each cycle lasting 24s. Participants performed the fixation task throughout all scans (Chapter 2, section 2.4).

3.2.4. Data Processing

As outlined in Chapter 2, all functional data were acquired using GE 3 T HDx Excite MRI scanner at York Neuroimaging Centre using a 16-channel posterior surface coil covering the occipital pole. Functional data were aligned to previously obtained high-resolution structural scans and processed using the VISTA software running under MATLAB.

Retinotopic and pRF data were analysed using the mrVista pRF modelling algorithm. Sizes and positions were estimated for each voxel from the amblyopic and fellow eye (left/right eye in controls), using the standard pRF modelling algorithm described by Dumoulin and Wandell (2008). Modelling was performed on time series data averaged across repetition for each eye using a 'difference of gammas' hemodynamic response function (HRF) from the SPM analysis package (Friston et al., 2006). This enabled visual areas to be defined using the polar angle and eccentricity maps produced by the pRF model. Flat maps of the brain were used to visualise the maps and define boundaries between visual areas V1, V2 and V3 using the phase reversals on the polar angle map in both the left and right hemispheres. The phase-encoded retinoptic mapping scans (Fig. 3B and 3C) were analysed using standard Fourier methods (DeYoe et al., 1996; Engel et al., 1997). These were compared to the retinotopic

maps generated by the pRF stimuli and ROIs were tweaked in order to provide the most accurate location for each visual area. Once each visual area was defined in both the left and right hemisphere, they were combined to create bilateral ROIs for V1, V2 and V3 (e.g. V1 left and V1 right were combined).

3.3. Results

3.3.1 Retinotopic maps and ROIs

Boundaries of early visual areas V1, V2 and V3 were identified in both hemispheres using the retinotopic output of the phase encoded ring/wedge data and the output of the pRF modelling, which were consistent with previous studies (Dumoulin & Wandell, 2008; Engel et al., 1997). ROIs of each visual area were drawn by hand on a flattened representation of the cortical surface and the calcarine sulcus was used to orientate to the location of V1. Examples of the boundaries between visual areas are shown on a flattened cortical surface for one control (Figure. 3.2) and one amblyopic participant (Figure. 3.3) in the left and right hemispheres. The size of each visual area was calculated using the Flat View in mrVista and are displayed in Table 3.1, showing that on average the surface area of each ROI gets smaller with progression through the visual processing hierarchy.

	Visual Area	Mean ROI size (mm^2)	SD across observers (mm^2)
Controls	V1	1527.10	385.10
	V2	1566.90	328.79
	V3	1344.10	299.66
Amblyopes	V1	1741.33	474.67
	V2	1647.42	397.21
	V3	1324.12	250.43
All Participants	V1	1643.95	439.88
	V2	1610.82	361.47
	V3	1333.36	267.27

Table 3.1. The mean surface area (mm^2) and standard deviation (SD) for visual areas V1, V2 and V3 (once combined across both hemispheres) for the control and the amblyopic group.

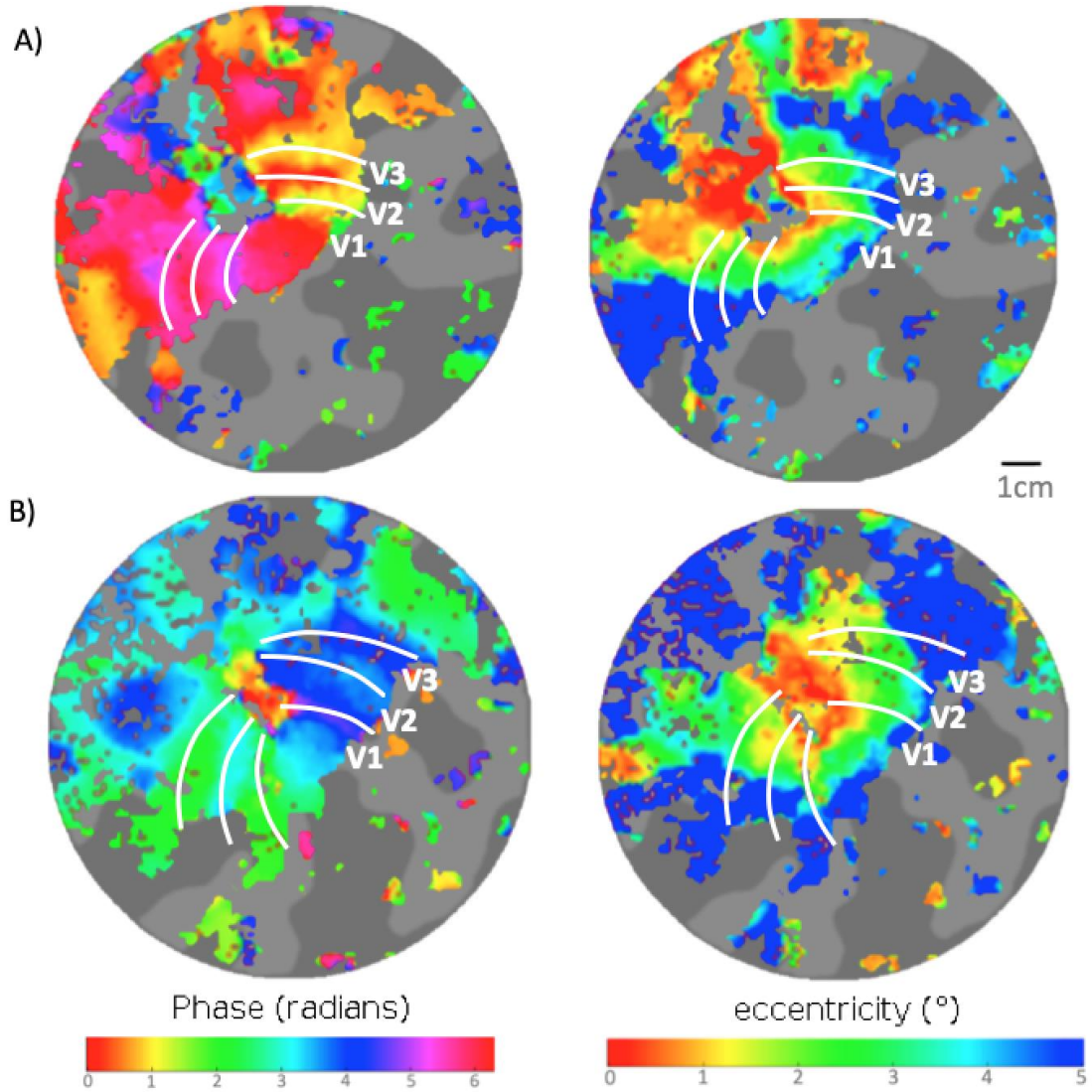

Figure 3.2 Retinotopic maps for one control participant (FL). Polar angle (left) and eccentricity (right) phase maps are shown, which were used to identify visual area ROIs in the left (A) and right (B) hemispheres. Boundaries of the visual areas are overlaid on the maps.

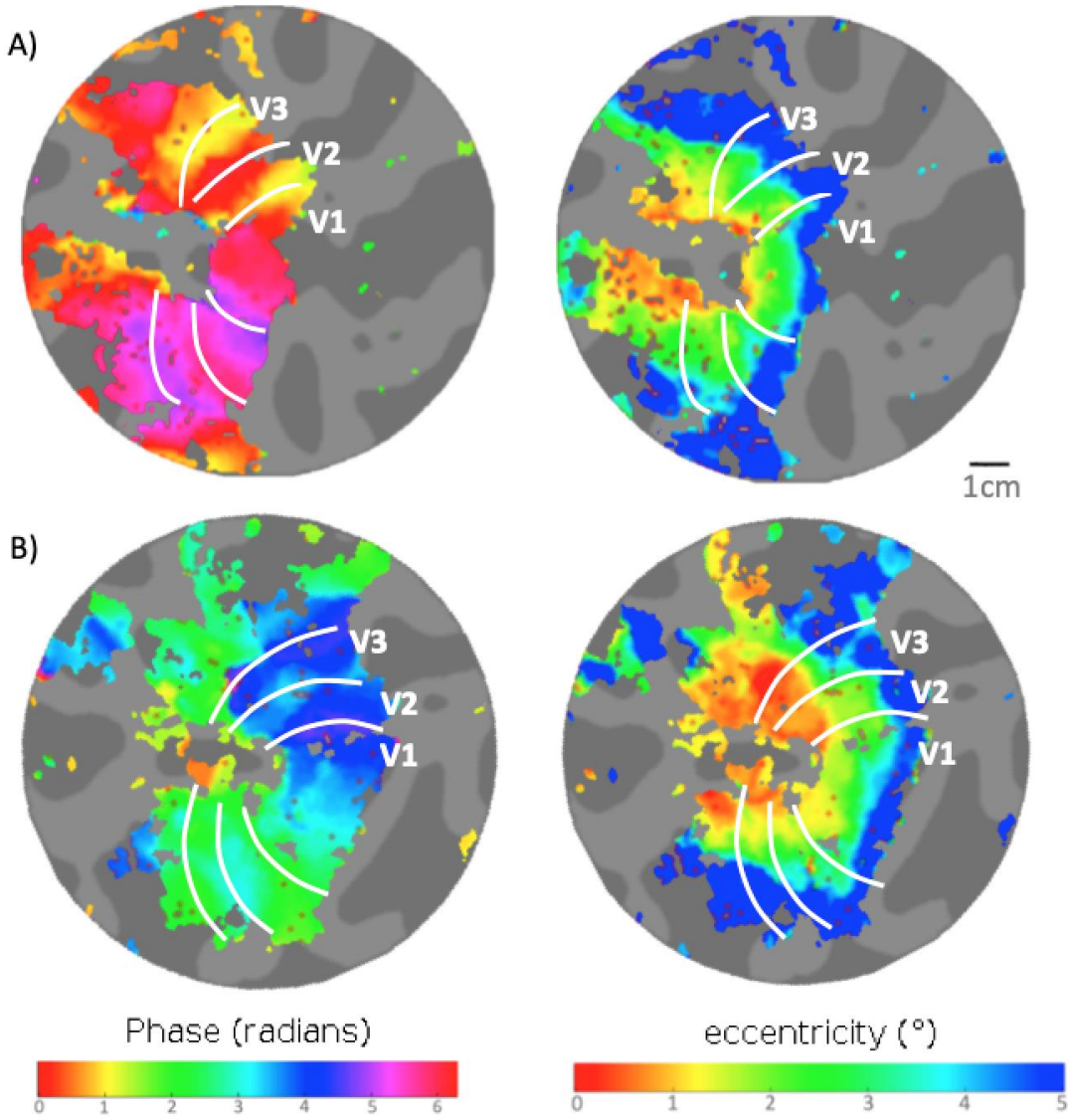

Figure 3.3. Retinotopic maps for an amblyopic participant (SA). Polar angle (left) and eccentricity (right) phase maps are shown, which were used to identify visual area ROIs in the left (A) and right (B) hemispheres. Boundaries of the visual areas are overlaid on the maps.

3.3.2 pRF size verses eccentricity

One control participant was removed from the analysis as the pRF model failed to converge, leaving nine control participants and twelve amblyopic participants included in all further analyses. The average pRF sizes for each eye in both the control group (left/right eyes) and amblyopic group (amblyopic/fellow eyes) were plotted as a function of eccentricity and displayed separately for visual areas V1, V2 and V3 (Fig. 3.4). The pattern of responses for

each condition appear consistent with previous studies, showing that pRF sizes increase as a function of eccentricity from the fovea to periphery, and throughout the visual processing hierarchy from V1-V3 (Clavagnier et al., 2015; Dumoulin & Wandell, 2008).

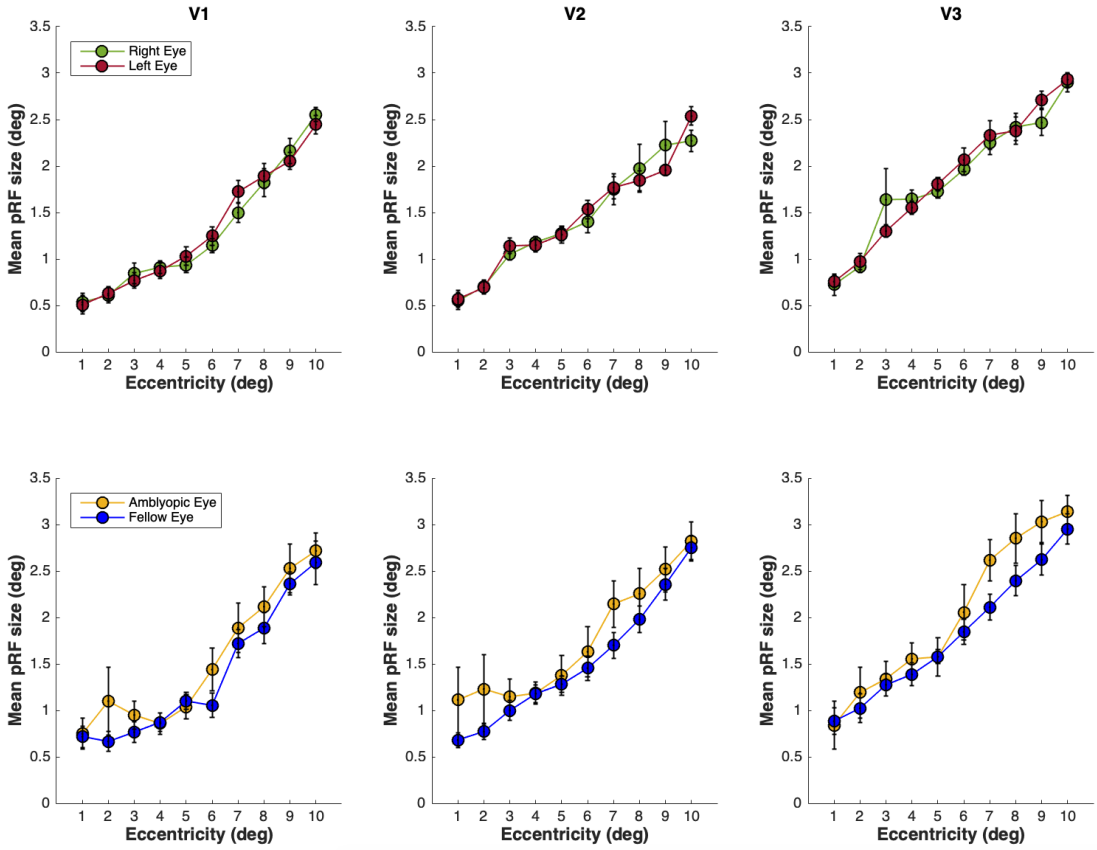

Figure 3.4 Average pRF sizes plotted against eccentricity for visual areas V1, V2 and V3 (left to right). The top panel shows the results from the left (red) and right (green) eyes in the control group (N=9). The bottom panel shows the results from the amblyopic (yellow) and fellow (blue) eyes for the amblyopic group (N=12). Error bars represent the standard error of the mean.

For three control participants and four amblyopic participants, the pRF model was unable to fit for some eccentricities resulting in some missing cases (see Table 3.2). Due to this, it was not possible to run repeated measures comparisons within one analysis. Therefore, statistical comparisons were conducted in two parts: firstly in order to account for the missing cases, a series of Generalized Linear Mixed Models (GLMMs) were used to compare the effects within each visual area (fovea – periphery) (Breslow & Clayton, 1993; Schafer & Yucel,

2002); and secondly a mixed ANOVA was used to compare the effects between the visual areas (V1 – V3).

Table 3.2. The percentage of cases that were included and excluded in the GLMMs analysis due to the pRF model being unable to fit for certain eccentricities for three control participants and four amblyopic participants.

	Visual Area	Cases Included (%)	Cases Excluded (%)
Controls	**V1**	95.6	4.4
	V2	99.4	0.6
	V3	97.8	2.2
Amblyopes	**V1**	92.9	7.1
	V2	97.5	2.5
	V3	96.7	3.3

3.3.2.1 Comparisons within visual areas

A series of Generalized Linear Mixed Models (GLMMs) were conducted to assess the effects within each visual area by comparing the effect of eye (left/right, amblyopic/fellow) and eccentricity (1-10 degrees) on the pRF size (degrees). A separate GLMM was conducted for each visual area (V1, V2 and V3) and participant group (amblyopes and controls) to avoid over fitting the models. Eye and Eccentricity were entered as fixed factors in the models and pRF size was the dependent measure. All GLMMs were run in IBM SPSS (version 24) using a normal probability distribution and identity link function. The participant variable was entered as a random factor in order to control for repeated sampling of each participant.

Results of the GLMMs are shown in Table 3.3. For the control participants, the GLMMs revealed a significant main effect of eccentricity but not for eye or for the interaction between eye and eccentricity, in each visual area. In line with previous studies, this finding indicates that pRF size increased as a function of eccentricity (Dumoulin & Wandell, 2008) but there

was no difference between the left eye and right eye in V1, V2 or V3. For the amblyopic group, the GLMMs revealed a significant main effect of both eye and eccentricity but no significant interaction between eye and eccentricity, in each visual area. As with the control group, this finding indicates that pRF sizes increased as a function of eccentricity, however, larger pRF sizes were found for the amblyopic eye compared to the fellow eye. As no interaction was found, this suggests that eccentricity did not significantly influence the pRF size when testing the amblyopic or fellow eye.

Table 3.3 Results of GLMMs exploring the effect of eye (left/right, amblyopic/fellow), eccentricity (1-10), as well as the interactions between eye and eccentricity on the average pRF size. A separate GLMM was conducted for each visual area (V1-V3) in both participant groups. Significant results are indicted, where ** denotes $p < .005$ and *** denotes $p < .001$.

		Controls			**Amblyopes**		
	df	**V1** **F(*p*)**	**V2** **F(*p*)**	**V3** **F(*p*)**	**V1** **F(*p*)**	**V2** **F(*p*)**	**V3** **F(*p*)**
Eye	1, 19	0.21 (.646)	0.05 (.819)	1.42 (.236)	11.33 (.001)***	10.31 (.002)**	8.13 (.005)**
Eccentricity	9, 19	119.05 (<.001)***	67.35 (<.001)***	152.11 (<.001)***	47.94 (<.001)***	34.18 (<.001)***	47.78 (<.001)***
Eye * Eccentricity	9, 19	0.87 (.551)	0.71 (.703)	0.44 (.912)	0.58 (.817)	0.56 (.830)	0.62 (.783)

3.3.2.2 Comparisons between visual areas

In order to see whether there were any differences between V1, V2 and V3, the pRF response was averaged across all eccentricities for each participant's left/amblyopic eye and right/fellow eye and analysed using a mixed ANOVA. Mauchley's test of sphericity indicated that the data did not violate the assumption of sphericity for visual area ($p = .102$) or for the interaction between eye and contrast ($p = .510$).

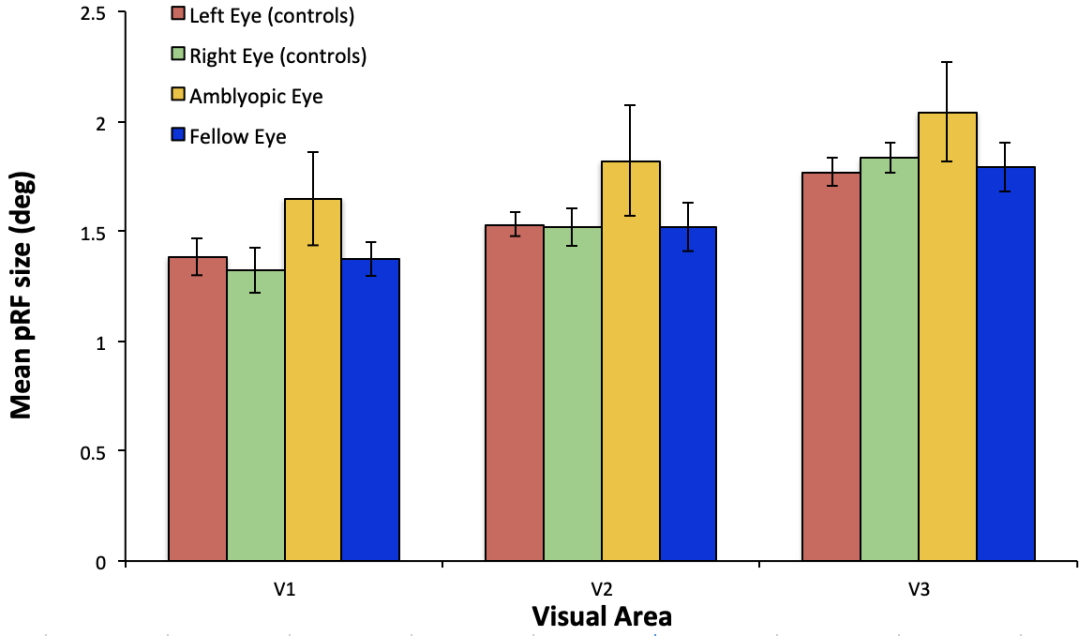

Figure 3.5. pRF sizes averaged across all eccentricities for each eye condition (left/right eye for controls and amblyopic/fellow eye for amblyopes) and grouped by visual area (V1-V3). A mixed ANOVA revealed a main effect of visual area on pRF size but no effect of eye or for the interaction between eye and visual area, for pRF size in both participant groups. Error bars represent the standard error of the mean.

The results of a mixed ANOVA revealed no significant main effect of eye (F (1, 19) = 0.75, p = .398, partial η^2 = 0.04) on pRF size. There was also no significant interaction effect between amblyopic and control participant groups on the eye that was tested (F (1, 19) = 0.32, p = .577, partial η^2 = 0.02). A significant main effect was found for visual area (F (2, 38) = 80.18, p < .001, partial η^2 = 0.81) on pRF size. Planned contrasts (repeated) revealed significant differences between V1 and V2 (p < .001) and V2 and V3 (p < .001). Again, no significant interaction was found between amblyopic and control participant groups on the visual area (F (2, 38) = 0.54, p = .590, partial η^2 = 0.03). There was no significant interaction found between the eye and visual area (F (2, 38) = 0.01, p = .987, partial η^2 = 0.01). Finally, no significant interaction effect between amblyopic and control groups on the eye that was tested and the visual area (F (2, 38) = 0.32, p = .727, partial η^2 = 0.02).

3.4. Discussion

In this fMRI study, pRF modelling was carried out on a group of amblyopic and control observers in order to further understand the nature of the neural deficit caused in amblyopia. For both groups each eye was tested separately and the responses from within and between visual areas V1, V2 and V3 were compared. Retinotopic maps were acquired to enable ROIs for each visual area to be carefully obtained from the phase and eccentricity maps from each individual.

As predicted, for both groups the pattern of responses showed that pRF size increased as a function of eccentricity from the fovea to the periphery, for all visual areas. Furthermore, it was found that in amblyopic observers pRF sizes were significantly larger when viewing the stimulus with their amblyopic eye compared to viewing it with their fellow eye, whereas in healthy controls there were no differences between their left and right eyes. However, no significant interaction was found between eye and eccentricity, suggesting that differences between the amblyopic eye and fellow eye were not larger in the fovea within each visual area.

When comparing between visual areas, the averaged pRF sizes (averaged across all eccentricities) increased between V1 – V3 for all eye conditions, supporting the hypothesis that pRF sizes would increase with progression throughout the visual processing hierarchy. Despite the trend of the responses shown in Figure 3.5, no significant effects were found of eye or participant groups suggesting that pRF sizes increase between V1, V2 and V3, regardless of which eye is being tested for both participant groups. This result is somewhat surprising as it was hypothesised that larger pRF sizes would be measured from the amblyopic eye between visual areas due to the reduced spatial resolution of the amblyopic eye. One explanation for this result could be that responses were measured from a wider range of neurons in each visual area due to the pink noise carrier used in the pRF bar stimulus, and the narrower bar width compared with previous studies (1.5° in Clavagnier et

al., 2015, 0.5° here). This stimulus may have been able to evoke responses from neurons with smaller receptive fields, perhaps resulting in smaller differences between the amblyopic and fellow eye. Additionally the sample of amblyopic participants may have influenced the findings. For example, the group of observers in the current study were not as severely amblyopic as those recruited by Clavagnier et al, (2015). This could have been reflected in smaller pRF sizes therefore contributing to the lack of significant findings of eye and participant groups between visual areas in this study.

Another potential issue that could have affected these findings is the impact of uncorrected optical blur on the neural responses. This has been demonstrated in both electrophysiology and fMRI studies, which have shown that uncorrected blur can disturb responses recorded from the occipital cortex (Berman & Seki, 1982; Mirzajani, Sarlaki, Kharazi, & Tavan, 2011; Sokol & Moskowitz, 1981). For example, an fMRI study investigating the impact of inducing different levels of myopia (short sightedness) found significant decreases in the level and extent of BOLD responses recorded from the visual cortex (Mirzajani et al., 2011). This suggests that optical blur created by refractive errors can potentially have considerable effects on measurements of cortical activity. In terms of pRF responses, it is possible that uncorrected optical blur could have impacted neurons with small receptive field sizes, whereas neurons with bigger receptive field sizes would be largely unaffected. However, this is unlikely to have impacted the findings of the current study, as we would have found an increase in pRF responses at the fovea. Nevertheless, the impact of refractive error and optical blur on pRF responses has not to this date been formally investigated, and therefore future studies should carefully consider the impact that optical blur could potentially have on pRF sizes.

The findings from the current study are consistent with the explanation put forward by Clavagnier et al. (2015), suggesting that the enlarged pRF sizes from the amblyopic eye demonstrate a loss of spatial resolution of the cells in V1, V2 and V3. This provides support

for previous psychophysical studies demonstrating reduced spatial resolution from the amblyopic eye (Hess & Howell, 1977; Levi & Harwerth, 1977). These findings are also consistent with electrophysiology studies conducted on animal models of amblyopia, showing reduced spatial resolution in V1 neurons (Movshon et al., 1987; Wiesel & Hubel, 1963). Furthermore, the amblyopic deficit seen in V2 and V3 provides further evidence that extrastriate processing is also affected in amblyopia (Barnes et al., 2001; Li et al., 2007).

3.5. Conclusion

This study used pRF modelling to compare the projections from the amblyopic and fellow eyes in amblyopic observers and left and right eyes in healthy control observers. A similar method was used to Clavagnier et al. (2015), with improvements made to the stimulus and binocular separation method, to enable a more natural viewing situation. The findings agree well with previous studies, showing that pRF size scaled with eccentricity and ascending visual area (V1 – V3) (Alvarez et al., 2015; Binda et al., 2013; Dumoulin & Wandell, 2008). It also supports previous findings by Clavagnier et al. (2015), revealing larger pRF sizes measured from the amblyopic eye across V1, V2 and V3. This study lends support for the idea that the amblyopic deficit lies within V1 and extends into V2 and V3. However, the extent of the amblyopic deficit within these visual areas was smaller than previous studies have reported. Overall, these results are consistent with the explanation that neurons responding to the amblyopic eye have reduced spatial resolution.

CHAPTER 4

Interocular fMRI responses in human amblyopia

4.1. Introduction

The computational process of how visual information from each eye is combined in the brain has been the source of much research over the years. In a healthy visual system, presenting stimuli to both eyes has very little improvement on our two-dimensional spatial perceptual experience, compared to viewing a stimulus through one eye only. Psychophysical studies have shown that improvements in contrast sensitivity following binocular presentation only appear at very low contrasts or for very brief presentation periods, however these effects are negligible at higher contrasts (Baker et al., 2007; Legge, 1984). Equally, binocular presentation has little impact on the response magnitude of neurons in the visual cortex. Stimulating two eyes instead of one eye should double the input from pre-cortical stages (retina and LGN) to V1. This would increase the overall neuronal activity in V1 by activating twice the number of monocular cells and the binocular cells receiving double the excitatory input from the LGN (Heeger, 1992a, 1992b). However, suppressive mechanisms in V1 control for this increased excitatory response through a process of 'normalisation', where the activity of a given neuron is normalized with respect to the activity of other surrounding neurons, so activity from each eye reduces the gain for the other eye (Albrecht & Geisler, 1991; Moradi & Heeger, 2009).

The process of cortical normalisation was examined in a study by Moradi and Heeger (2009) using an fMRI paradigm to measure how binocular information is combined in early visual cortex. They measured the BOLD response to stimuli (ringed spiral gratings at one orientation or as a plaid) presented to one eye or both eyes (monocularly or dichoptically) at a range of different contrasts. Results were similar to that of psychophysical studies, revealing greater contrast sensitivity in V1 when stimulating both eyes compared to one eye for low contrast

stimuli, but these differences were negligible at higher contrasts. Taken together, these results show that suppression between two eyes was comparable to the suppression measured from one eye. Based on these findings, Moradi and Heeger (2009) put forward a contrast normalization model, which assumes inputs from each eye contribute equally to the normalization for both eyes and accounts for any excessive excitation in response to doubling the input. This normalization model is consistent with models derived in previous psychophysical research and is computationally very similar to the two-stage model of binocular gain control, as described in Chapter 1 (section 1.2, Fig. 1.1B) (Meese et al., 2006). Therefore, these findings are consistent with the idea that suppressive mechanisms prevent excessive excitation in early visual cortex and that normalisation plays an important role in how binocular information is combined in a healthy visual system.

This type of normalisation model is also useful in understanding the computational process of how binocular information is combined in amblyopia. A major contributing factor to the loss of binocularity in amblyopia is greater suppression of one eye's input into the visual cortex, however, direct evidence of this has proven difficult to research (Sengpiel & Blakemore, 1996). However, more recent psychophysical studies have found that responses from the amblyopic eye were best predicted by a model simulating an attenuated response gain shift, where the response is reduced compared to the fellow eye (Baker et al., 2008). Support for this model can also be seen in fMRI studies, which reveal an attenuated response in the visual cortex (Conner et al., 2007; Farivar et al., 2017) and the lateral geniculate nucleus (LGN) (Hess, Li, Mansouri, Thompson, & Hansen, 2009). However, a limitation of these studies is that the method used to achieve monocular stimulus presentation involves occluding one eye. This presents a problem as it creates an unnatural viewing situation where one eye is kept in darkness, which also minimises suppression (Farivar et al., 2017). Therefore, it is unclear whether these findings are truly reflective of how visual information is combined in individuals with amblyopia.

The aim of this study was to carefully examine how binocular information is combined in V1 in amblyopes and healthy controls. A similar paradigm to Moradi and Heeger (2009) was used to measure monocular, binocular and dichoptic contrast responses using fMRI. It also aimed to improve on previous studies by using a polariser and passive stereo-glasses within the scanner to carefully control the presentation of stimuli to each eye. This method required no input from participants whilst in the scanner and enabled both eyes to be open throughout all conditions. It was predicted that the control participants would show a pattern of contrast responses consistent with the two-stage model, whereby amplitude increases monotonically with stimulus contrast. The amblyopic group were predicted to show a similar pattern of contrast responses to the control group but a significantly reduced response from the amblyopic eye compared to the fellow eye and binocular conditions. Results from the amblyopic group were compared to three variations of the two-stage model that had been disturbed in different ways to simulate the binocular abnormalities in amblyopia.

4.2. Methods

4.2.1 Participants

The same participants as described in Chapter 3 (Section 3.2.1) completed this experiment (12 amblyopes and 10 controls). All demographic and clinical details for the amblyopes can be found in Chapter 2 (section 2.2).

4.2.2 Materials

As described in Chapter 2 (section 2.3.1 and Fig. 2.1), stimuli consisted of four sinusoidal gratings with a spatial frequency of 3 cycles/° at five different contrast values (0, 1.5, 6, 24 and 96% Michelson Contrast), as indicated in Figure 4.1. Stimuli flickered (on-off contrast modulation) at a rate of 4Hz and were presented monocularly, binocularly, and dichoptically to participants for trials of 12 seconds.

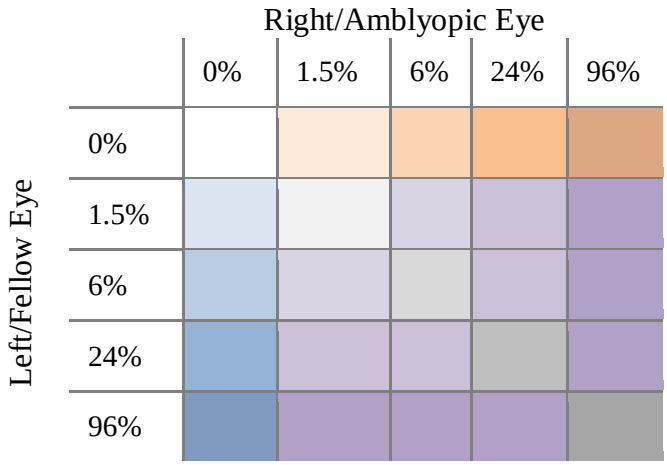

Figure 4.1. All possible stimulus combinations when each contrast is presented to one eye or both eyes together. The white square (0%) indicates the baseline condition (no grating presented to both eyes). Monocular conditions are shown by the blue squares (contrast only presented to the left/fellow eye) and orange squares (contrast only presented to the right/fellow eye). Grey squares indicate binocular conditions and Purple squares indicate dichoptic conditions. For each condition the colour gets darker for increasing contrast level (1.5 - 96% contrast).

4.2.3 Procedure

Responses were measured for all 25 conditions once in each block. Stimuli flickered on the screen for 12 seconds, followed by a 12 second 'blank' where no gratings were presented. As outlined in Chapter 2 (section 2.4), participants were asked to maintain fixation and click a button every time there was a change in the fixation point. Four blocks were conducted lasting around 10 minutes each. All structural and functional MRI acquisition parameters are outlined in Chapter 2 (section 2.3.2).

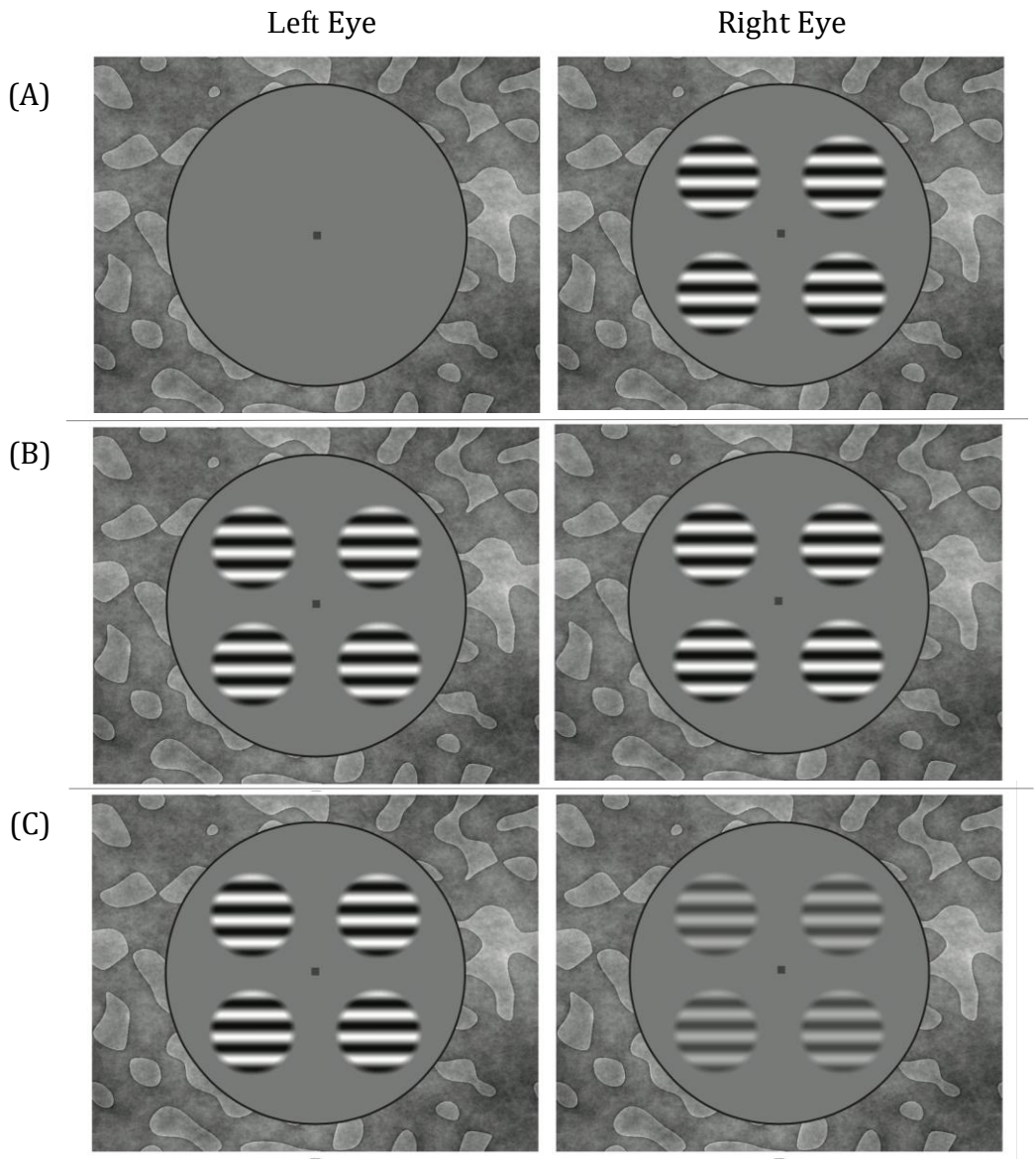

Figure 4.2. An example of the stimulus display achieved by using a stereo-projector and polarizing glasses inside the MRI scanner. (A) demonstrates a monocular condition where the stimulus was presented to one eye (e.g. right eye) and no gratings to the other eye (e.g. left eye). (B) demonstrates a binocular condition where both eyes were presented with gratings of the same contrast. (C) demonstrates a dichoptic condition where each eye is presented with a grating of different contrast (e.g. left eye sees a high contrast and right eye sees a low contrast stimulus).

4.2.4 Data processing

4.2.4.1 Defining regions of interest

All fMRI data were preprocessed using the mrVista software package and FSL, as described in Chapter 2 (section 2.3.2). V1 was identified in all participants from retinotopic maps acquired in the pRF study, as described in Chapter 3 (see section 3.3.1). V1 was identified in both hemispheres based on the reversals of the polar angle maps, which were consistent with previous studies (Dumoulin & Wandell, 2008; Engel et al., 1997). Further regions of interest (ROIs) were identified in sub regions of each visual area based on the activity from a binocularly-presented phase-encoded localiser stimulus, in order to select voxels that responded to both eyes at the stimulus presentation (see Table 4.1). This localiser consisted of a circular black and white radial plaid (4° in diameter), which was presented binocularly (temporal period = 24s, contrast reversal = 4Hz) and moved to each location of the four gratings (Figure 4.3). We measured the phase coherence for each voxel (see Figure 4.3) and retained voxels with a coherence above 0.3.

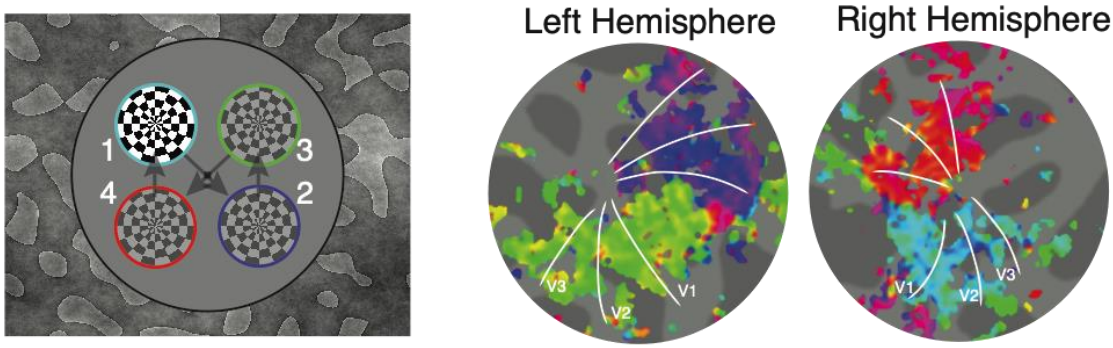

Figure 4.3. An example of the phase-encoded localiser plaid that moved in the location of each grating. The numbers (1-4) next to the plaid represent the order in which it moved and the colour encircling the plaid (which was absent during the experiment) indicates the hemisphere and location of the voxels that responded to the stimulus location, as seen on the flattened cortical surface for one example control participant (right). The left hemisphere represents the right hand side gratings, with green showing ventral regions (V1/V2v/V3v) and purple showing dorsal regions (V1/V2d/V3d). The right hemisphere represents the left hand side gratings, with blue showing ventral regions (V1/V2v/V3v) and red showing dorsal regions (V1/V2d/V3d).

Table 4.1. The mean surface area (mm^2) and standard deviations (SD) of localiser ROIs within V1 (combined left and right hemispheres), for the amblyopes, controls and averaged across all participants.

Participants	Mean ROI size (mm^2)	SD across observers (mm^2)
Controls	612.75	199.54
Amblyopes	583.63	200.80
All Participants	596.86	198.43

4.2.4.2 Response time course

The responses for each stimulus contrast condition in V1 were taken from the BOLD signal (%) change averaged across time points at 6, 9 and 12 seconds. The haemodynamic response function (HRF) used SPM's difference-of-gammas to enable better estimates of activity by accounting for both the positive and negative BOLD signals in the time series. This enabled group averages to be produced for the ROIs derived from the localiser scan, within each visual area. An example of the fMRI timeseries for amblyopes and control participants can be seen in Figure 4.4.

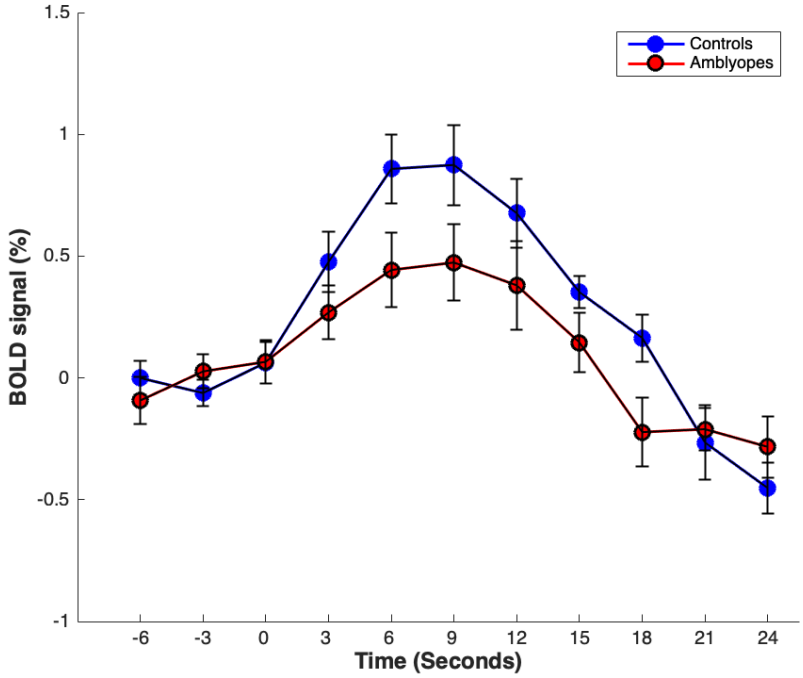

Figure 4.4. An example fMRI timecourse in V1 for 96% contrast presented binocularly, averaged across controls (blue) and amblyopes (red).

4.2.4.3 Models

The responses recorded from each group of participants were compared to different model predictions of binocular combination, in order to assess the subtleties of the deficits seen in amblyopia. The first two models below outline how binocular information is summed together (Equation 4.1) and considers how binocular information is combined in a healthy visual system (Equation 4.2), taken from the two-stage model of binocular gain control (Meese et al., 2006). The subsequent models each explore a different adjustment to the two-stage model, which encompasses a different aspect of how binocular information might be combined in amblyopia. Firstly, the attenuator model (Equation 4.3) has previously been found to successfully predict the pattern of responses from psychophysical studies. It predicts a reduced response from the amblyopic eye simulating a response gain shift (e.g. a reduction in the maximum response (Rmax)). Secondly, a contrast gain shift model is compared (Equation 4.4), which predicts a reduced response that is shifted to the right (e.g. a change in contrast sensitivity (increase in C50)) simulating a change in contrast gain. Finally, a model predicting unbalanced interocular suppression from one eye is compared (Equation 4.5). Many researchers have predicted that unbalanced suppression is a major contributing factor in amblyopia but studies have struggled to reliably measure this effect (Freeman, Nguyen, & Jolly, 1996; Huang, Baker, & Hess, 2012; Zhou et al., 2014). The results from this study are compared to the qualitative pattern of responses predicted by these models, rather than fitted directly to the data, due to the lack of saturation in the responses at the higher contrasts making it difficult to constrain.

Binocular summation

The process of binocular combination first requires the visual inputs from each eye to be squared before being summed together, resulting in the output being the square root of the summed value (Legge, 1984):

$$B = \sqrt{L^2 + R^2} \tag{4.1}$$

where L and R are the input contrasts to the left and right eyes respectively and B is the binocular response.

Two-stage model of binocular gain control

The two-stage model of binocular gain control model was developed to explain the processes of binocular combination in a healthy visual system (Meese et al., 2006) and is described by:

$$\frac{L^m}{S+L+R}+\frac{R^m}{S+R+L} \tag{4.2}$$

where S and m are model parameters, and L and R are the input contrasts to the left and right eyes (Georgeson, Wallis, Meese, & Baker, 2016). The left and right eye channels contain interocular suppression from the opposite eye before being summed together (as outlined in Chapter 1 section 1.1B). The pattern of responses predicted for the conditions in the fMRI experiment can be seen in Figure. 4.5A.

Attenuator model

The attenuator model was developed by Baker et al. (2008) and implements attenuation of signal (and originally an increase in monocular noise, though this is not included here) in one eye, to account for the binocular visual deficit in amblyopia. The model is described by:

$$\frac{aL^m}{S+aL+R}+\frac{R^m}{S+R+aL} \tag{4.3}$$

where the attenuation factor (a) is a free parameter and is implemented in the left eye, and all other parameters retain their meanings from equation 4.2. The behaviour of this model simulates a response gain shift in the amblyopic eye (Fig. 4.5B).

Contrast gain shift model

A model simulating a contrast gain shift was also compared. This model implements a fixed gain difference in the amblyopic eye, which is independent of the input to the fellow eye. This model is described by:

$$\frac{L^m}{aS + L + R} + \frac{R^m}{S + R + L} \tag{4.4}$$

where a larger saturation constant (aS) is implemented in the left (amblyopic) eye only. The pattern of this response can be seen in Figure 4.5C.

Interocular suppression model

Finally, an unbalanced interocular suppression model was explored, where suppression increases in one eye only. This model is described by:

$$\frac{L^m}{S + L + wR} + \frac{R^m}{S + R + L} \tag{4.5}$$

where a suppressive weight (w) is implemented. The behaviour for this model can be seen in Figure 4.5D.

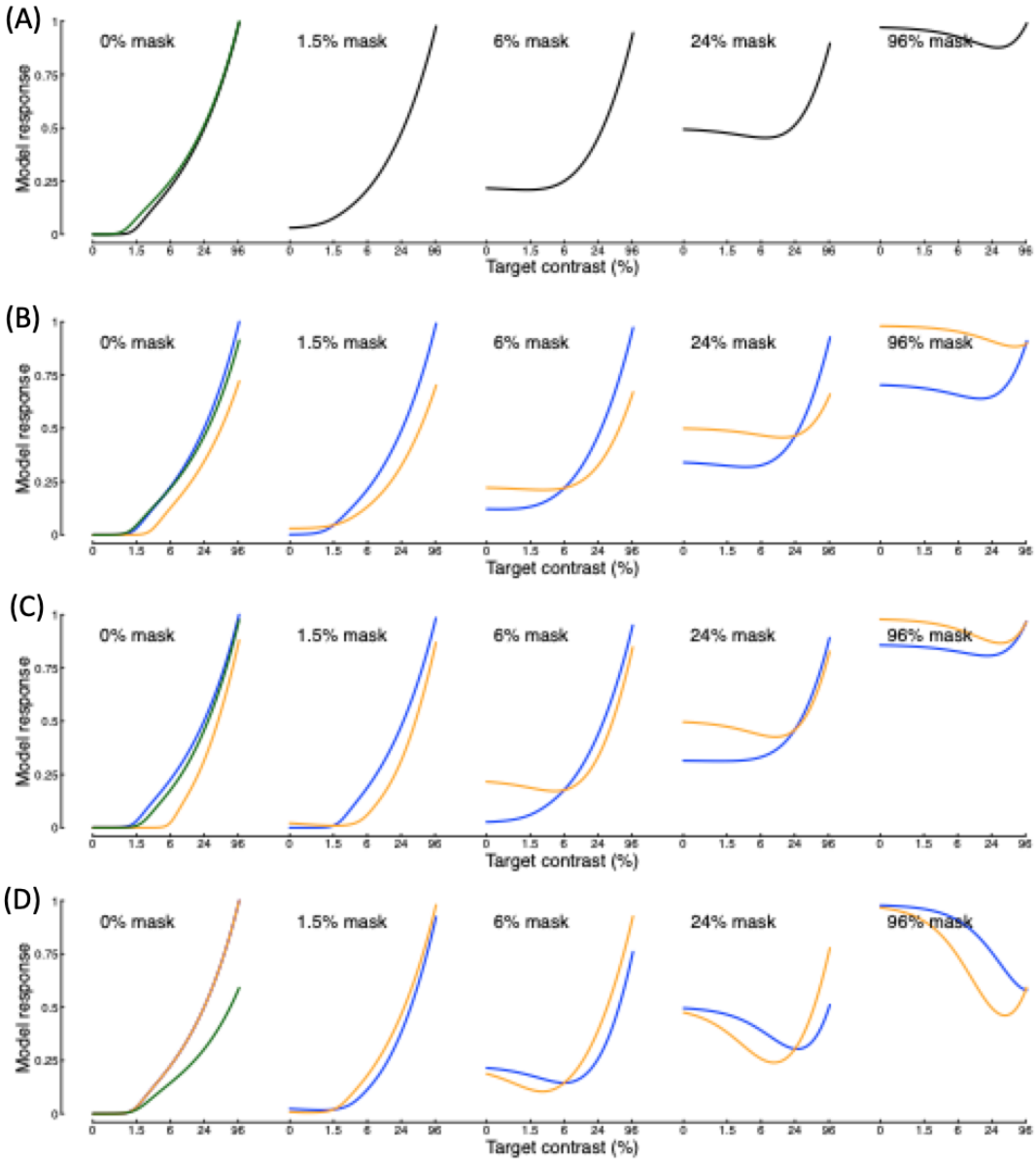

Figure 4.5 Behaviour of the four different computational models explored in this study, for the range of conditions tested empirically. Within each subplot, the model response is plotted as a function of increasing target contrast, when a mask contrast is set in one eye. (A) displays the pattern of response from the two-stage model of binocular gain control (no difference between the eyes). B-D shows three different models response predictions for the amblyopic eye (yellow) and the fellow eye (blue): attenuator model (B), contrast gain shift model (C) and interocular suppression model (D). The first subplot for each model displays the binocular response (green). For all models m =1.3, S =1, and an output nonlinearity follows binocular combination.

4.3. Results

4.3.1. Comparisons between monocular and binocular responses

The average BOLD response at each condition was calculated for each participant and then averaged to give an overall response for each stimulus contrast condition (Fig. 4.1). In order to assess the response deficit of the amblyopic eye, comparisons were made between the average BOLD responses at each stimulus contrast for the monocular and binocular conditions (Fig. 4.6A). The left eye, right eye and binocular responses were also compared for the control group (Fig. 4.6B). In the amblyopic group, it was predicted that the monocular response from the amblyopic eye would show a significantly reduced response compared to that of the fellow eye and binocular response, whereas there would be no difference between the monocular and binocular conditions in the control group. The averaged responses from each monocular and binocular condition were compared using a mixed ANOVA.

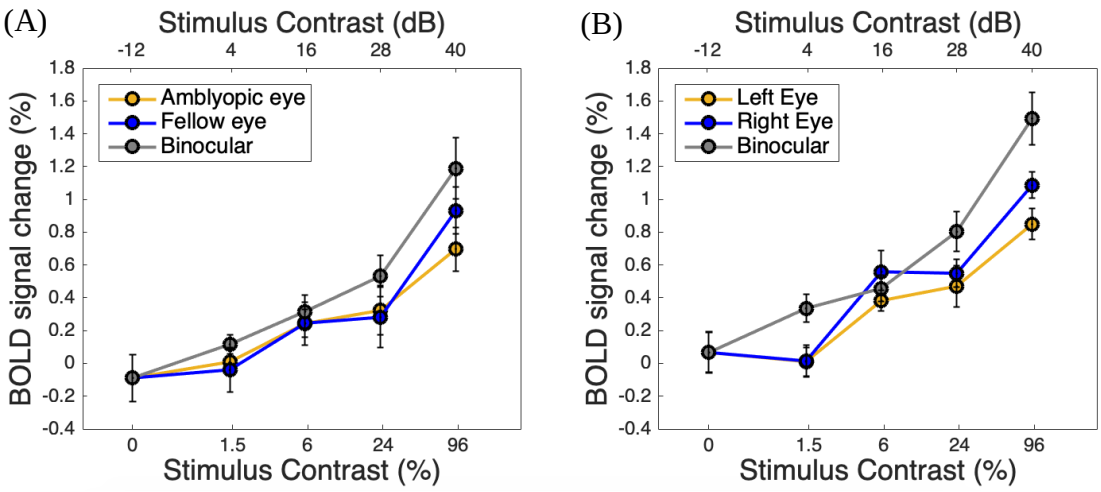

Figure 4.6. Averaged BOLD signal change (%) for each eye's monocular response and the binocular response at each stimulus contrast (0, 1.5, 6, 24 and 96%), for the amblyopes (A) and control (B) group. Error bars indicate ± 1 standard error of the mean. A Mixed ANOVA revealed significantly larger binocular compared to amblyopic/left and fellow/right eye responses, but showed no significant differences between the amblyopic and control participant groups.

Mauchley's test of sphericity indicated that the data did not violate the assumption of sphericity for eye condition (p = .993), stimulus contrast (p = .694) or for the interaction between eye and contrast (p = .580). There was a significant main effect of eye (F (2,40) = 13.98, p < .001, partial η^2 = 0.41) on BOLD response. Planned contrasts (simple) revealed that the response during the binocular condition was significantly higher than the amblyopic/left eye (p = .001) and the fellow/right eye (p < .001). However, there was no significant interaction effect between amblyopic and control participant groups on the eye that was tested (F (2,40) =1.50, p = .236, partial η^2 = 0.07).

A significant main effect was found for stimulus contrast (F (4,80) = 40.80, p < .001, partial η^2 = 0.67) on BOLD response. Planned contrasts (simple) revealed significant differences between 6% (p = .002), 24% (p < .001) and 96% (p < .001) contrast compared to a baseline of 0% contrast. No significant interaction was found of participant group on the stimulus contrast (F (4, 80) = 0.17, p = .953, partial η^2 = 0.01). A significant interaction was found between the eye and stimulus condition (F (8,160) =2.65, p = .009, partial η^2 = 0.12). Contrasts revealed significant interactions when comparing amblyopic/left eye response and the binocular response to stimulus contrasts at 1.5% (p = .014) and 96% (p = .001) compared to the 0% contrast. Significant interactions were also found between the fellow/right eye and the binocular response to stimulus contrasts at 1.5% (p = .047), 24% (p = .025) and 96% (p = < .001) compared to the 0% contrast. However, the participant group did not reveal any significant interaction between the eye that was tested and the stimulus contrast (F (8,160) =0.86, p = .507, partial η^2 = 0.04). Overall this analysis suggests that binocular responses were significantly larger than monocular responses (particularly at the highest stimulus contrasts, 96%) for all participants and showed no differences between the amblyopic and control group.

4.3.2. Interocular contrast responses and model comparisons

Interocular contrast responses for all 25 conditions were compared and the results from this can be seen in Figure 4.7, for healthy controls (Fig. 4.7A) and amblyopic observers (Fig. 4.7B). As predicted, the control group showed typical contrast response functions, where the BOLD response increased monotonically as a function of stimulus contrast. As shown in Figure 4.7A, the BOLD response also gradually increased when a higher mask contrast was presented in the other eye. These results are somewhat consistent with the two-stage model of binocular gain control (Meese et al., 2006), as shown in Figure 4.5A.

The contrast response functions for the amblyopic group were predicted to show a similar pattern to the control group, in that the BOLD response would increase for greater target contrast and for greater mask contrast. However, we expected to observe a reduction in BOLD response from the amblyopic eye compared to that of the fellow eye. In the 0% mask condition, the contrast responses show very little differences between the amblyopic and fellow eye except at the highest-level target contrast (96%). This pattern indicates some level of response gain difference between the amblyopic and fellow eyes at the highest contrast, however, these differences are not as marked as the attenuator model predicts (Fig. 4.5B). For the mask conditions at 1.5%, 6% and 24% contrast, only very small differences between the amblyopic and fellow eye were observed. Interestingly, the response pattern for 96% mask contrast indicates a greater interocular suppression effect of the fellow eye from the amblyopic eye, which is consistent with the model predicting unbalanced interocular suppression (Fig. 4.5D).

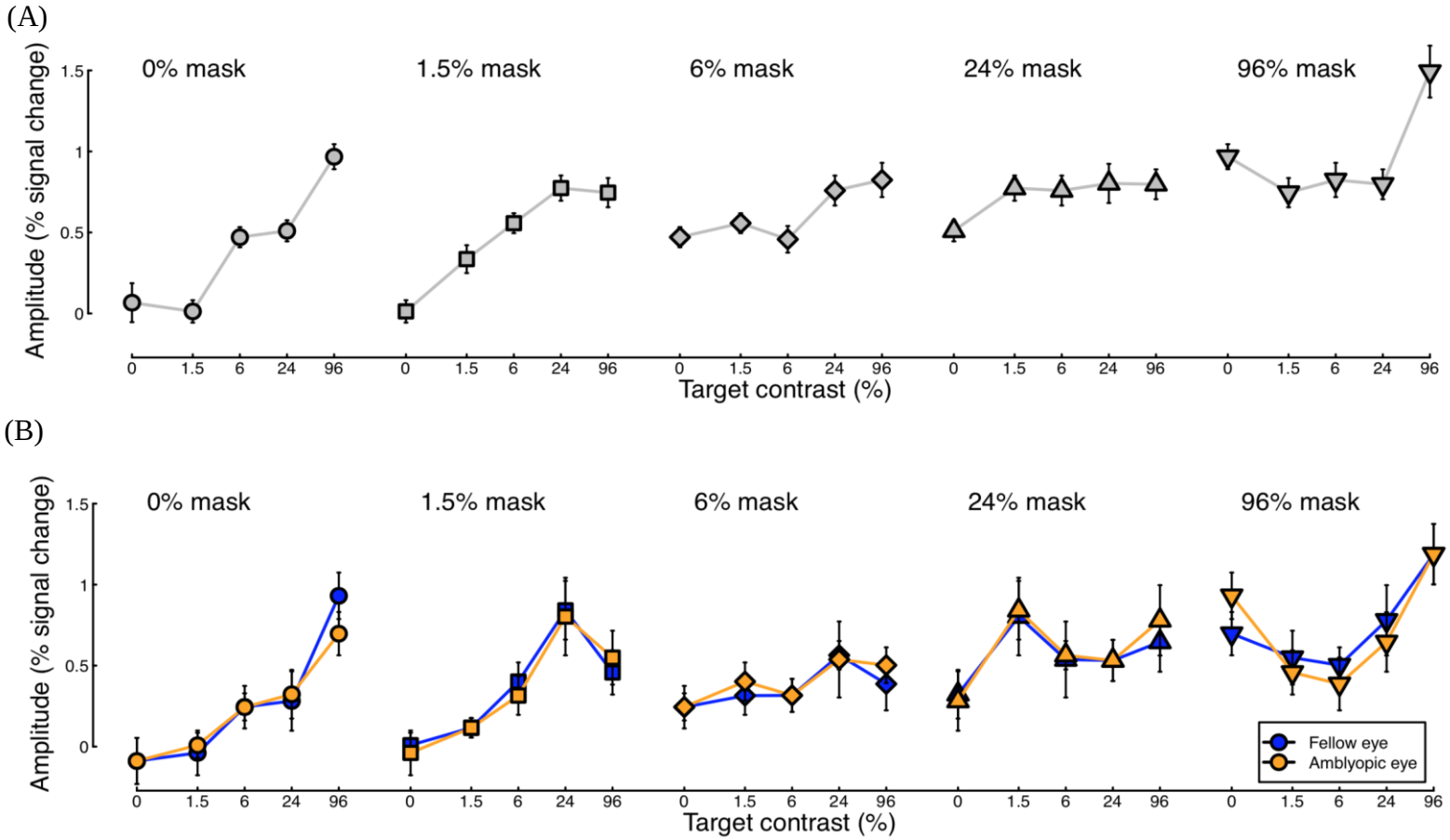

Figure 4.7 Averaged V1 responses for all 25 conditions, for control observers (A) and amblyopic observers (B). Within each subplot, the amplitude response (% signal change) is plotted as a function of increasing target contrast, when a mask contrast is fixed in one eye. In (A) the response is averaged across the left and right eyes. In (B) the response from the amblyopic eye is plotted in yellow and the fellow eye is plotted in blue. Error bars indicate standard error.

4.3.3. Measuring interocular suppression

To explore whether there was significantly greater suppression of the fellow eye from the amblyopic eye, we calculated a suppression ratio for each eye by taking the average response between 1.5% and 6% contrast and dividing it by the 0% contrast, at the 96% mask condition (((1.5%+6%)/2)/0%). The average suppression ratio of the fellow eye and amblyopic eye were compared within the amblyopic group. These ratios were also compared to the averaged left and right eye suppression ratio in the control group. These results are displayed in Figure 4.8. One case was removed from the fellow eye data, as it was more than three standard deviations above the mean.

As anticipated from inspection of Figure 4.8, a paired samples t-test revealed significantly greater suppression of the fellow eye than the amblyopic eye (t (10) = -2.33, p = .042). Differences between the fellow eye and the control group were compared using unpaired t-tests. Results found that the response from the fellow eye showed significantly greater suppression than the control group (t (19) = -3.77, p = .001). Unpaired t-tests were also used to measure the differences between the amblyopic eye and the control group but revealed no significant difference (t (20) = 0.32, p = .750).

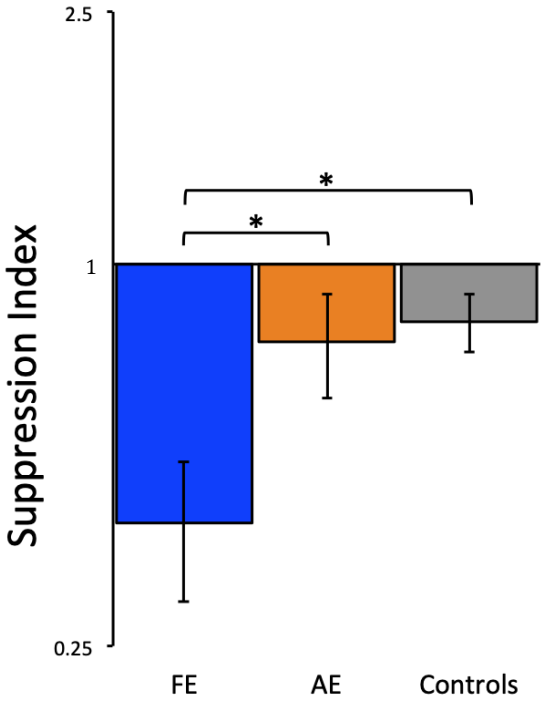

Figure 4.8. The suppression ratio of the fellow eye response (FE), amblyopic eye response (AE) and the averaged left and right eye responses in control participants. The suppression ratio was calculated from 0% target contrast and the average of 1.5% and 6% target contrast (((1.5% + 6%)/2)/0%) at 96% mask contrast. Error bars indicate the standard error of the mean. Brackets with an asterisk indicate statistically significant differences ($p < .05$).

4.4. Discussion

This study measured neural responses in V1 to sine wave gratings using fMRI, in amblyopic and control participants. Previous research found that contrast responses recorded from participants with a healthy visual system are subject to a process of normalisation, which prevents excessive excitation to doubling the input to visual cortex when stimulating both eyes (Moradi & Heeger, 2009). The results from the control group showed similar contrast response functions to those recorded by Moradi and Heeger (2009), in which BOLD responses increased monotonically with increasing stimulus contrast. Unexpectedly, the responses recorded from the control participants revealed significantly larger binocular responses compared to the monocular responses and therefore are not consistent with computational models, such as two-stage model of contrast gain control (Baker et al., 2008;

Moradi & Heeger, 2009). It is unclear why this pattern is seen, as all participants were experienced viewers, familiar with scanning procedure and all motion artefacts were controlled for in the data analysis (see Chapter 2, section 2.3.2 for more details). Various explanations for these findings are discussed below.

Several studies measuring responses from amblyopic observers have reported attenuated responses from the amblyopic eye, compared to that of the fellow eye and binocular responses (Baker et al., 2008; Conner et al., 2007; Farivar et al., 2017; Hess et al., 2009). The pattern of responses from the current study revealed a mild deficit of the amblyopic eye, which was mainly apparent at the higher contrast levels. Although only small, the reduction in response from the amblyopic eye at the higher contrasts appeared consistent with the pattern predicted by the attenuator model. On further investigation, no significant reduction in BOLD response was found for the amblyopic eye but binocular responses were significantly greater than monocular responses.

The results from this study are somewhat surprising, as no significant difference in responses were found between the amblyopes and controls and both groups revealed a significantly greater response to binocular stimuli, compared to monocular stimuli. One possible explanation for the greater response to binocular conditions could be attributed to a bias caused by the localiser stimulus towards binocularly selective voxels. The localiser was presented binocularly and used to select voxels that only responded at the location of each of the four gratings (see Fig. 4.3). It is possible that voxels with a monocular bias did not respond strongly to the binocularly presented stimulus and therefore were not included in analysis.

It is possible that the location of the stimuli presentation could have impacted these results. Studies have shown that the amblyopic deficit for strabismus is strongest at the fovea (Babu, Clavagnier, Bobier, Thompson, & Hess, 2013; Jampolsky, 1955). As a consequence,

presenting the stimuli in the central visual field may have enabled larger amblyopic effects to be measured in some participants. However, this could also mean that it would be harder to record measurable responses from the amblyopic eye in some more severely amblyopic participants. Therefore, offsetting the stimuli parafoveally enabled a level of reassurance that measureable responses could be obtained from within our sample of amblyopes.

A further explanation for these unusual findings could be due to the temporal constraints of fMRI. It is possible that the attenuation of signals in amblyopia stems from a temporally sensitive process, which cannot be measured accurately using fMRI. This would also provide an explanation for previous studies that also found small differences between the amblyopic and fellow eye using fMRI, compared to other studies that have reported much larger differences using EEG and psychophysics (Baker et al., 2015; Conner et al., 2007; Li et al., 2007). This issue is explored further in Chapter 5.

Equally, many other participant or methodological factors could also be contributing to these discrepancies between these findings and the results of previous studies. For example, the heterogeneous nature of amblyopia as a condition and different recruitment criteria, will likely present problems when comparing responses across different techniques. As mentioned previously, various methodological constraints like the technique for achieving binocular separation may have also had an adverse effect on the different responses measured in fMRI and EEG. Some studies achieve monocular viewing conditions by patching one eye which is not particularly reliable as it creates an unrealistic viewing condition where one eye is in darkness (Moradi & Heeger, 2009). Other studies have used a haploscope which the participants adjust themselves for each viewing condition (Conner et al., 2007). This is also prone to error as is it requires the participant themselves to adjust a mirror in order to suitably align the stimuli presented to each eye. The present study used a much more reliable method of stimulus presentation by using a stereo projector within the MRI scanner, which did not require any adjustment from the participant and enabled a natural viewing situation where

both eyes were open during monocular viewing conditions. Therefore, it is unlikely that the stimulus presentation had any adverse impact on the findings of this study. This issue of discrepancies in responses derived from different neuroimaging methods is addressed in the next chapter (see Chapter 5). By running exactly the same study in EEG, using the same group of participants and the same stimuli, this will establish whether the temporal properties of these different techniques are comparable when measuring contrast responses in amblyopes.

Finally, one finding that is particularly interesting was evidence of unbalanced interocular suppression in the amblyopic group. The responses recorded at the 96% mask condition revealed measurable suppression of the amblyopic eye and also within the control participants. Critically, findings revealed significantly greater suppression of the fellow eye from the amblyopic eye. This demonstrates a pattern whereby the response to presenting a mask stimulus in the fellow eye is supressed by the increasing contrast of the stimulus to the amblyopic eye. Whilst these findings strongly support a computational model simulating unbalanced interocular suppression, these results are a direct contradiction of what many previous studies have predicted, i.e. that there would be greater suppression of the amblyopic eye from the fellow eye (Agrawal, Conner, Odom, Schwartz, & Mendola, 2006; Harrad & Hess, 1992; Holopigian, Blake, & Greenwald, 1988; Sengpiel & Blakemore, 1996). This is a counter intuitive finding and one that has not been clearly identified in previous studies of amblyopia.

One possible explanation for this finding could be that the signals derived from fMRI are a consequence of tapping into a different stage of neural processing, which was not measurable in previous psychophysical or electrophysiology methods. To that end the attenuator model, which was developed to explain responses in psychophysical data, may not fully explain the pattern of neural responses recorded in amblyopes using fMRI. The responses derived from fMRI in this study would suggest that some level of unbalanced suppression of the fellow eye

from the amblyopic eye occurs and should be taken into consideration when interpreting responses from amblyopic participants.

4.5. Conclusion

In conclusion, both the amblyopic and control groups revealed contrast responses that increased monotonically with increasing stimulus contrast. Surprisingly, both groups showed significantly greater responses to binocular stimuli compared to monocular stimuli. The pattern of responses from the amblyopic eye revealed only a mild attenuation effect at the higher contrasts. However, responses from the 96% mask condition showed evidence of greater interocular suppression of the fellow eye from the amblyopic eye, contrary to previous studies that found the opposite effect. These findings support a combination of computational models simulating a response gain attenuation shift and unbalanced interocular suppression. These unusual findings could be due to a number of different methodological reasons, such as the stimulus used for localising regions of cortical activation, individual differences in participants or the limitation of temporal insensitivity in fMRI. In order to further investigate these findings, the same experiment was repeated using exactly the same group of participants and the same stimuli but using steady-state EEG, and the results for this can be found in Chapter 5.

CHAPTER 5

Interocular steady-state EEG responses in human amblyopia

5.1. Introduction

Previous studies using EEG to measure neural activity from amblyopic observers at the scalp, have found similar response patterns to those using psychophysical methods. Studies measuring visual evoked potentials (VEP's) have shown abnormalities in the responses derived from the amblyopic eye, both in terms of the amplitude and latency, such as in the P100 and N170 (Bankó, Körtvélyes, Németh, Weiss, & Vidnyánszky, 2013; Joosse et al., 2005; Oner, Coskun, Everekliogluu, & Dogan, 2004). Studies have also revealed a significantly reduced response in amplitude from the amblyopic eye when measuring steady-state visual evoked potentials (SSVEP's) to flickering stimuli, in both children (Johansson & Jakobsson, 2006) and adults (Bagolini, Falsini, Cermola, & Porciatti, 1994; Baker et al., 2015). These findings suggest that responses recorded using EEG reveal an attenuation effect of the amblyopic eye, however, evidence of abnormal interocular suppression between the eyes has not been found (Chadnova, Reynaud, Clavagnier, & Hess, 2017; Huang et al., 2012). This supports the predictions made by the attenuator model, suggesting that inputs to the amblyopic eye are attenuated permanently, rather than being supressed moment-by-moment through a dynamic process of interocular suppression (Baker et al., 2008, 2015).

The aim of this study was to further test the predictions made by the attenuator model to explain the pattern of contrast responses derived using steady-state EEG, in order to examine the binocular deficit seen in amblyopia. Contrary to previous research, the fMRI results from Chapter 4 found only a mild attenuation effect but did find evidence of greater suppression of the fellow eye from the amblyopic eye when a 96% mask was presented to the fellow eye. Therefore, this study used exactly the same participants and an identical experimental design to Chapter 4. This enabled a direct comparison to be drawn between the SSVEP responses in

this study and the fMRI results from the previous chapter. It was predicted that both healthy controls and amblyopic observers would show a pattern of responses whereby amplitude increases with stimulus contrast, however, the amblyopes would show a significantly reduced response from the amblyopic eye but no evidence of abnormal interocular suppression. To our knowledge this will be the first study to directly test quantitative predictions of the attenuator model using the same methods and participants, across two different neuroimaging techniques.

5.2. Methods

5.2.1 Participants

The same participants from the fMRI study in Chapter 4 were recruited for this study, with the addition of thirteen more amblyopes who were also recruited via posters located around the University of York campus and on the Department of Psychology website. In total, twenty-five amblyopes (14 females, mean age = 23.84, standard deviation of age = 7.65) and ten controls (7 females, mean age = 26.70, standard deviation of age = 3.97) took part in this study. All demographic and clinical details for the amblyopes can be found in Chapter 2 (section 2.2). All control participants had normal or corrected to normal visual acuity.

5.2.2 Materials

The stimuli were exactly the same sinusoidal gratings as described in Chapter 4 (see section 4.2.2), which were presented at five contrast levels (0, 1.5, 6, 24 and 96% Michelson Contrast) and factorially combined across the eyes, giving 25 separate conditions.

5.2.3 Procedure

Contrast response functions were measured for all 25 conditions using a WaveGuard cap recording from 64 electrode locations (1000Hz recording frequency). Stimuli were displayed using a VIEWPixx 3D monitor (120Hz refresh rate) and binocular separation was achieved through stereo shutter goggles. Stimuli flickered on the screen for 12 seconds, followed by a 3

second ‘blank’ where no gratings were presented. Observers completed eight trials per stimulus contrast and viewing condition (total of 200 trials). The stimuli were presented in a random order across eight blocks, between which participants were offered a break. As outlined in Chapter 2, participants were asked to maintain fixation and click a button every time the fixation point changed in contrast. Further details of the apparatus and experimental procedure used for the EEG data acquisition can be found in Chapter 2 (section 2.3.3 and 2.4).

5.2.4 Data processing

EEG signals were acquired using whole-head reference of 64 electrodes. The first second of each trial was discarded to eliminate onset transients and the following ten seconds were Fourier transformed. For all conditions, the largest Fourier component was at the fundamental frequency of the stimulus flicker (4Hz). Therefore, this analysis focused on the amplitude (measured in μV) and phase values of the fundamental frequency and did not include values from higher harmonics. As expected, there was a strong response from electrodes located in the occipital region; therefore the data presented are averaged across electrodes Oz, O1, O2 and POz (Fig. 5.1). Data were first averaged across trials and then averaged across observers.

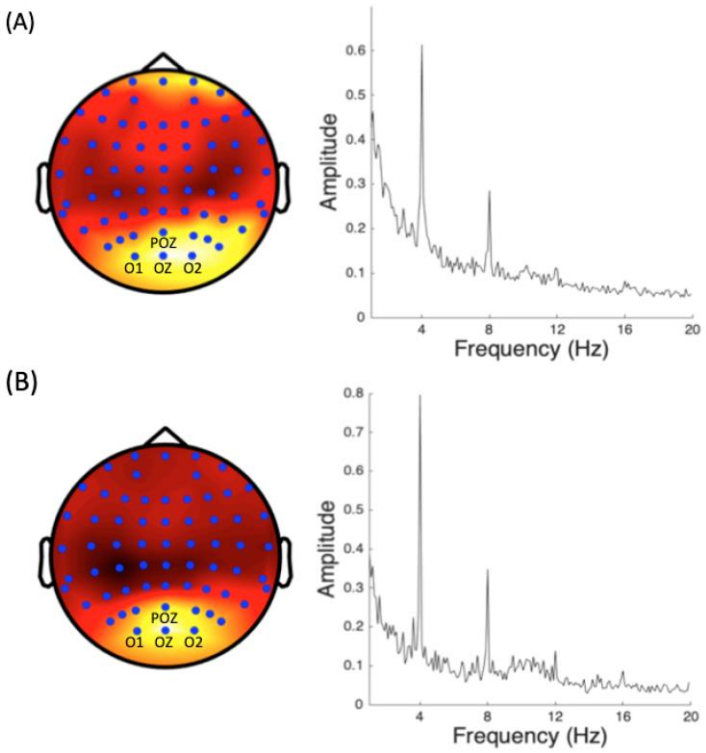

Figure 5.1 The Fourier spectra for SSVEPs up to 20Hz averaged across observers and conditions for both the amblyopic (A) and control (B) groups. In both cases the Fourier amplitude (measured in μV) is greatest at the fundamental frequency of the stimulus flicker (4Hz), with the second harmonic appearing to be smaller (8Hz). The head plots display the distribution of activity across all 64 electrodes averaged across all conditions. Yellow/white indicates a high level of activity and dark red/black indicates a low level of activity. The strongest activity appears to be concentrated over the occipital regions around the visual cortex.

5.3. Results

5.3.1. Comparisons between monocular and binocular responses

In order to assess the response deficit of the amblyopic eye, comparisons were made between the average amplitude responses at each stimulus contrast (0, 1.5, 6, 24 and 96%) for the monocular and binocular conditions. The responses for all 25 amblyopic participants that participated in this study are shown in Figure 5.2A. A subsection of this group containing the results from the 12 amblyopic participants that also participated in the fMRI experiment from

in Chapter 4, can be seen in Figure 5.2B. The left eye, right eye and binocular responses were compared for the control group, which can be seen in Figure 5.2C. It was predicted that amblyopic participants would show a significantly reduced response from the amblyopic eye compared to that of the fellow eye and binocular response, whereas there would be no difference between the monocular and binocular conditions in the control group.

Firstly, a mixed ANOVA was carried out to compare the differences between the control group and the 12 amblyopic participants that also took part in the fMRI study in Chapter 4 (Fig.5.2 B and C). This was in order to directly compare the responses from the same participants across the different techniques. Mauchley's test of sphericity was violated for the eye condition ($p = .001$), stimulus contrast ($p < .001$) and the interaction between eye and contrast ($p < .001$), so the Greenhouse-Geisser correction was applied for all conditions. There was a significant main effect of eye (F (1.31, 26.22) = 6.97, $p < .009$, partial $\eta^2 = 0.26$) on SSVEP amplitude. Planned contrasts (simple) revealed that the response during the binocular condition was significantly higher than the amblyopic/left eye ($p < .001$) but not significantly different to the fellow/right eye ($p = .269$). Despite these results, the effect of the participant group on eye condition was just on the edge of significance (F (1.31, 26.22) = 3.24, $p = .050$, partial $\eta^2 = 0.14$).

A significant main effect was found for stimulus contrast (F (1.53, 30.52) = 44.72, $p < .001$, partial $\eta^2 = 0.69$) on SSVEP amplitude. Planned contrasts (simple) revealed significant differences between 24% ($p < .001$) and 96% ($p < .001$) contrast compared to 0% contrast. A marginally significant interaction was found between amblyopic and control participant groups on the stimulus contrast (F (1.53, 30.52) = 3.64, $p = .049$, partial $\eta^2 = 0.15$). Contrasts revealed only one significant interaction at 96% contrast ($p = .032$), suggesting that the amblyopic group revealed significantly smaller responses than the control group at the highest contrast only. However, there was no significant interaction found between eye and stimulus contrast (F (3.49, 69.87) = 1.90, $p = .130$, partial $\eta^2 = 0.09$) or for the interaction between

amblyopic and control groups on the eye that was tested and the stimulus contrast (F (3.49, 69.87) = 1.19, p = .324, partial η^2 = 0.06).

A repeated-measures ANOVA was also conducted to compare the monocular and binocular responses for all 25 amblyopic participants that took part in this EEG study (Fig 5.2 A). Mauchley's test of sphericity indicated that the data did not violate the assumption of sphericity for eye condition (p = .072). However, sphericity was violated for stimulus contrast (p < .001) and the interaction between eye and contrast (p < .001), so the Greenhouse-Geisser correction was applied for both conditions. A significant main effect was found for eye condition (F (2, 48) = 21.80, p < .001, partial η^2 = 0.48). Planned contrasts (simple) revealed significantly lower response amplitudes for the amblyopic eye (p < .001) and fellow eye (p < .001) compared to the binocular responses. Stimulus contrasts also revealed a significant main effect (F (1.67, 40.04) = 36.04, p < .001, partial η^2 = 0.60) revealing significantly larger responses for 24% (p < .001) and 96% (p < .001) compared to the baseline of 0% stimulus contrast. Finally, a main effect was also seen for the interaction between eye and contrast (F (4.07, 97.58) = 3.40, p = .012, partial η^2 = 0.12). Contrasts showed no differences between the fellow eye and binocular responses at any contrast level, however, significantly lower responses were observed from the amblyopic eye at 1.5% (p = .028), 24% (p < .001) and 96% (p = .006) contrast compared to binocular responses.

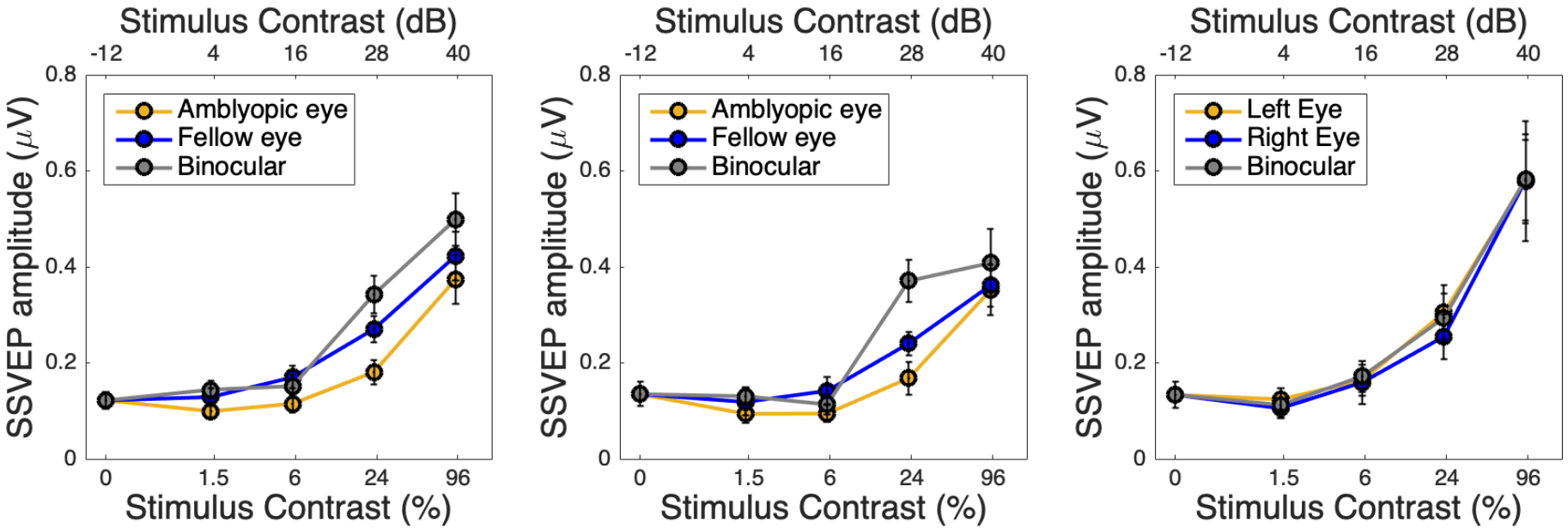

Figure 5.2. Averaged SSVEP response amplitude (μV) at 4Hz for each eye's monocular response and the binocular response at each stimulus contrast (0, 1.5, 6, 24 and 96%), for all amblyopes (N = 25) that participated in the EEG study (A), the group of amblyopes (N = 12) that participated in both the EEG and fMRI study (B), and control group (C, N = 10). Error bars indicate ±1 standard error of the mean. A Mixed ANOVA between amblyopes in (B) and controls in (C) revealed main effects of eye condition and stimulus contrast but only marginally significant differences between the participant groups. A repeated measures ANOVA based on responses from amblyopes in (A) revealed significantly smaller responses from the amblyopic eye compared to that of the fellow eye and binocular responses.

5.3.2. Interocular contrast responses and model comparisons

The SSVEP amplitude response for all conditions was calculated for each participant and then averaged to give an overall response for each of the 25 conditions. The results from this can be seen in Figure 5.3, for healthy controls (Fig. 5.3A) and all amblyopic observers (Fig. 5.3B, N=25).

As predicted, both the control group and amblyopic group revealed typical contrast response functions, where the amplitude response increased monotonically as a function of stimulus contrast. The pattern of response seen from the control group fit extremely well with the prediction made by the two-stage model of binocular gain control (Meese et al., 2006) as described in Chapter 4 (Fig. 4.5A). In the amblyopic group, the overall response amplitude was much lower compared to that of the control group. Furthermore, the amblyopic eye response revealed a reduced and rightward shift in the contrast response curve compared to the fellow eye response, which is particularly evident when no mask contrast is present. This pattern of response is mostly consistent with a model simulating a contrast gain shift, which describes the amblyopic eye response as a rightward shift in the psychometric curve by increasing the saturation constant (increase in C50) in the amblyopic eye (see Chapter 4, Fig 4.5C).

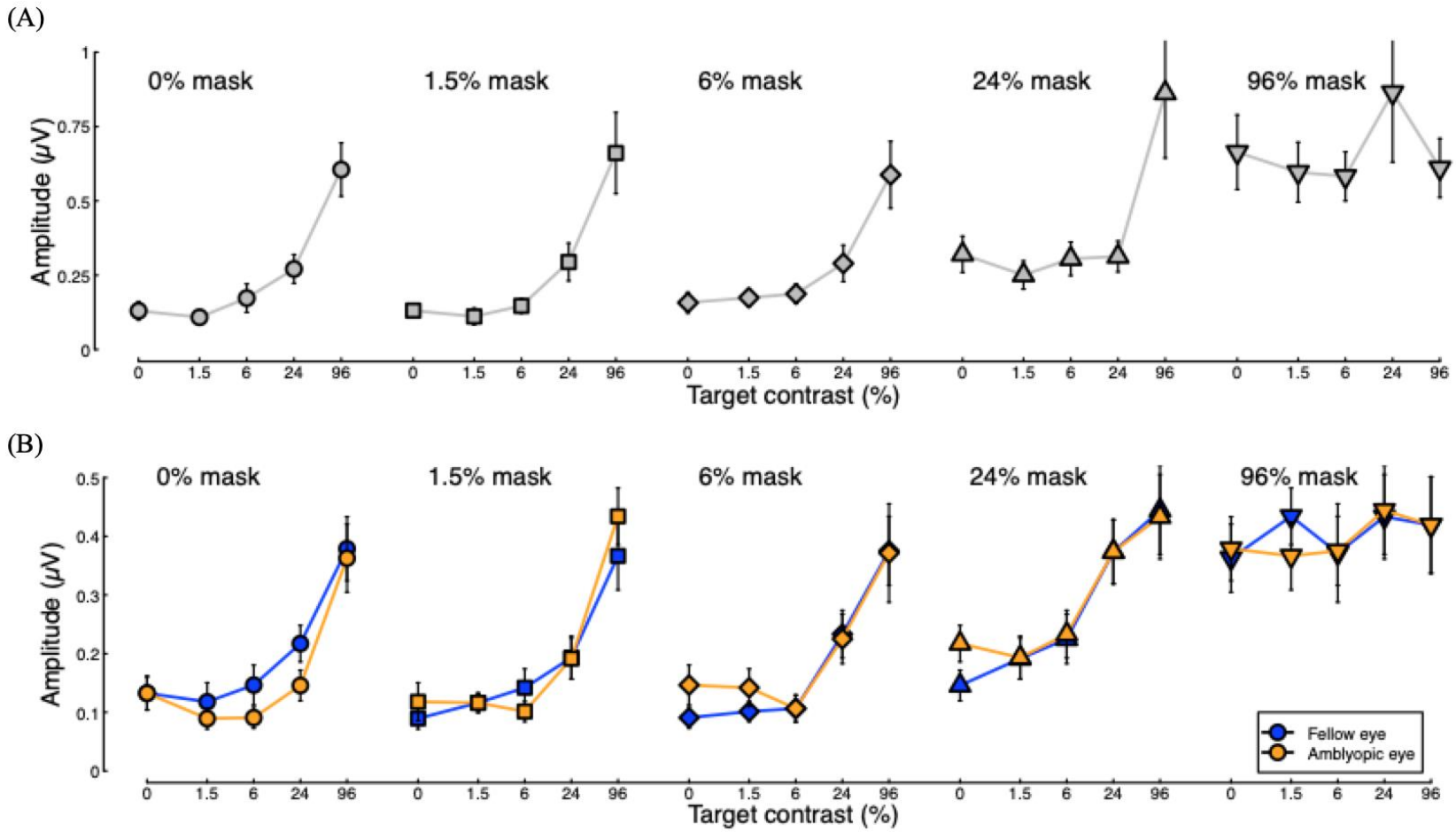

Figure 5.3 Averaged SSVEP responses for all 25 conditions, for control (A) and all amblyopic observers (N=25) (B). Within each subplot, the amplitude response (μV) is plotted as a function of increasing target contrast, when a mask contrast is fixed in one eye. In (A) the response is averaged across the left and right eyes. In (B) the response from the amblyopic eye is plotted in yellow and the fellow eye is plotted in blue. Error bars indicate standard error.

5.3.3. Measuring interocular suppression

The findings from fMRI data in Chapter 4 revealed greater suppression of the fellow eye from the amblyopic eye in the 96% mask condition, but no clear evidence of increased interocular suppression from the amblyopic eye relative to the control group. To examine whether the same pattern is present in the EEG data, the suppression ratio of each eye was calculated in the same way, by taking the average response between 1.5% and 6% contrast and dividing it by the 0% contrast, at the 96% mask condition (((1.5%+6%)/2)/0%). This was done for the same group of participants that had previously taken part in the fMRI study in Chapter 4 (N=12) and the results are displayed in Figure 5.4 alongside the suppression ratios calculated from the fMRI data for comparison.

A series of t-tests were conducted to compare the suppression ratios between the fellow eye and amblyopic eye, as well as the averaged response for the left and right eye in the control group. A paired samples t-test revealed no difference in suppression ratio between the fellow eye and the amblyopic eye (t (11) = -0.20, p = .849). Differences between the fellow eye and the control group were compared using unpaired t-tests. Results comparing the fellow eye to the control group were found to violate Levene's test of homogeneity (p = .039) and therefore equal variances were not assumed. The unpaired t-test revealed no significant differences between the suppression ratio of the fellow eye response and the control group (t (17.48) = 1.04, p = .313). An unpaired t-test was also used to measure the differences between the amblyopic eye and the control group. These groups were found to violate Levene's test (p = .042), so equal variances were not assumed. This test revealed no significant difference between the suppression ratios for the amblyopic eye and the control group (t (16.03) = 1.170, p = .259).

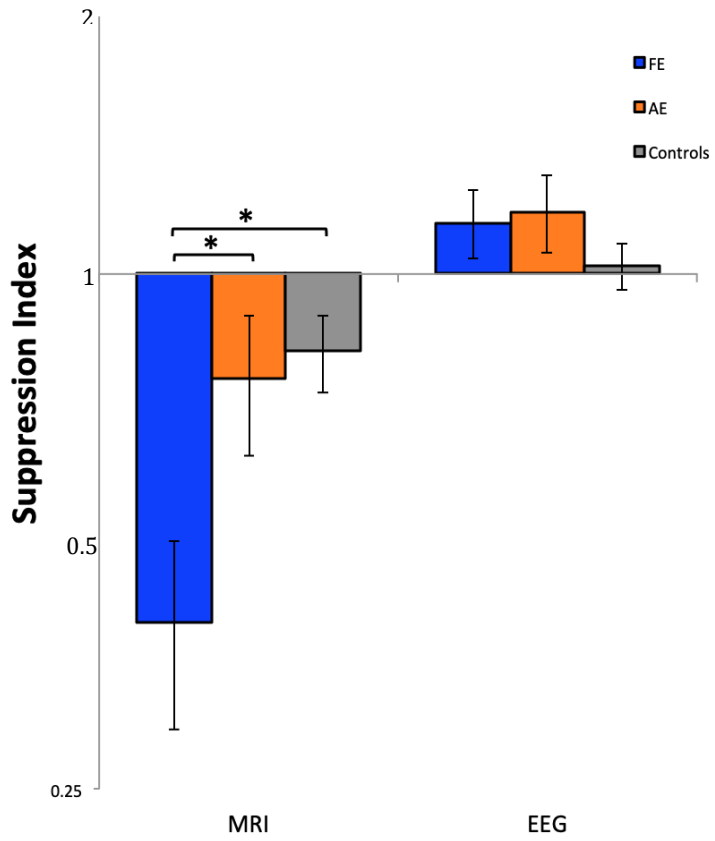

Figure 5.4 The suppression ratio of the fellow eye (FE), amblyopic eye (AE) and the averaged left and right eye responses for the control participants (Controls), for the EEG data (right) and the fMRI data (included in Chapter 4) for comparison (left). The suppression ratio was calculated from 0% target contrast and the average of 1.5% and 6% target contrast (((1.5% + 6%)/2)/0%) at 96% mask contrast. Error bars indicate the standard error of the mean. Brackets with an asterisk indicate statistically significant differences ($p < .05$).

5.4. Discussion

This study measured SSVEPs to sine-wave grating stimuli in amblyopic and control observers. The contrast response functions for both participant groups followed a similar pattern to Moradi and Heeger (2009), with SSVEP amplitudes increasing monotonically with stimulus contrast. Firstly, an analysis was conducted to compare the differences in monocular and binocular responses between the amblyopes (N=12, Fig. 5.2B) and controls (N=10, Fig. 5.2C) that had previously participated in Chapter 4. For both participant groups, the amplitude at the target frequency (4Hz) increased as a function of the stimulus contrast, but differences

between the groups were only apparent at the higher contrasts (96%). Furthermore, only marginal differences between amblyopic eye, fellow eye and binocular responses were observed between the groups. A second analysis was conducted comparing the monocular and binocular responses from a larger group of amblyopes (N=25). As predicted, findings revealed significantly smaller response amplitudes for the amblyopic eye (at 1.5, 24 and 96% contrast) compared to binocular responses, whereas this difference was not found for the fellow eye. This finding shows a more robust difference in SSVEPs between the eyes when a larger sample of amblyopes is compared.

On examination of the nature of the deficit measured from the amblyopic eye, the pattern of response appears to be best predicted by a model simulating a contrast gain shift. This model predicts a contrast response function that is shifted to the right (increase in C50 relative to the fellow eye), rather than purely a response gain shift where the amblyopic eye response is shifted downwards (reduction in Rmax). Contrary to previous studies, this suggests that the attenuator model that was designed to explain psychophysical responses is not able to fully account for the pattern of neural responses recorded using SSVEPs. This further illustrates the architectural differences between responses recorded using behavioural methods compared to neural responses. Therefore, this highlights the need for more sensitive computational models to be developed that can account for patterns of contrast and response gain when interpreting responses from the amblyopic eye.

In the previous chapter a significant effect of unbalanced interocular suppression was found, revealing greater suppression of the fellow eye from the amblyopic eye. This was also compared for the SSVEP responses in the same group of amblyopes that took part in the fMRI study (N=12). Unlike the fMRI results, no evidence of unbalanced interocular suppression was found. It is unclear why such different patterns in response are found within the same group of participants in EEG and fMRI. It is possible that by carefully selecting voxels from V1 in fMRI, the responses are specific to what is happening in V1, whereas in

EEG the responses might be picking up on various feed-forward or feedback effects from other regions of visual cortex.

One exciting possibility for future research stemming from this study includes the possibility of using EEG within a clinical setting as a direct measure of visual improvement during amblyopia therapy. The successful recording of SSVEPs from amblyopic participants in this study provides evidence that substantial responses could be measured from the amblyopic eye and therefore could be used as a sensitive and objective measure of visual improvements following treatment for amblyopia (Baker et al., 2015). Furthermore, due to good signal-to-noise ratios, quick set up and low costs, this steady state technique could be easily deployed within in a clinical setting. This possibility is examined in the next chapter, by using a dry-electrode EEG system to measure contrast responses in children (4-6 years old) undertaking treatment for amblyopia.

5.5. Conclusion

In conclusion, this study investigated the pattern of contrast responses from each eye using steady-state EEG, in amblyopic and control participants. As predicted, the results showed that responses recorded from the amblyopic eye were significantly weaker than those from the fellow eye, whereas this difference was not found for control participants. The pattern of responses suggests that the amblyopic deficit is due to a change in contrast gain, rather than a change in response gain. These findings suggest that the attenuator model, which was designed to account for psychophysical responses, does not fully explain the neural deficit in amblyopia. The successful ability to measure SSVEPs from the amblyopic eye provides evidence to suggest that this method can be used within a clinical setting as an objective measure of visual improvement following treatment for amblyopia.

CHAPTER 6

Objective measures of visual improvement following amblyopia therapy in children and adults

6.1. Introduction

Several methods have been developed in recent years to treat not only children, but also adults with amblyopia. Traditionally, treating amblyopia was only successful for children within the 'critical period' up to around 7 years old, during which occlusion therapy (eye patching) is effective. Greater understanding of the binocular deficit caused in amblyopia has enabled new techniques to be developed to treat both children and adults with amblyopia. Some of these methods include perceptual learning and brain stimulation techniques, such as transcranial direct current stimulation (t-DCS) and transcranial magnetic stimulation (TMS) (Clavagnier, Thompson, & Hess, 2013; Polat, Ma-Naim, Belkin, & Sagi, 2004; Spiegel, Byblow, Hess, & Thompson, 2013; Thompson et al., 2008). As outlined in Chapter 1 (section 1.4), dichoptic game paradigms have also been shown to improve on traditional treatments by encouraging binocular cooperation through contrast imbalance (Hess et al., 2010; Li, Ngo, Nguyen, & Levi, 2011). This means that the amblyopic eye can be strengthened over time without occluding the fellow eye. This has a number of wide reaching benefits, including a reduction in the psychosocial side effects commonly experienced by children during occlusion therapy, which should in turn improve compliance to the treatment (Hess et al., 2010).

However, one major issue surrounds the psychophysical methods used to examine the effectiveness of these treatments. Over time these behavioural measures can be prone to response bias and practice effects when consistently testing the same participants. Neuroimaging techniques like electroencephalography (EEG) have been shown to provide a more objective measure of visual improvement during amblyopia therapy (Baker et al., 2015;

Bankó et al., 2013; Joosse et al., 2005). One study by Baker et al. (2015) designed a steady-state EEG paradigm that measured contrast response functions (at a range of contrasts between 3 – 51%) from both eyes in a group of amblyopes and healthy controls. Results showed that the response amplitude increased as a function of contrast for both groups, however, responses from the amblyopic eye were significantly attenuated, supporting predictions made by the attenuator model (Chapter 1, section 1.2). These findings provide evidence that steady-state EEG offers a sensitive measure to record differences between the eyes at a range of different contrasts. Therefore, the authors suggest that this paradigm is ideally suited for objectively measuring visual improvements due to the good signal-to-noise ratio in steady-state responses and avoiding issues of practice and response bias (Baker et al., 2015).

One potential pitfall of using EEG to measure visual improvements are the lengthy set up times to apply the electrodes using conductive gel (Teplan, 2002). This could be especially impractical for testing within a clinical environment, particularly when assessing young children. However, the development of dry-electrode EEG systems that do not require any conductive gel, provide a good solution to this problem. Due to its portability and quick set up times, these systems enable researchers to measure EEG responses in both research and clinical situations that were not previously possible (Kam et al., 2019). Crucially, the performance and signal quality of the dry-electrode systems have been shown to be comparable to that of the traditional 'wet' EEG electrode systems (Kam et al., 2019; Lopez-Gordo, Sanchez-Morillo, & Valle, 2014). Along with the other benefits of EEG like good temporal precision and affordability (Teplan, 2002), these dry-electrode systems make an attractive alternative to the traditional 'wet' electrode systems and other more expensive neuroimaging techniques (e.g. fMRI).

In this chapter, two studies were conducted with the aim of measuring visual improvements following amblyopia therapy, using a dry-electrode EEG system. The first study measured

improvements in steady-state responses in children before, during and after undertaking traditional treatment for amblyopia (patching or atropine drops). The second presents the findings of a pilot study to assess whether a similar paradigm can be used to measure visual improvements in adults, whilst undertaking a 3D gaming treatment. To assess whether a full-scale project would be feasible, steady-state responses were measured from four adult participants before, during and after undertaking this gaming therapy. A similar steady-state paradigm to Baker et al., (2015) was used in both experiments to measure visual responses to sinusoidal gratings at a range of contrasts (as outlined in Chapter 2, section 2.3.1). Based on the findings from Baker et al., (2015), it was predicted that the amblyopic eye for both children and adults would initially show a weaker response compared to the fellow eye. However, the differences between the eyes should improve as treatment progresses.

Experiment 1: Visual improvement following amblyopia treatment in children

6.2. Methods

6.2.1. Participants

Thirty-two children aged 4-5 years old (at the start of the study) with strabismic amblyopia were recruited to take part in this study (9 females; mean age = 4.39; standard deviation of age = 0.49). Demographic and clinical details, including visual acuity measurements, are presented for each participant in Table 6.1. All children had been referred for treatment at the Ophthalmology Department at the Hull Royal Infirmary Eye Clinic. Participants were paid £10 for each testing session that they completed. All parents or guardians gave informed consent on behalf of their child and were made aware that they could withdraw from the study at any time. This study was ethically approved by the Department of Psychology at the University of York and Leeds East Research Ethics Committee (Yorkshire & The Humber - reference number: 15/YH/0532).

Table 6.1 Demographic details for each participant and visual acuity (logMAR) measurements taken at the start of each session (AE = amblyopic eye; FE = fellow eye; M = male; F = Female; L = left; R = right; SD = standard deviation).

				Session 1 (before treatment)		Session 2 (after 6-8 weeks)		Session 3 (after treatment)	
ID	**Age**	**Gender**	**AE**	**AE**	**FE**	**AE**	**FE**	**AE**	**FE**
1	5	M	L	0.425	0.125	0.125	0	0.1	0
2	4	F	R	0.725	0.05	0.275	-0.05	0.125	-0.02
3	4	M	R	0.55	0.15	0.4	-0.05	0.2	-0.025
4	4	M	L	0.525	0.075	0.35	0.1	0.22	0.1
5	4	F	R	1	0.05	0.175	0.05	0.175	0
6	4	F	R	0.725	0.225	0.375	0.025	0.175	0.1
7	5	M	R	0.425	0.175	0.2	0	0.55	0.15
8	5	M	L	0.6	0.175	0.65	0.125	0.7	0.125
9	4	F	R	0.65	0.15	0.325	0.1	0.1	0.025
10	4	F	L	0.725	0	0.325	0.025	0.225	0.05
11	4	M	L	0.85	0.15	0.3	0.125	0.35	0.175
12	5	M	L	0.65	0.1	-	-	0.275	0.025
13	5	F	R	0.425	0.15	0.1	0.05	-	-
14	5	F	R	0.625	0.0025	0.225	0	-	-
15	4	M	L	0.8	0.1	0.6	0.1	-	-
16	5	M	R	0.425	0.175	0.2	0	-	-
17	4	M	R	0.85	0.125	0.35	0.1	-	-
18	4	F	R	0.55	0.25	0.2	0.125	-	-
19	5	M	R	0.35	0.15	-	-	-	-
20	5	M	L	0.875	0.125	-	-	-	-
21	5	M	R	0.575	0.275	-	-	-	-
22	5	M	R	0.4	0	-	-	-	-
23	4	M	R	0.8	0.1	-	-	-	-
24	4	M	R	0.575	0.275	-	-	-	-
25	4	M	R	0.35	0.1	-	-	-	-
26	4	M	L	0.875	0.275	-	-	-	-
27	4	M	R	0.35	0.05	-	-	-	-
28	4	M	L	0.5	0.3	-	-	-	-
29	4	M	L	0.95	0.225	-	-	-	-
30	4	F	L	0.575	0.1	-	-	-	-
31	4	M	L	0.575	0.125	-	-	-	-
32	5	M	L	0.675	0.05	-	-	-	-
Average Visual Acuity (SD)				**0.62 (0.18)**	**0.14 (0.08)**	**0.30 (0.14)**	**0.05 (0.06)**	**0.27 (0.18)**	**0.06 (0.07)**

6.2.2. Materials

Steady-state responses were measured using a dry-electrode EEG system, as outlined in Chapter 2 (section 2.3.4). Stimulus presentation and binocular separation were achieved by using an Oculus Rift DK2 virtual reality headset, originally intended for 3D gaming purposes. The Oculus was mounted and secured on an adjustable stand so it could be positioned at the correct height for the child and to avoid using the head strap, which would disrupt the positioning of the cap or electrodes (see Appendix 1). The same stimuli as Chapters 4 and 5 were used, consisting of four sinusoidal gratings (4Hz on-off flicker), as outlined in Chapter 2 (section 2.3.1). Stimuli were presented monocularly to each eye at 6, 24 and 96% Michelson contrast. Stimuli flickered for trials of 12 seconds, followed by a 3 second 'blank' where no gratings were presented. Three blocks were conducted lasting 4.5 minutes each, containing three repetitions of each contrast for each eye (18 trials presented in a randomised order within each block). Participants were given an opportunity to have a break in-between each block. A modification was made to the central fixation point to make it more appealing for children to fixate at the centre of the screen. The fixation point consisted of a series of small animations in Graphics Interchange Format (GIFs) of characters from the popular children's film 'Despicable Me' (Illumination Entertainment, Universal Studios), which were repeated throughout the experiment.

6.2.3. Procedure

The study was separated into three identical testing sessions. The first session occurred immediately after their appointment with the ophthalmologist on their initial visit to the hospital, before being given any treatment. The second session occurred during a follow-up appointment within 6 – 8 weeks of the first appointment (average of 54.13 days between sessions one and two). The third session occurred at the end of the treatment between 6-12 months after the first initial appointment (average of 304.82 days between session two and three). Ophthalmologists took measures of visual acuity for all children at the time of each testing session (Table 6.1). Treatment prescribed included occlusion therapy (eye patch) or

atropine eye drops, with the duration or dosage of the treatment depending on the severity of amblyopia in each individual. Some children were also given optical correction to help with misalignment of the eyes, which was always worn during any subsequent testing sessions.

All testing took part in the Eye Clinic at Hull Royal Infirmary. Before the first session, participants were invited to take part in the study by the Ophthalmologist and an information sheet outlining the experiment's aims and procedures was given to the parent or guardian to read. A simplified version of the information sheet was also provided for the adult to read to the child. During the study, the children were held on the adults lap to try and keep the children as still as possible. Children were first shown the cap and stimulus through the Oculus and then were instructed to ignore the 'black and white circles' but watch the 'character' very carefully on screen. They were also encouraged to sit as still as possible whilst looking inside the Oculus. Children were given a break and a reward sticker at the end of each block.

6.2.4. Data processing

The combination of a dry-electrode system and young participants led to a much higher noise baseline than for the EEG data in Chapter 5. For this reason, we present results as signal-to-noise ratios (SNRs) rather than amplitudes. Each SNR was calculated by dividing the amplitude at the signal frequency by the mean amplitude in the surrounding frequency bins (5 bins above and below with a frequency resolution of 0.1Hz). An SNR of 1 indicates no measurable signal, as the amplitude at the signal frequency equals that at the adjacent frequencies. For each individual, responses were taken from the electrode that produced the largest SNR in the 96% contrast condition for the fellow eye, as demonstrated in Figure 6.1. Responses were first coherently averaged across trials and then the absolute SNRs were averaged across participants.

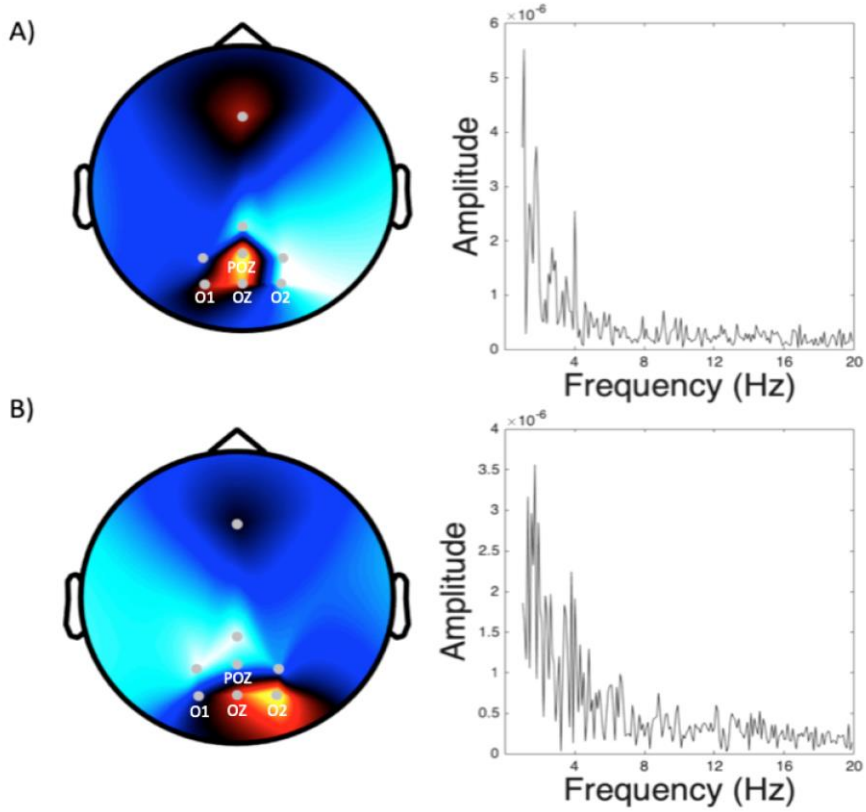

Figure 6.1 Example Fourier spectra showing the amplitude response for SSVEPs up to 20Hz for two different testing sessions in one participant. Head plots show the electrode locations and distribution of activity centred on electrode POz (A) and O2 (B) averaged across all trials in one session. Yellow/red regions indicate a high level of activity and blue/black regions indicate a low level of activity.

6.3. Results

Thirty-two children participated in the first testing session with 16 of these children returning for the second session. Out of these 16 children, 11 returned for the third session. One child that participated in the first session failed to attend the second session but did take part in the third session. Therefore, in total there were 12 children that participated in the third session but only 11 that completed all three sessions.

Firstly, in order to assess whether the treatment undertaken by the children was effective in improving their vision, a Generalized Linear Mixed Model (GLMM) was conducted to compare the effect of eye (amblyopic and fellow eye) and testing session (1-3) on visual acuity (see Figure 6.2). The analysis was conducted on participants that completed at least two testing sessions: session 1 N=17; session 2 N=16; session 3 N=12. Eye and session were entered as fixed factors in the model and the visual acuity was the dependent measure. A normal probability distribution and identity link function were used and the participant variable was entered as a random factor in order to control for repeated sampling of each participant.

Table 6.2 Results of a GLMM exploring the effect of eye (amblyopic verses fellow eye), session (1-3), as well as the interactions between eye and session on visual acuity. Significant results are indicted, where *** denotes $p < .001$.

	F	**df**	**P**
Eye	193.00	1, 82	<.001***
Session	43.48	2, 82	<.001***
Eye*Session	20.77	2, 82	<.001***

The results of the GLMM are shown in Table 6.2, revealing significant main effects of eye, session and for the interaction between eye and session. Furthermore, fixed coefficients revealed a significant interaction of the amblyopic eye between sessions one and two (p = <.001), suggesting that the amblyopic eye had significantly worse visual acuity than the fellow eye but this improved following the first stage of treatment. These findings demonstrate the effectiveness of conventional treatment for improving acuity in children. They suggest that most of the gains in acuity occurred quickly, between sessions one and two, and that further improvements between sessions two and three were minimal.

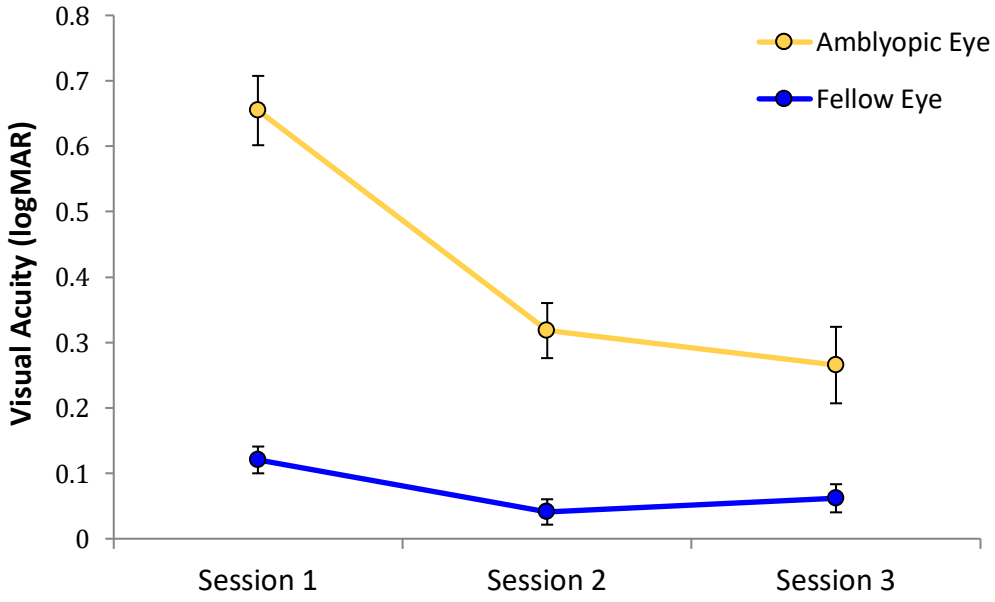

Figure 6.2. Average visual acuity (logMAR) measurements for the amblyopic and fellow eyes for the patients that completed all three sessions (N=11). Error bars represent ±1 standard error of the mean. GLMM analysis revealed a significant main effect for eye, session and the interaction between eye and session.

To analyse the steady-state responses, the SNR from each eye was calculated for each participant and then averaged over trials to give an overall SNR for each of the three stimulus contrasts at each testing session. Results are presented in Figure 6.3, with separate plots indicating different testing sessions split across the number of participants that completed the first session (A, N=32), second session (B-C, N=16) and all three sessions (D-F, N=11). The pattern of results shows no above-baseline SNRs at lower contrasts (6 and 24%). Therefore, the analysis was focused on SNRs at the highest contrast (96%) for all sessions.

A GLMM was conducted to compare the effect of eye (amblyopic and fellow eye) and testing session (1 - 3) on the SNR for 96% contrast. The analysis was conducted on the same group of participants as the visual acuity GLMM. Eye and session were entered as fixed factors in the model and the SNR was the dependent measure. A normal probability distribution and identity link function were used and the participant variable was entered as a random factor. The results of the GLMM are shown in Table 6.3, revealing a significant main effect of eye but not for session or for the interaction between eye and session. This finding indicates that SNRs were larger for the fellow eye compared to the amblyopic eye but that no significant changes occurred between each testing sessions. As no interaction was found, this suggests that the time or treatment undertaken between testing sessions did not significantly influence the SNRs when comparing the amblyopic or fellow eye.

Table 6.3 Results of a GLMM exploring the effect of eye (amblyopic verses fellow eye), session (1-3), as well as the interactions between eye and sesison on the average SNR at the 96% stimulus contrast condition. Significant results are indicted, where *** denotes $p < .001$.

	F	**df**	**P**
Eye	13.71	1, 84	<.001***
Session	0.68	2, 84	.508
Eye*Session	0.38	2, 84	.682

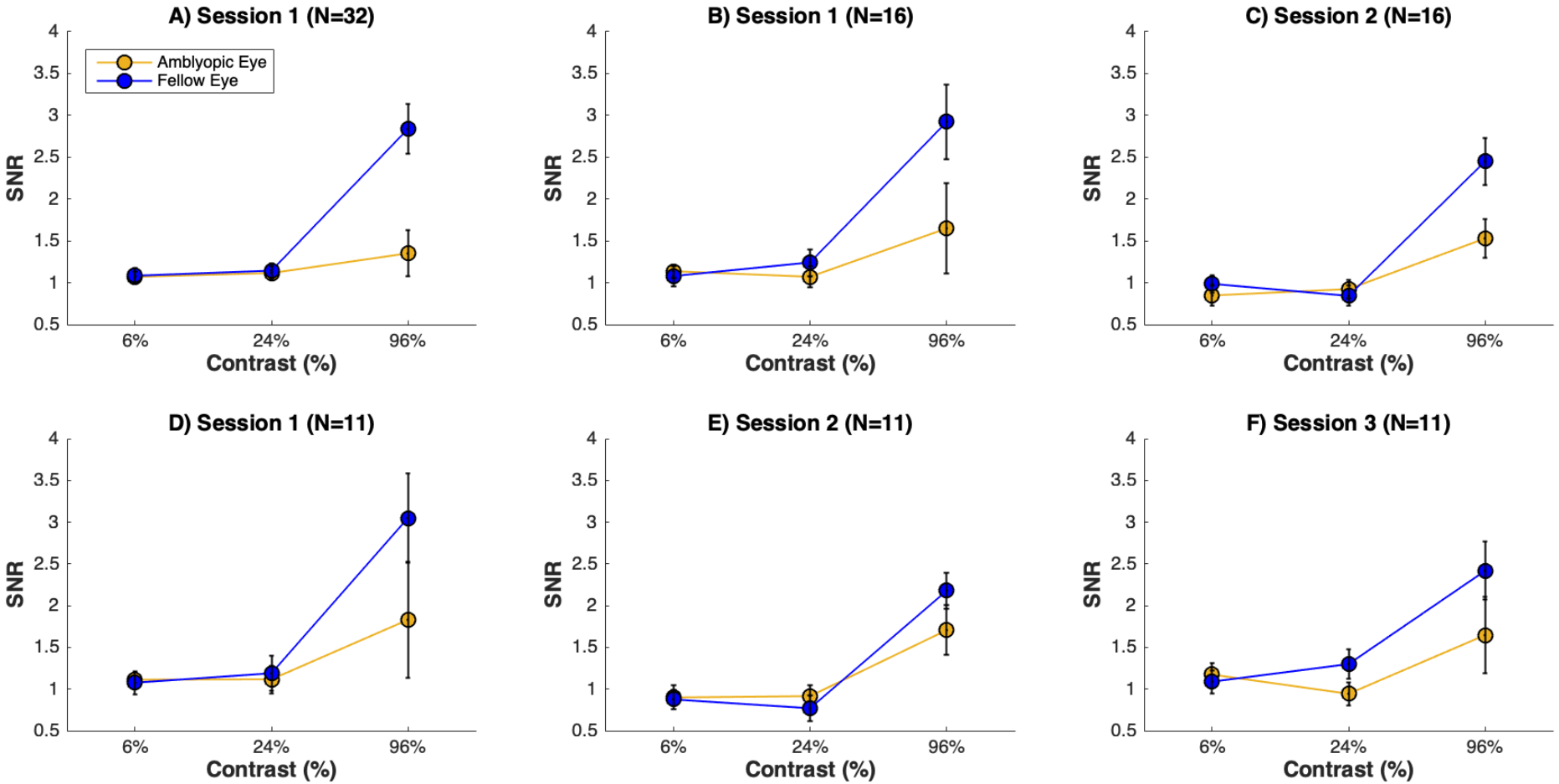

Figure 6.3. Signal-to-noise ratios (SNR's) at each stimulus contrast for the amblyopic (yellow) and fellow eye (blue). Separate plots represent different testing sessions. (A) All participants that completed Session 1 (N=32); (B) Session 1 results for participants that returned in Session 2 (N=16); (C) All participants that completed session 2; (D – F) results from participants that attended all three testing sessions (N=11). Error bars represent ±1SE.

In order to investigate further whether there was a reduction of SNR between the eyes at 96% stimulus contrast, ratios between the fellow eye and the amblyopic eye were calculated. A series of paired samples t-tests were conducted to examine whether there were any significant differences in the ratio between the amblyopic and fellow eyes across the different testing sessions (Fig. 6.3). Firstly, a paired samples t-test revealed no significant differences between ratios at session 1 and 2 for the 16 participants that returned at session 2 (t (15) = -0.67, p = .515). Paired samples t-tests were also conducted for the 11 participants that returned for all three sessions. However, no significant differences found between ratios at session 1 and 2 (t (10) = 1.23, p = .248) or between session 2 and 3 (t (10) = -0.12, p = .905).

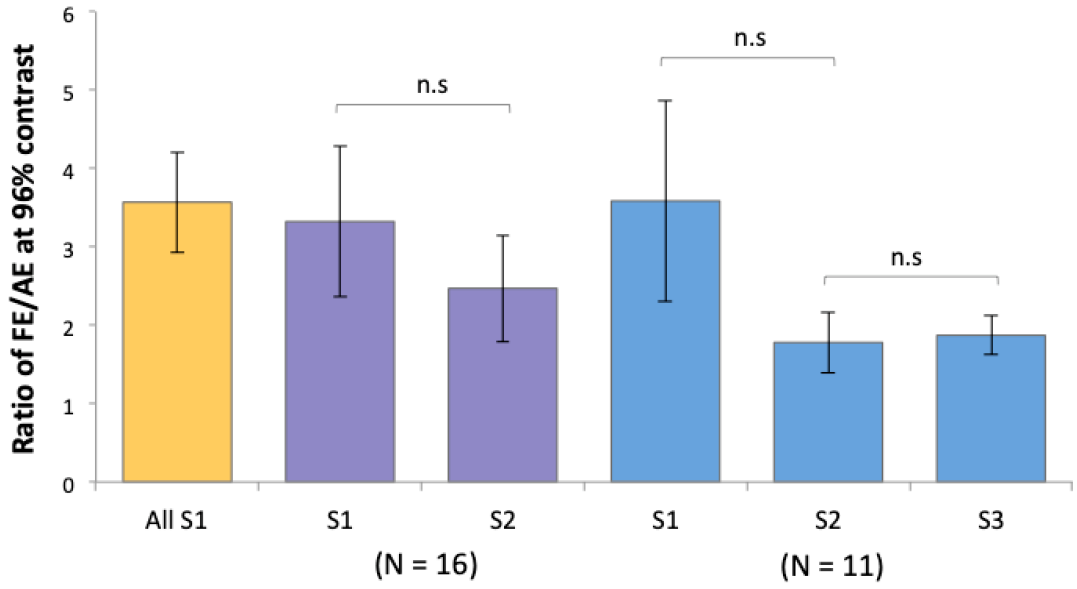

Figure 6.4. Ratios between the amblyopic and fellow eyes (fellow eye / amblyopic eye) taken from the SNR response at 96% stimulus contrast. The yellow bar represents ratios for all participants tested at session 1 (N=32). Purple bars represent ratios from participants that returned for session 2 only (N=16). Blue bar represent ratios from participants that completed all three sessions (N=11). Error bars represent ±1SE and n.s denotes non-significant comparisons as revealed by paired-samples t-tests.

6.4. Discussion

The aim of this study was to use a dry-electrode EEG system to objectively measure visual improvements in children following treatment for amblyopia. SSVEPs were recorded in response to sine wave gratings presented to the amblyopic and fellow eyes at three different stages throughout their treatment. SNRs rather than amplitude responses were compared due to high noise baselines for all participants. For stimuli presented at 96% contrast, SNRs for the fellow eye were found to be better than the amblyopic eye but these differences were not found to improve significantly between testing sessions. Furthermore, no differences were found between the ratio of response from the fellow and amblyopic eyes across the different testing sessions, although these did go in the predicted direction. However, measures of visual acuity from the amblyopic eye were found to significantly improve between the first and second session but not between the second and third sessions. These findings support the predictions that steady-state responses would be better for the fellow eye than the amblyopic eye, but provide no convincing evidence of improvements between testing sessions. The improvements in visual acuity suggest that the treatment undertaken was successful in improving the children's vision over time but these changes were not reflected in the SSVEPs measured using the dry-electrode EEG system. It is likely that the high attrition rate, combined with highly variable measurements, reduced our statistical power so that the changes evident in Figure 6.3 did not reach statistical significance.

There are a number of explanations for why no significant differences in the SSVEPs were measured between testing sessions. Firstly, one of the biggest challenges during the data collection was making sure that the children were fixating centrally. Using an Oculus to present the stimuli meant that it was difficult to check whether the children were fixating at the centre of the screen as their eyes were obscured from view. It is possible that they found it difficult to focus their attention selectively on watching the central animation whilst ignoring the stimulus. For future studies, engaging the children with an easy fixation task (e.g. press a button when a picture appears) may help to maintain attention to the centre of the screen.

Furthermore, tiredness, boredom and time of day when testing took place could have been other critical factor in the child's ability to maintain attention (Ruff & Lawson, 1990). Splitting the conditions over six blocks rather than three would require the children to maintain their attention for shorter time periods and enable them to have more frequent breaks. This would allow them to move and for the height of the Oculus to be adjusted to accommodate any changes in their position.

Another problem that frequently occurred was that many of the children struggled to sit still for the duration of the block or wanted to talk during the stimulus presentation. The nature of using EEG to measure electrical signals means that any muscle movement will generate a much larger response in comparison to the small electrical signals in the brain. This is especially the case when using a dry-electrode system, due to the higher impedance levels of the electrodes when no conductive gel is used. Therefore any source of motion, such as eye or head movement, adjusting their position on the parent's lap, talking or laughing, is likely to cause an artefact and contribute noise to the data. Again, future studies should consider adapting the design of this study by incorporating shorter blocks to help them stay still for the duration of the block and a small behavioural task at fixation to encourage children to maintain concentration during data collection.

For a number of years there has been some debate as to whether the spatial frequency of the stimulus can influence the level of binocular imbalanced observed in amblyopes. Studies have shown that mid-to-high spatial frequencies (e.g. 5 – 9 cycles/°) enable a larger amblyopic deficit to be observed in some cases, however, this could also make it more difficult to record measurable responses from the amblyopic eye in some more severely amblyopic participants (Kwon, Wiecek, Dakin, & Bex, 2015; Levi & Harwerth, 1977). Equally, deficits have been shown to be less pronounced at lower spatial frequencies (e.g. 1 cycle/°) (Hess & Howell, 1977; Kwon et al., 2015). Other research has found that spatial frequencies of around 3

cycles/° provide a good compromise between the higher and lower spatial frequencies when measuring binocular imbalance (Baker et al., 2008). Due to this trade off, the spatial frequency of 3 cycles/° used within this study is unlikely to have strongly influenced the findings.

In conclusion, steady-state responses were measured from both eyes of the children undertaking treatment for amblyopia. SSVEPs revealed better SNR for the fellow eye compared to the amblyopic eye. No improvements in SNR were observed after undertaking treatment for amblyopia; however, improvements in the visual acuity of the amblyopic eye were measured after 6-8 weeks of treatment. This suggests that the treatment that the children received was effective in improving their vision between the sessions but any neural changes between the eyes were unable to be measured using SSVEPs. Due to the level of noise in the data set, it is clear that some adjustments need to be made to the design of this study to enable objective measures of visual improvement to be measured in children. Reducing the length of time for each block and including an easy fixation task might help encourage young participants to stay still for longer and fixate at the centre of the screen.

Experiment 2: Visual improvement following amblyopia treatment in adults

6.5. Methods

6.5.1. Participants

Participants who had previously taken part in the experiments from Chapters 3-5 were all invited to take part in this pilot study to measure visual improvements whilst undertaking a 3D gaming treatment. Initially six adults agreed to take part, however, two withdrew leaving only four participants that completed the study (see Chapter 2, section 2.2). All four participants were female with an average age of 20 years old (SD: 0.71). Visual acuity measurements were taken at the time of each testing session using a Snellen eye chart (read at

6 meters) and are reported in Table 6.4. This study was ethically approved by the Department of Psychology at the University of York.

Table 6.4 Demographic details visual acuity measurements taken at the start of each session (AE = amblyopic eye; FE = fellow eye; L = left; R = right). Visual acuity was measured using a Snellen Chart (logMAR equivalents provided).

			Session 1		Session 2		Session 3	
	Age	AE	AE	FE	AE	FE	AE	FE
SA	20	R	6/7.5 (0.1)	6/9.5 (0.2)	6/9 (0.17)	6/9.5 (0.2)	6/9 (0.17)	6/9.5 (0.2)
MRW	19	L	6/12 (0.3)	6/6 (0)	6/12 (0.3)	6/6 (0)	6/12 (0.3)	6/6 (0)
ECD	20	L	6/4.8 (-0.1)	6/4.8 (-0.1)	6/4.8 (-0.1)	6/4.8 (-0.1)	6/4.8 (-0.1)	6/4.8 (-0.1)
IKL	21	L	6/6 (0)	6/4.8 (-0.1)	-	-	6/6 (0)	6/4.8 (-0.1)

6.5.2. Materials

6.5.2.1. Experimental equipment and stimuli

The current study followed a similar design to Experiment 1, using the same dry-electrode system to record SSVEPs. Stimuli consisted of sinusoidal gratings (4Hz on/off flicker) and were displayed using Oculus Rift headset (as described in Experiment 1). Three different viewing conditions were included: stimuli were presented monocularly at 6, 12, 24, 48 and 96% contrast; binocularly at 6, 24 and 96% contrast; and dichoptically where a mask of 48% contrast flickering at 6Hz was fixed in one eye whilst targets (flickering at 4Hz) with contrasts of 6, 24 and 96% were presented to the other eye. Trials lasted 12 seconds each, followed by a 3 second 'blank' where no gratings were presented (Chapter 4, Fig.4.2). Eight blocks were conducted lasting 5 minutes each, containing two repetitions of each contrast for each eye (20 trials presented in a randomised order within each block).

6.5.2.2. Game treatment

The treatment undertaken in this study was a binocular training regime that consisted of playing a specially designed game, called 'Dig Rush' (Amblyotech, Inc, Ubisoft, Montréal, Canada). The game works by presenting different components (the characters and obstacles)

to each eye separately, in order to train the brain to use the amblyopic eye. Participants were required to wear red-green glasses whilst playing the game in order to achieve binocular separation. These glasses were worn over the top of any normally used prescription glasses or contact lenses. The aim of the game was to move a character around the game environment to collect gold and return it within an allocated amount of time. Points are rewarded to the player for collecting the gold quickly and successfully navigating around obstacles.

The game was installed on Nexus tablets (Google LLC, CA, USA) running the Android operating system, which were loaned to the participants for the duration of the treatment, along with a set of red-green glasses. An example of the screen setup is shown in Figure 6.4. Parts of the game displayed in blue were presented to the amblyopic eye and parts displayed in red were presented to the fellow eye. The background information presented in grey was displayed to both eyes. The game was played for one hour every day over a two-month period. The difficulty automatically increased throughout the treatment by reducing the contrast presented to the fellow eye, according to the score achieved by the participants each day.

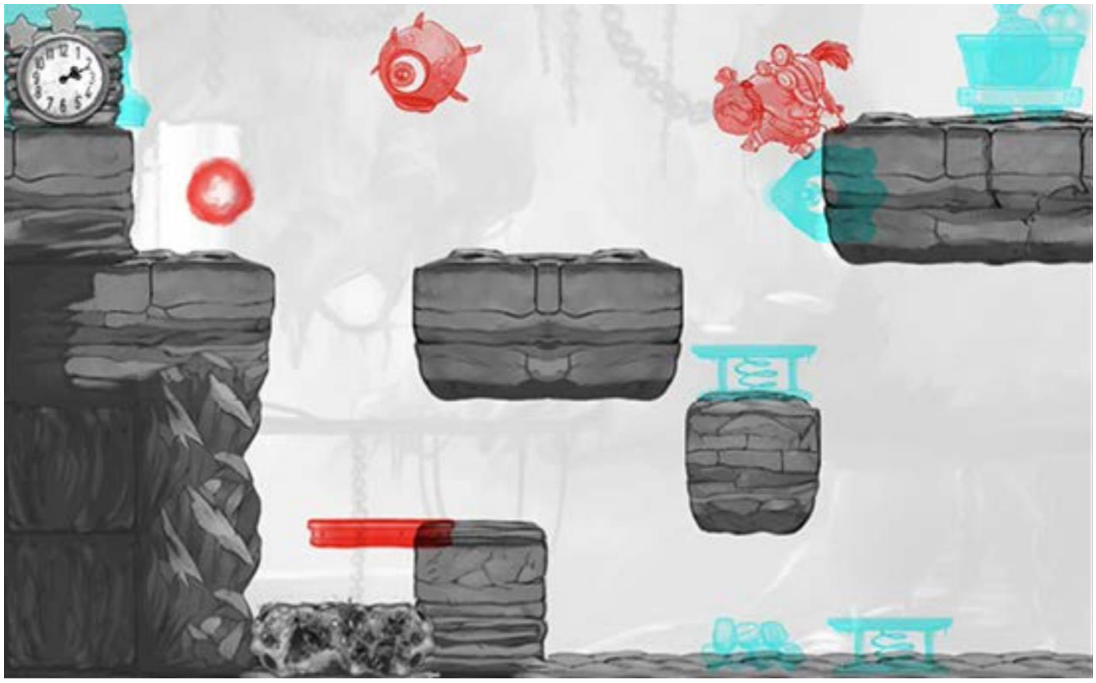

Figure 6.5 An example of the ‘Dig Rush’ treatment game. Participants had to move the character (shown in red in the top right corner) around the game environment, by swiping left and right with their finger, to collect gold (shown in blue at the bottom). The objects in blue were presented to the amblyopic eye, the red objects were presented to the fellow eye and the grey background was presented binocularly.

6.5.3. Procedure

The current study followed a similar procedure to that of Experiment 1, where SSVEPs were recorded during three identical testing sessions. All testing took place over a two-month period at the Department of Psychology, University of York. Prior to the first session, participants received an information sheet detailing what was required during the testing sessions and details of the treatment. Participants were shown how to use the tablet and were instructed to play the game for at least an hour every day (which could be played in one go or split across multiple periods throughout the day). The second session occurred after participants had played the game for one month and the third session occurred at the end of the two-month period.

During each testing session, participants completed the EEG experiment where they were asked to maintain central fixation throughout (as outlined in Chapter 2, section 2.4) and were given an opportunity to have a break in-between each block. Participants were rewarded £100 for participating in the whole study.

6.5.4. Data processing

In order to compare these findings to the results from Experiment 1, results from this study were also presented as signal-to-noise ratios (SNRs). Each SNR was calculated in the same way as Experiment 1 and responses were taken from the electrode that produced the largest SNR. Responses were first coherently averaged across trials and then the absolute SNRs were averaged across participants.

6.6. Results

The results reported for this study present the preliminary findings from four participants to assess the feasibility of conducting a larger study into the effectiveness of EEG to measure visual improvements following a gaming treatment. All four participants completed the first and the third testing session. One participant (IKL) failed to attend the second testing session but did take part in the first and third session. Statistical tests were not conducted due to the lack of power from using a small sample size. However, the patterns of these responses are described and discussed in terms of conducting this study on a larger scale. Results are presented in Figure 6.6, with plots separated across testing sessions (left to right) and viewing condition (top to bottom).

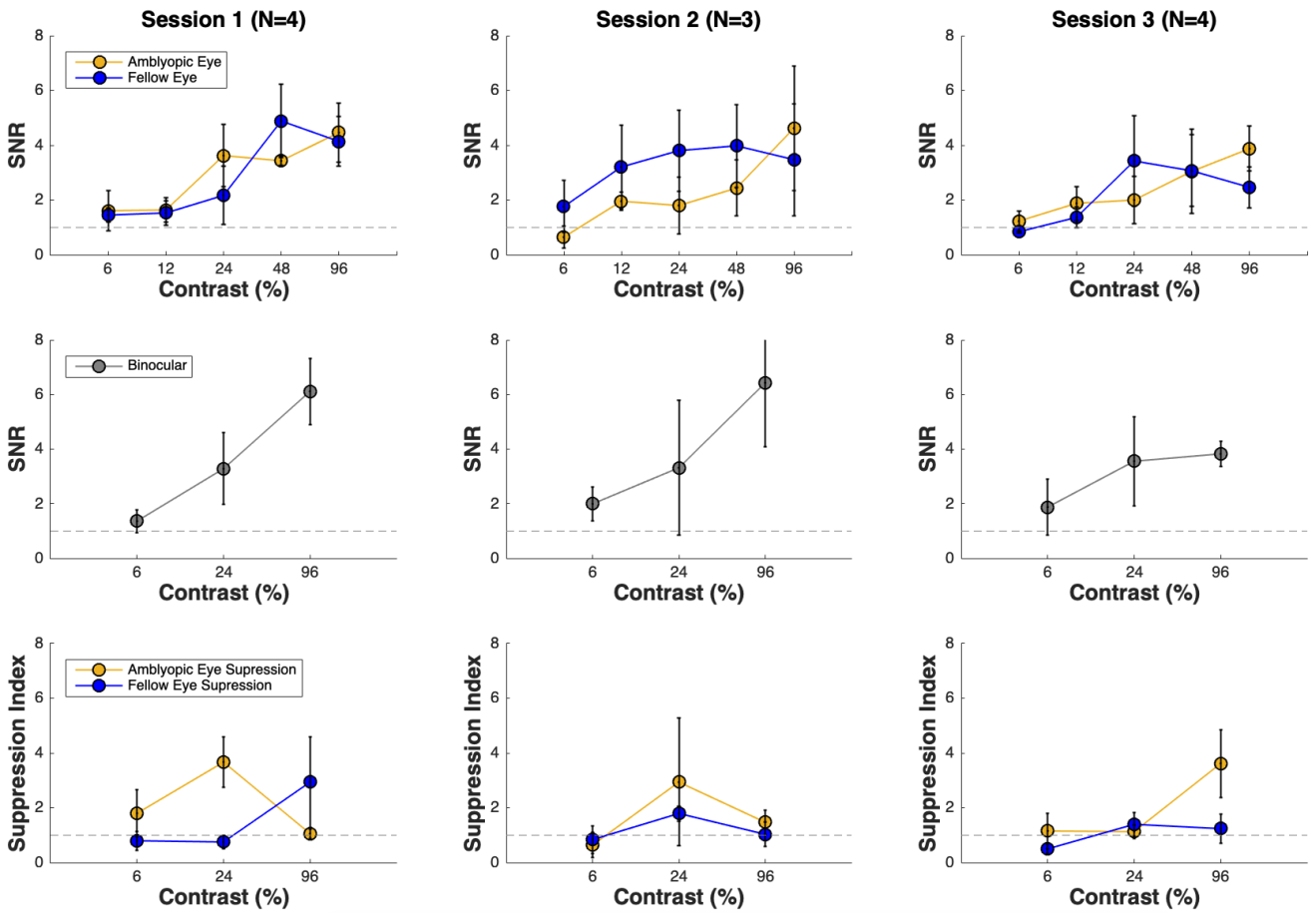

Figure 6.6. Signal-to-noise ratios (SNR's) for sessions 1 – 3 (left to right) at each stimulus contrast: the top row shows monocular conditions; the middle row shows binocular conditions; and the bottom row displays the suppression of each eye (taken from the monocular condition / dichoptic mask conditions). Dashed line represents a baseline of 1 (indicating no measurable SNR). Error bars represent ±1SE.

The SNR from each viewing condition was calculated by averaging across trials and then averaged across participants. Measurable contrast responses were seen for both the monocular and binocular viewing conditions, suggesting that this paradigm was successful in measuring responses from each eye. The patterns of these responses appear to increase with stimulus contrast, supporting findings from previous EEG studies (and the results of Chapter 5) that find that steady-state responses increase monotonically with increasing stimulus contrast (Baker et al., 2015). Suppression ratios were generally higher for targets presented in the amblyopic eye, compared to when targets were presented to the fellow eye, potentially indicating greater suppression of the amblyopic eye. Furthermore, the responses recorded from the adults appear to show larger SNRs across a wider range of stimulus contrasts, compared to the responses recorded from children in Experiment 1. This perhaps suggests that it is possible to record more substantial SSVEP measurements in adults due to the fact that they are better able to maintain central fixation and stay still for longer.

It is unclear whether any improvements are seen for the amblyopic eye response across testing sessions. Responses from the monocular conditions seem to show that the difference in SNRs between the eyes seems to reduce between the second and third sessions, which could indicate that the treatment was successful in reducing some of the amblyopic deficit. However, visual acuity measures appear to be relatively unchanged throughout the course of the study, with only one participant (SA) showing a minor change in the acuity of their amblyopic eye (see Table 6.4). It is clear that the treatment would need to be undertaken by more people, in order to assess whether the game is effective in improving visual responses over time.

6.7. Discussion

The aim of this study was to use dry-electrode EEG to objectively measure visual improvements in amblyopic adults following a gaming treatment. This experiment reports the preliminary findings of a pilot study containing just four participants, in order to assess the feasibility of conducting a larger scale study. Due to the low sample size, statistical tests were not conducted and instead the patterns of steady-state responses recorded from this sample are discussed.

Measureable contrast responses were recorded in all viewing conditions and appear to increase monotonically with stimulus contrast, following patterns recorded in other EEG studies (Baker et al., 2015). Substantial SNRs were recorded for both the amblyopic and fellow eyes, providing evidence that this dry-electrode EEG system could be used to measure differences between the eyes if conducted on a larger scale. Due to the lack of statistical power from testing only four participants, it is unclear whether visual improvements are made over time between testing sessions. However, the improvements in SNRs between the amblyopic and fellow eyes for the third session could be an indication of a significant improvement if more participants were tested. These preliminary findings provide a good indication that this EEG paradigm could be used on a larger scale to successfully measure visual improvements following treatment for amblyopia.

However, a few suggestions are made to address some of the issues surrounding the game treatment, which could potentially influence its effectiveness. One common problem that participants faced was that the expectation to play the game every day for two months was quite demanding of their time and energy. One change that could be implemented is a measure built into the game or tablet that could record exactly how long each participant is undertaking the treatment each day. This should enable researchers to know exactly when and for how long participants are interacting with the game each day and if any days have been missed. This would enable a higher level of control by ensuring that the treatment has been

carried out for the correct duration in order to achieve the maximum benefit for each participant. It could also help avoid any response bias that might occur by relying on participants to self-report when they were able to play the game.

Similarly, participants reported that they struggled to remember to play the game every day. If this treatment were to be given to a larger group of participants, they should be encouraged to set reminders and devise a plan of when to play the game to experience the fully potential of the treatment. Future studies should encourage participants to view this game like any other treatment that may be prescribed by a doctor, so that in order to experience the benefits of the treatment they need to adhere to the instructions. As discussed in section 6.1, the dry-electrode EEG system is portable and easy to set up, which enables testing to occur quickly outside of the laboratory environment. Researchers should make the most of this flexibility by conducting the EEG sessions from a place that may be more convenient to the participant (e.g. their homes) to ensure that each session occurs at the correct time point.

In conclusion, the preliminary data presented in this study provide promising indications that this dry-electrode EEG paradigm could be used as a measure of visual improvement following amblyopia therapy in adults. Data presented here show observable contrast responses under monocular, binocular and dichoptic viewing conditions. Furthermore, the patterns of responses provide a promising indication that improvements in amblyopic eye responses might be seen across sessions. Various improvements to the protocol have been suggested which should enable more accurate data to be recorded. Therefore, the findings from this pilot study suggest that a larger-scale project would be feasible with some changes made to the current protocol.

6.8. Overall conclusion

The studies undertaken in this chapter tested a dry-electrode EEG paradigm to measure visual improvements following treatment for amblyopia, in both children and adults. The findings from both studies revealed a higher noise baseline than originally anticipated. These dry-electrode systems appear to contribute more noise to the SSVEP responses than the traditional wet EEG systems, mainly due to higher intrinsic impedances of the electrodes. Despite this, substantial steady-state responses were recorded from each eye in both participant groups, which revealed measurable SNRs particularly at the higher stimulus contrasts. Although the patterns of responses appear to show a reduction in the deficit from the amblyopic eye, the improvements in visual function between testing sessions fell outside of significance. This is likely to be a result of several factors, including: low sample sizes caused by high attrition rates; a higher noise level from measuring responses from children (as discussed in section 6.4); and high impedances of the dry-electrode EEG system. However, successful recordings of steady-state responses further demonstrate its usefulness as an objective method for measuring improvements in visual responses. Some changes are suggested to improve the protocol and design of the study, to help minimise some of the factors that may affect its validity. Overall, these studies show the ease at which neural responses can be measured quickly and effectively, demonstrating the wider potential to apply dry-electrode EEG as an objective measure within mainstream clinical settings.

CHAPTER 7

General Discussion

7.1. Summary of findings

The aim of this thesis was to further understand the nature of the binocular visual deficit caused by amblyopia. The studies undertaken in this thesis have enabled insights into the neural and computational mechanisms involved in processing binocular vision, both in cases of amblyopia and in healthy visual systems. Using two different neuroimaging methods has enabled unique comparisons to be drawn across these studies and provided a more complete picture of how contrast is processed in the amblyopic brain.

In Chapter 3, fMRI was used to compare the pRF sizes from each eye in a group of amblyopic and control observers. It improved on the method used to measure projections from each eye in previous studies by carefully controlling binocular separation using a stereo projector and polarising glasses inside the scanner (Clavagnier et al., 2015). Furthermore, adaptations were made to the stimulus by incorporating a narrower drifting bar containing a $1/f$ 'pink' noise carrier. This was in order to create a more natural stimulus and to drive responses from a wider range of neurons compared to the traditional checkerboard carrier. The pattern of responses from both participant groups agreed well with previous studies, showing that pRF size increased as a function of eccentricity (fovea – periphery) and ascending visual area (V1 – V3) (Clavagnier et al., 2015; Dumoulin & Wandell, 2008). As predicted, it was found that the amblyopic eye showed significantly larger pRF sizes across all visual areas compared to the fellow eye, whereas no differences were found between the left and right eyes of the control participants. However, the difference between the amblyopic and fellow eyes across each visual area was smaller than predicted. One explanation given for this finding was that neurons with smaller receptive field sizes were able to be measured due to the changes made to the stimulus. Overall, these findings suggest that enlarged pRF sizes

from the amblyopic eye reflect a loss of spatial resolution (Clavagnier et al., 2015; Hess & Howell, 1977; Levi & Harwerth, 1977) in cells within both striate and extrastriate areas (Barnes et al., 2001; Li et al., 2007).

Chapter 4 used fMRI to investigate how binocular visual information is combined across the eyes, in amblyopic and control observers. Four sine wave gratings were presented monocularly, binocularly and dichoptically at a range of contrasts (0, 1.5, 6, 24, 96 %). As predicted, the findings showed that contrast response functions increased monotonically with increasing stimulus contrast for both participant groups (Moradi & Heeger, 2009). Surprisingly, these results only revealed a mild attenuation effect of the amblyopic eye at the higher contrasts. However, findings did show evidence of greater interocular suppression of the fellow eye from the amblyopic eye for the highest masking contrast. This result directly contradicts suggestions made in previous studies that predicted the opposite to be true (Agrawal et al., 2006; Harrad & Hess, 1992; Holopigian et al., 1988; Sengpiel & Blakemore, 1996). Therefore, these findings support a computational model involving a combination of response gain attenuation shift (reduction in Rmax) and unbalanced interocular suppression.

The study reported in Chapter 5 used steady-state EEG to measure contrast responses using the same experimental design and the same participants as Chapter 4. Substantial SSVEPs were recorded, revealing contrast response functions that increased monotonically with increasing stimulus contrast, in both participant groups. As predicted, the amblyopic eye revealed a significantly reduced response compared to that of the fellow eye and binocular responses, however, no evidence of unbalanced interocular suppression was found. On further examination, the pattern of responses recorded from the amblyopic eye seems to be best predicted by a computational model involving a contrast gain shift (increase in C50 relative to the fellow eye). These findings illustrate the architectural differences between responses recorded using different neuroimaging methods and highlights the need for more sensitive

computational models to be developed that can account for different response patterns across the eyes (these findings are discussed in more detail in section 7.2).

The successful recording of steady-state responses in Chapter 5 demonstrates the effectiveness of using EEG to record differences between the eyes (Baker et al., 2015). Therefore, the studies in Chapter 6 used a dry-electrode EEG system to objectively measure visual improvements at different stages throughout treatment for amblyopia. Experiment 1 measured contrast responses from the amblyopic and fellow eyes of children. Findings revealed better signal to noise ratios (SNRs) for the fellow eye compared to the amblyopic eye, however, no improvements in SNRs were measured throughout treatment. The combination of using a dry-electrode system and young participants led to a much higher noise baseline than the EEG data in Chapter 5. Therefore, improvements to the design of this study (e.g. shorter blocks and a fixation task) are needed in order to be able to use this technique to objectively measure visual improvements in children.

Experiment 2 presents the findings from a pilot study to test the effectiveness of the same dry-electrode EEG system at measuring improvements in four amblyopic adults whilst undertaking a 3D gaming treatment. Findings appeared to show that adults produced more substantial SNRs at a wider range of contrasts, compared to the pattern of responses recorded from children in Experiment 1. Due to the low sample size, limited improvements in the response from the amblyopic eye were noticed over the duration of the treatment. Various suggestions are made to improve the impact of the 3D game treatment, such as systematically recording the number of days spent playing the game, which would enable a direct measure of compliance to the treatment. However, the successful recording of SSVEPs in this pilot study provides good evidence to believe that a larger-scale project would be feasible with some small changes made to the current protocol.

7.2. Multimodal neuroimaging

Over the years studies have implicitly assumed that EEG and fMRI index similar neural mechanisms, as they have complementary spatial and temporal resolutions. However, there are some inconsistencies in the literature relating to amblyopia, in terms of the pattern of responses measured from each eye when using different neuroimaging techniques (Chapter 1, section 1.5). Even when measuring responses from severely amblyopic participants, fMRI studies have reported much smaller differences between the amblyopic and fellow eyes, compared to responses derived from EEG (Baker et al., 2015; Conner et al., 2007; Li et al., 2007). One of the main aims of this thesis was to address this issue by comparing whether fMRI and EEG produced similar types of neural patterns from the amblyopic and fellow eyes, when all sources of variability (e.g. stimulus, task, procedure and participants) are controlled for. Despite this, different patterns of responses were still observed between fMRI and EEG. BOLD responses showed that the amblyopic deficit was best predicted by computational models simulating a response gain shift and unbalanced interocular suppression, whereas SSVEP responses support a contrast gain shift model. These findings challenge the assumption that fMRI and EEG reflect the same neural processes measured at different spatial and temporal resolutions.

Another recent study investigating visual attention found a similar discrepancy between neuroimaging techniques (Itthipuripat, Sprague, & Serences, 2019). Here fMRI and EEG were used to measure attention modulations of neural contrast responses within the same group of participants. Findings revealed different patterns of attentional modulations between the techniques, with fMRI results showing that activation scaled additively with attention, whereas EEG scaled multiplicatively. Further investigation revealed that fMRI measures of attentional modulations respond in a similar way to later EEG components, such as alpha-band oscillations (Itthipuripat et al., 2019). These findings suggest that both neuroimaging techniques are able to uniquely tap into different physiological processes and aspects of neural signals that go beyond a tradeoff in temporal and spatial resolutions. Therefore, in

order to make inferences about the neural underpinnings of cognitive operations both techniques need to be considered, particularly when using them as diagnostic tools within clinical populations (Calderone et al., 2013) or for developing treatments for conditions like amblyopia.

It is clear that more investigation is needed to further understand the patterns of response from the amblyopic eye measured in different neuroimaging techniques. Following the suggestions made by the attention study above (Itthipuripat et al., 2019), the differences in responses derived from fMRI and EEG could be as a consequence of tapping into different stages of binocular processing in amblyopia. A more detailed investigation into where the similarities and differences in responses for both techniques lie would enable a broader picture of the neural underpinnings of amblyopia. This would also help in developing more sophisticated computational models of amblyopia that can account for other neural patterns, including response gain, contrast gain and unbalanced interocular suppression.

7.3. Future directions

The main aim of the studies undertaken in this thesis was to provide insight into the computational processes involved in binocular vision in amblyopia, in order for new and more effective forms of treatment to be developed. The dry-electrode EEG paradigm used in Chapter 6 is currently being applied in a large-scale project at Moorfields Eye Hospital (NHS Foundation Trust), to measure visual improvements in amblyopic children. This project aims to compare traditional methods for treating amblyopia (occlusion/atropine drops) with a new dichoptic treatment known as 'Balanced Binocular Viewing Therapy' (BBV) (Bossi et al., 2017). This treatment works in a similar way to the game treatment described in Chapter 6, where children (between the ages of 3 – 8 years old) watch dichoptic movies on a 3D game console whilst wearing shutter glasses (to achieve binocular separation) for around one hour a day over a 16 week period. BBV works by presenting images to both eyes separately but the image presented to the fellow eye is blurred in an attempt to balance the input received by

primary visual cortex (Tailor, Bossi, Greenwood, & Dahlmann-Noor, 2016). Previous research found substantial and rapid improvements in visual acuity following BBV, along with high levels of compliance due to the engaging nature of the movies (Bossi et al., 2017). Recording dry-electrode EEG measurements, along with other behavioural and clinical tests, should provide a clear insight into the effectiveness of this new treatment and how it compares to traditional methods. It will also provide further understanding into how the neural patterns change over the course of treatment, which is still not well understood.

Recent developments in other neuroimaging techniques, such as magnetoencephalography (MEG), could also provide an interesting alternative to EEG measures. MEG uses sensors on the outside of the head to measure the magnetic fields generated by the electric currents produced during neural activity (Cohen, 1972). Although the magnetic signals generated by the brain are extremely small, when many neurons respond at the same time it creates a measurable magnetic field outside the head. Traditional MEG systems use superconducting sensors (SQUIDs) that detect and amplify these magnetic fields. These sensors are highly sensitive and have to be used within a magnetically shielded room to prevent interference, whilst being cryogenically cooled using liquid helium (Singh, 2014). Sensors are encased in a fixed 'one-size-fits-all' helmet that is placed around the subject's head. MEG has advantages over other neuroimaging methods, as it provides superior spatial resolution to EEG and much better temporal resolution than fMRI (Singh, 2014). However, as the sensors remain in fixed positions inside the helmet, this can mean that they are not optimally positioned relative to the head. This makes it a particularly inaccessible technique for testing certain participant groups, such as children, as the brain-to-sensor distance is too large (Boto et al., 2018; Holmes et al., 2018).

As a result of these limitations, a compact scalp-mounted MEG system has been developed, using Optically Pumped Magnetometers (OPMs) (Tierney et al., 2019). This method is founded on similar principles to MRI, as it relies on the manipulation of 'spin' (a quantum

property that underlies a particle's magnetic moment and therefore its responses to a magnetic field) (Shah & Wakai, 2013). OPMs use a laser that emits electromagnetic waves to establish the magnetically sensitive state in a heated vapour of spin-polarised alkali atoms. A major advantage of these systems is that they do not require cryogenic cooling, which means it is also significantly cheaper to operate than SQUID-based MEG (Boto et al., 2016). Studies have shown that measurements recorded using OPMs are comparable to traditional MEG systems, showing that they remain highly sensitive at measuring weak magnetic fields within millimetres of the scalp (Budker, Kimball, Rochester, Yashchuk, & Zolotorev, 2000; Shah & Wakai, 2013). Over recent years OPMs have been applied within a variety of sensory studies, such as those investigating the somatosensory (Borna et al., 2017), auditory (Johnson, Schwindt, & Weisend, 2013) and visual systems (Labyt et al., 2019), including retinotopy (Holmes et al., 2018).

The compact nature and wearability of OPMs present exciting possibilities to measure MEG responses from participants with a range of head-sizes and within settings that were not previously possible. As established from the studies undertaken in Chapter 6, one of the biggest challenges with measuring neural responses from clinical populations, especially children, is the requirement to remain as still as possible. OPMs are much more robust in terms of compensating for motion compared to traditional MEG methods, as well as other neuroimaging techniques like fMRI and EEG (Boto et al., 2018; Holmes et al., 2018). In fact, studies have even begun to use these systems as a method for measuring responses from the motor cortex when participants are free to move (Boto et al., 2018). This is hugely beneficial as it places fewer restrictions on participants making it easier to measure neural responses, especially for participants within clinical populations.

Furthermore, studies comparing the effectiveness of different neuroimaging techniques in children, including EEG, OPM and a version of MEG designed for children (known as 'babyMEG') are currently being undertaken at the University of Colorado (CO, USA). The

long-term goal of this research is to over come the current restrictions of present technology and establish a practical, lower cost solution to non-invasively measure neural responses from both children and adults. The portability and quick set up time, along with the flexibility of measuring MEG responses from a range of head sizes, make OPMs an attractive technique that could be implemented within research and clinical environments. There are many clinical applications of this technique and suggestions have already been made to use it to further understand epilepsy and schizophrenia (Barkley & Baumgartner, 2003; Holmes et al., 2018; Robson et al., 2016). However, it also has the potential for widespread application to be used as a common method for measuring visual improvements during treatment for amblyopia.

7.4. Overall conclusion

The experiments in this thesis contribute to the wider understanding of the neural basis of amblyopia. Different neuroimaging approaches have been used to explore how binocular visual inputs are combined in the brain, as well as understanding how these patterns can change over time with treatment. For the first time, two neuroimaging methods have been directly compared within the same group of participants and using the same experimental design. These findings of how binocular inputs are combined in the brain have built on previous research and provide evidence for ways in which current computational models of amblyopia could be improved. Possible future directions have been discussed to improve on current neuroimaging methods for objectively measuring visual improvements during amblyopia therapy. Ultimately, it is hoped that these studies will help further the development of new and more effective forms of treatment, so that more people can achieve normal binocular vision.

Appendix 1: Dry-electrode EEG equipment set up

Figure 1. A photo taken of the equipment set up during a testing session at Hull Royal Infirmary. Displaying (left to right) the testing laptop, the dry-electrode EEG kit, and the Oculus Rift headset mounted on an adjustable stand. Exactly the same set up was used for Experiment 1 and 2 in Chapter 6.

References

Aaen-Stockdale, C., Ledgeway, T., & Hess, R. F. (2007). Second-Order Optic Flow Deficits in Amblyopia. *Investigative Opthalmology & Visual Science*, *48*(12), 5532. https://doi.org/10.1167/iovs.07-0447

Agrawal, R., Conner, I. P., Odom, J. V., Schwartz, T. L., & Mendola, J. D. (2006). Relating Binocular and Monocular Vision in Strabismic and Anisometropic Amblyopia. *Archives of Ophthalmology*, *124*(6), 844. https://doi.org/10.1001/archopht.124.6.844

Albrecht, D., & Geisler, W. (1991). Motion selectivity and the contrast-response function of simple cells the visual cortex. *Visual Neuroscience*, *7*(1991), 531–546. https://doi.org/10.1017/S0952523800010336

Algaze, A., Roberts, C., Leguire, L., Schmalbrock, P., & Rogers, G. (2002). Functional magnetic resonance imaging as a tool for investigating amblyopia in the human visual cortex: A pilot study. *Journal of American Association for Pediatric Ophthalmology and Strabismus*, *6*(5), 300–308. https://doi.org/10.1067/mpa.2002.124902

Alvarez, I., Haas, B. De, Clark, C. A., Rees, G., Schwarzkopf, D. S., & Harvey, B. M. (2015). Comparing different stimulus configurations for population receptive field mapping in human fMRI, *9*(February), 1–16. https://doi.org/10.3389/fnhum.2015.00096

Assaf, A. A. (1982). The sensitive period: transfer of fixation after occlusion for strabismic amblyopia. *British Journal of Ophthalmology*, *66*(1), 64–70. https://doi.org/10.1136/bjo.66.1.64

Babu, R. J., Clavagnier, S. R., Bobier, W., Thompson, B., & Hess, R. F. (2013). The Regional Extent of Suppression: Strabismics Versus Nonstrabismics. *Investigative Opthalmology & Visual Science*, *54*(10), 6585. https://doi.org/10.1167/iovs.12-11314

Bagolini, B., Falsini, B., Cermola, S., & Porciatti, V. (1994). Binocular interactions and steady-state VEPs. A study in normal and defective binocular vision (Part II). *Graefe's Archive for Clinical and Experimental Ophthalmology*, *232*(12), 737–744. https://doi.org/10.1007/BF00184277

Baker, D., Lygo, F., Meese, T. S., & Georgeson, M. A. (2018). Binocular summation revisited : beyond Ö 2.

Baker, D.H., Meese, T. S., & Summers, R. J. (2007). Psychophysical evidence for two routes to suppression before binocular summation of signals in human vision. *Neuroscience*, *146*(1), 435–448. https://doi.org/10.1016/j.neuroscience.2007.01.030

Baker, Daniel H., Meese, T. S., & Hess, R. F. (2008). Contrast masking in strabismic amblyopia: Attenuation, noise, interocular suppression and binocular summation. *Vision Research*, *48*(15), 1625–1640. https://doi.org/10.1016/j.visres.2008.04.017

Baker, Daniel H., Meese, T. S., Mansouri, B., & Hess, R. F. (2007a). Binocular summation of contrast remains intact in strabismic amblyopia. *Investigative Ophthalmology and Visual Science*, *48*(11), 5332–5338. https://doi.org/10.1167/iovs.07-0194

Baker, Daniel H., Meese, T. S., Mansouri, B., & Hess, R. F. (2007b). Binocular Summation of Contrast Remains Intact in Strabismic Amblyopia. *Investigative Opthalmology & Visual Science*, *48*(11), 5332. https://doi.org/10.1167/iovs.07-0194

Baker, Daniel H., Simard, M., Saint-Amour, D., & Hess, R. F. (2015). Steady-state contrast response functions provide a sensitive and objective index of amblyopic deficits. *Investigative Ophthalmology and Visual Science*. https://doi.org/10.1167/iovs.14-15611

Baker, Daniel H, Meese, T. S., & Georgeson, M. a. (2007). Binocular interaction: contrast matching and contrast discrimination are predicted by the same model. *Spatial Vision*, *20*(5), 397–413. https://doi.org/10.1163/156856807781503622

Bankó, É. M., Körtvélyes, J., Németh, J., Weiss, B., & Vidnyánszky, Z. (2013). Amblyopic deficits in the timing and strength of visual cortical responses to faces. *Cortex*, *49*(4), 1013–1024. https://doi.org/10.1016/j.cortex.2012.03.021

Barkley, G. L., & Baumgartner, C. (2003). MEG and EEG in epilepsy. *Journal of Clinical Neurophysiology : Official Publication of the American Electroencephalographic Society*, *20*(3), 163–178. Retrieved from http://www.ncbi.nlm.nih.gov/pubmed/12881663

Barnes, G. ., Hess, R. ., Dumoulin, S. ., Achtman, R. ., & Pike, G. . (2001). The cortical

deficit in humans with strabismic amblyopia. *Journal of Physiology*, *11584*(533), 281–297.

Berman, M. S., & Seki, S. (1982). Blur-Induced Changes in the Visual Evoked Potential. *Optometry and Vision Science*, *59*(7), 556–560. https://doi.org/10.1097/00006324-198207000-00002

Bhola, R., Keech, R. V., Kutschke, P., Pfeifer, W., & Scott, W. E. (2006). Recurrence of Amblyopia after Occlusion Therapy. *Ophthalmology*, *113*(11), 2097–2100. https://doi.org/10.1016/j.ophtha.2006.04.034

Binda, P., Thomas, J. M., Boynton, G. M., & Fine, I. (2013). Minimizing biases in estimating the reorganization of human visual areas with BOLD retinotopic mapping. *Journal of Vision*, *13*(7), 1–16. https://doi.org/10.1167/13.7.13.doi

Borna, A., Carter, T. R., Goldberg, J. D., Colombo, A. P., Jau, Y.-Y., Berry, C., … Schwindt, P. D. D. (2017). A 20-channel magnetoencephalography system based on optically pumped magnetometers. *Physics in Medicine & Biology*, *62*(23), 8909–8923. https://doi.org/10.1088/1361-6560/aa93d1

Bossi, M., Tailor, V. K., Anderson, E. J., Bex, P. J., Greenwood, J. A., Dahlmann-Noor, A., & Dakin, S. C. (2017). Binocular Therapy for Childhood Amblyopia Improves Vision Without Breaking Interocular Suppression. *Investigative Opthalmology & Visual Science*, *58*(7), 3031. https://doi.org/10.1167/iovs.16-20913

Boto, E., Bowtell, R., Krüger, P., Fromhold, T. M., Morris, P. G., Meyer, S. S., … Brookes, M. J. (2016). On the Potential of a New Generation of Magnetometers for MEG: A Beamformer Simulation Study. *PLOS ONE*, *11*(8), e0157655. https://doi.org/10.1371/journal.pone.0157655

Boto, E., Holmes, N., Leggett, J., Roberts, G., Shah, V., Meyer, S. S., … Brookes, matthew J. (2018). Moving magnetoencephalography towards real-world applications with a wearable system. https://doi.org/10.1038/nature26147

Brainard, D. H. (1997). The Psychophysics Toolbox. *Spatial Vision*, *10*(4), 433–436. Retrieved from http://www.ncbi.nlm.nih.gov/pubmed/9176952

Breslow, N. E., & Clayton, D. G. (1993). Approximate Inference in Generalized Linear Mixed Models. *Journal of the American Statistical Association*, *88*(421), 9. https://doi.org/10.2307/2290687

Budker, D., Kimball, D. F., Rochester, S. M., Yashchuk, V. V., & Zolotorev, M. (2000). Sensitive magnetometry based on nonlinear magneto-optical rotation. *Physical Review A*, *62*(4), 043403. https://doi.org/10.1103/PhysRevA.62.043403

Buxton, R. B. (2013). The physics of functional magnetic resonance imaging (fMRI). *Reports on Progress in Physics. Physical Society (Great Britain)*, *76*(9), 096601. https://doi.org/10.1088/0034-4885/76/9/096601

Calderone, D. J., Martinez, A., Zemon, V., Hoptman, M. J., Hu, G., Watkins, J. E., … Butler, P. D. (2013). Comparison of psychophysical, electrophysiological, and fMRI assessment of visual contrast responses in patients with schizophrenia. *NeuroImage*, *67*, 153–162. https://doi.org/10.1016/J.NEUROIMAGE.2012.11.019

Campbell, F. W., & Green, D. G. (1965a). Monocular versus binocular visual acuity. *Nature*, *208*(5006), 191–192. https://doi.org/10.1038/208191a0

Campbell, F. W., & Green, D. G. (1965b). With 13 text-figures OPTICAL AND RETINAL FACTORS AFFECTING VISUAL RESOLUTION, *181*, 576–593.

Campbell, F. W., & Robson, J. G. (1968). Application of Fourier analysis to the visibility of gratings. *The Journal of Physiology*, *197*(3), 551–566. https://doi.org/10.1113/jphysiol.1968.sp008574

Camprodon, J. A., Martínez-Raga, J., Alonso-Alonso, M., Shih, M. C., & Pascual-Leone, A. (2007). One session of high frequency repetitive transcranial magnetic stimulation (rTMS) to the right prefrontal cortex transiently reduces cocaine craving. *Drug and Alcohol Dependence*, *86*(1), 91–94. https://doi.org/10.1016/j.drugalcdep.2006.06.002

Chadnova, E., Reynaud, A., Clavagnier, S., & Hess, R. F. (2017). Latent binocular function in amblyopia. *Vision Research*, *140*, 73–80. https://doi.org/10.1016/j.visres.2017.07.014

Chatrian, G. E., Lettich, E., & Nelson, P. L. (1985). Ten Percent Electrode System for Topographic Studies of Spontaneous and Evoked EEG Activities. *American Journal of*

EEG Technology, *25*(2), 83–92. https://doi.org/10.1080/00029238.1985.11080163

Choi, M. Y., Lee, K. M., Hwang, J. M., Choi, D. G., Lee, D. S., Park, K. H., & Yu, Y. S. (2001). Comparison between anisometropic and strabismic amblyopia fMRI_CHOI_2001.pdf. *British Journal of Ophthalmology*, *85*(9), 1052–1056. Retrieved from http://bjo.bmj.com/content/85/9/1052.abstract

Clavagnier, S., Dumoulin, S. O., & Hess, R. F. (2015). Is the Cortical Deficit in Amblyopia Due to Reduced Cortical Magnification, Loss of Neural Resolution, or Neural Disorganization? *Journal of Neuroscience*, *35*(44), 14740–14755. https://doi.org/10.1523/JNEUROSCI.1101-15.2015

Clavagnier, S., Thompson, B., & Hess, R. F. (2013). Long Lasting Effects of Daily Theta Burst rTMS Sessions in the Human Amblyopic Cortex. *Brain Stimulation*, *6*(6), 860–867. https://doi.org/10.1016/J.BRS.2013.04.002

Cohen, D. (1972). Magnetoencephalography: Detection of the Brain's Electrical Activity with a Superconducting Magnetometer. *Science*, *175*(4022), 664–666. https://doi.org/10.1126/science.175.4022.664

Conner, I. P., Odom, J. V., Schwartz, T. L., & Mendola, J. D. (2007). Monocular activation of V1 and V2 in amblyopic adults measured with functional magnetic resonance imaging. *Journal of American Association for Pediatric Ophthalmology and Strabismus*, *11*(4), 341–350. https://doi.org/10.1016/j.jaapos.2007.01.119

Crawford, M. L. J., & Harwerth, R. S. (2004). Ocular Dominance Column Width and Contrast Sensitivity in Monkeys Reared with Strabismus or Anisometropia. *Investigative Opthalmology & Visual Science*, *45*(9), 3036. https://doi.org/10.1167/iovs.04-0029

Dale, A. M., Fischl, B., & Sereno, M. I. (1999). Cortical Surface-Based Analysis. *NeuroImage*, *9*(2), 179–194. https://doi.org/10.1006/nimg.1998.0395

DeYoe, E. A., Carman, G. J., Bandettini, P., Glickman, S., Wieser, J., Cox, R., … Neitz, J. (1996). Mapping striate and extrastriate visual areas in human cerebral cortex. *Proceedings of the National Academy of Sciences of the United States of America*,

93(6), 2382–2386. https://doi.org/10.1073/PNAS.93.6.2382

Dumoulin, S. O., & Wandell, B. A. (2008). Population receptive field estimates in human visual cortex. *NeuroImage*. https://doi.org/10.1016/j.neuroimage.2007.09.034

Engel, S. A., Glover, G. H., & Wandell, B. A. (1997). Retinotopic organization in human visual cortex and the spatial precision of functional MRI. *Cerebral Cortex (New York, N.Y. : 1991)*, *7*(2), 181–192. Retrieved from http://www.ncbi.nlm.nih.gov/pubmed/9087826

Epelbaum, M., Milleret, C., Buisseret, P., & Duffer, J. L. (1993). The Sensitive Period for Strabismic Amblyopia in Humans. *Ophthalmology*, *100*(3), 323–327. https://doi.org/10.1016/S0161-6420(13)32170-8

Farivar, R., Zhou, J., Huang, Y., Feng, L., Zhou, Y., & Hess, R. F. (2017). Two cortical deficits underlie amblyopia: A multifocal fMRI analysis. *NeuroImage*. https://doi.org/10.1016/J.NEUROIMAGE.2017.09.045

Fischl, B. (2012). FreeSurfer. *NeuroImage*, *62*(2), 774–781. https://doi.org/10.1016/j.neuroimage.2012.01.021

Freeman, A. W., Nguyen, V. A., & Jolly, N. (1996). Components of Visual Acuity Loss in Strabismus. *Vision Research*, *36*(5), 765–774.

Georgeson, M. A., Wallis, S. A., Meese, T. S., & Baker, D. H. (2016). Contrast and lustre : A model that accounts for eleven different forms of contrast discrimination in binocular vision. *Vision Research*, *129*, 98–118. https://doi.org/10.1016/j.visres.2016.08.001

Gibson, J. J., & Flock, H. (1962). The Apparent Distance of Mountains. *The American Journal of Psychology*, *75*(3), 501. https://doi.org/10.2307/1419880

Glover, G. H. (2011). Overview of functional magnetic resonance imaging. *Neurosurgery Clinics of North America*, *22*(2), 133–139, vii. https://doi.org/10.1016/j.nec.2010.11.001

Goodyear, B. G., Nicolle, D. A., Humphrey, G. K., & Menon, R. S. (2000). BOLD fMRI Response of Early Visual Areas to Perceived Contrast in Human Amblyopia. *J Neurophysiol*, *84*(4), 1907–1913. Retrieved from http://jn.physiology.org/content/84/4/1907.short

Harrad, R. A., & Hess, R. F. (1992). Binocular integration of contrast information in amblyopia. *Vision Research*. https://doi.org/10.1016/0042-6989(92)90075-T

Harvey, B. M., & Dumoulin, S. O. (2011). The Relationship between Cortical Magnification Factor and Population Receptive Field Size in Human Visual Cortex: Constancies in Cortical Architecture. https://doi.org/10.1523/JNEUROSCI.2572-11.2011

Harwerth, R. S., Smith, E. L., & Levi, D. M. (1980). Suprathreshold binocular interactions for grating patterns. *Perception & Psychophysics*, *27*(1), 43–50. https://doi.org/10.3758/BF03199905

Heeger, D. J. (1992a). Half-squaring in responses of cat striate cells. *Visual Neuroscience*, *9*, 427–443.

Heeger, D. J. (1992b). Normalization of cell responses in cat striate cortex. *Visual Neuroscience*, *9*, 181–197.

Hess, R. F., & Howell, E. R. (1977). The threshold contrast sensitivity function in strabismic amblyopia: Evidence for a two type classification. *Vision Research*, *17*(9), 1049–1055. https://doi.org/10.1016/0042-6989(77)90009-8

Hess, R. F., & Pointer, J. S. (1987). Evidence for spatially local computations underlying discrimination of periodic patterns in fovea and periphery. *Vision Research*, *27*(8), 1343–1360. https://doi.org/10.1016/0042-6989(87)90211-2

Hess, R F, Mansouri, B., & Thompson, B. (2010). A new binocular approach to the treatment of Amblyopia in adults well beyond the critical period of visual development. *Restorative Neurology and Neuroscience*, *28*, 1–10. https://doi.org/10.3233/RNN-2010-0550

Hess, Robert F, Li, X., Mansouri, B., Thompson, B., & Hansen, B. C. (2009). Selectivity as well as Sensitivity Loss Characterizes the Cortical Spatial Frequency Deficit in Amblyopia. *Human Brain Mapping*, *30*, 4054–4069. https://doi.org/10.1002/hbm.20829

Hess, Robert F, Mansouri, B., & Thompson, B. (2010). A binocular approach to treating amblyopia: antisuppression therapy. *Optometry and Vision Science : Official Publication of the American Academy of Optometry*, *87*(9), 697–704.

https://doi.org/10.1097/OPX.0b013e3181ea18e9

Hess, Robert F, Thompson, B., & Baker, D. H. (2014). Binocular vision in amblyopia : structure , suppression and plasticity, *34*, 146–162. https://doi.org/10.1111/opo.12123

Himmelberg, M. M., & Wade, A. R. (2019). Eccentricity-dependent temporal contrast tuning in human visual cortex measured with fMRI. *NeuroImage*, *184*, 462–474. https://doi.org/10.1016/j.neuroimage.2018.09.049

Holmes, N., Leggett, J., Boto, E., Roberts, G., Hill, R. M., Tierney, T. M., … Bowtell, R. (2018). A bi-planar coil system for nulling background magnetic fields in scalp mounted magnetoencephalography. *NeuroImage*, *181*, 760–774. https://doi.org/10.1016/J.NEUROIMAGE.2018.07.028

Holopigian, K., Blake, R., & Greenwald, M. J. (1988). Clinical suppression and amblyopia. *Investigative Ophthalmology and Visual Science*, *29*(3), 444–451.

Holopigian, Karen, Blake, R., & Greenwald, M. J. (1986). Selective losses in binocular vision in anisometropic amblyopes. *Vision Research*, *26*(4), 621–630. https://doi.org/10.1016/0042-6989(86)90010-6

Huang, P., Baker, D. H., & Hess, R. F. (2012). Interocular suppression in normal and amblyopic vision : Spatio-temporal properties, *12*(2012), 1–12. https://doi.org/10.1167/12.11.29.Introduction

Hubel, D. H., & Wiesel, T. N. (1965). Receptive Archi- Tecture in Two Nonstriate Visual Areas (18 and 19) of the Cati. *Journal of Neurophysiology*.

Hussain, Z., Svensson, C.-M., Besle, J., Webb, B. S., Barrett, B. T., & McGraw, P. V. (2015). Estimation of cortical magnification from positional error in normally sighted and amblyopic subjects. *Journal of Vision*, *15*(2). https://doi.org/10.1167/15.2.25

Imamura, Richter, Fischer, Lennerstrand, Franzen, Rydberg, … Langstrom. (1997). Reduced activity in the extrastriate visual cortex of individuals with strabismic amblyopia.pdf, *225*, 173–176.

Jampolsky, A. (1955). Characteristics of Suppression in Strabismus. *A.M.A. Archives of Ophthalmology*, *54*(5), 683–696.

https://doi.org/10.1001/archopht.1955.00930020689010

Jenkinson, M., Bannister, P., Brady, M., & Smith, S. (2002). Improved optimization for the robust and accurate linear registration and motion correction of brain images. *NeuroImage*, *17*(2), 825–841. Retrieved from http://www.ncbi.nlm.nih.gov/pubmed/12377157

Johansson, B., & Jakobsson, P. (2006). Fourier-analysed Steady-state VEPs in Pre-school Children with and without Normal Binocularity. *Documenta Ophthalmologica*, *112*(1), 13–22. https://doi.org/10.1007/s10633-005-5889-4

Johnson, C. N., Schwindt, P. D. D., & Weisend, M. (2013). Multi-sensor magnetoencephalography with atomic magnetometers. *Physics in Medicine and Biology*, *58*(17), 6065–6077. https://doi.org/10.1088/0031-9155/58/17/6065

Joosse, M. V., Esme, D. L., Schimsheimer, R. J., Verspeek, S. A. M., Vermeulen, M. H. L., & van Minderhout, E. M. (2005). Visual evoked potentials during suppression in exotropic and esotropic strabismics: strabismic suppression objectified. *Graefe's Archive for Clinical and Experimental Ophthalmology*, *243*(2), 142–150. https://doi.org/10.1007/s00417-004-0994-8

Kam, J. W. Y., Griffin, S., Shen, A., Patel, S., Hinrichs, H., Heinze, H.-J., … Knight, R. T. (2019). Systematic comparison between a wireless EEG system with dry electrodes and a wired EEG system with wet electrodes. *NeuroImage*, *184*, 119–129. https://doi.org/10.1016/J.NEUROIMAGE.2018.09.012

Kim, S. G., Richter, W., & Ugurbil, K. (1997). Limits of temporal resolution in functional MRI. *Magnetic Resonance in Medicine*, *37*, 631–636.

Kiorpes, Kiper, O'Keefe, C. & M. (1998). Neuronal correlates of amblyopia in the visual cortex of macaque monkeys with experimental strabismus and anisometropia. *Survey of Ophthalmology*, *45*(2), 166. https://doi.org/10.1016/S0039-6257(00)00164-8

Kiorpes, L., Kiper, D. C., O'Keefe, L. P., Cavanaugh, J. R., & Movshon, J. A. (1998). Neuronal correlates of amblyopia in the visual cortex of macaque monkeys with experimental strabismus and anisometropia. *The Journal of Neuroscience : The Official*

Journal of the Society for Neuroscience, *18*(16), 6411–6424. https://doi.org/10.1523/JNEUROSCI.18-16-06411.1998

Kiorpes, L., & McKee, S. (1999). Neural mechanisms underlying amblyopia. *Current Opinion in Neurobiology*, (9), 480–486. Retrieved from http://invibe.net/biblio_database_dyva/woda/data/att/82d2.file.pdf

Klein, E., Kreinin, I., Chistyakov, A., Koren, D., Mecz, L., Marmur, S., … Feinsod, M. (1999). Therapeutic efficacy of right prefrontal slow repetitive transcranial magnetic stimulation in major depression: a double-blind controlled study. *Arch Gen Psychiatry*, *56*(4), 315–320. https://doi.org/10.1001/archpsyc.56.4.315

Koch, G., Brusa, L., Caltagirone, C., Peppe, A., Oliveri, P., Stanzione, P. & Centonze, D. (2005). rTMS of supplementary motor dyskinesias in Parkinson disease. *Neurology*, *65*, 623–625.

Koklanis, K., Abel, L. A., & Aroni, R. (2006). Psychosocial impact of amblyopia and its treatment: A multidisciplinary study. *Clinical and Experimental Ophthalmology*, *34*(8), 743–750. https://doi.org/10.1111/j.1442-9071.2006.01317.x

Kothari, R., Bokariya, P., Singh, S., & Singh, R. (2016). A Comprehensive Review on Methodologies Employed for Visual Evoked Potentials. *Scientifica*, *2016*. https://doi.org/10.1155/2016/9852194

Kumagami, T., Zhang, B., Smith, E. L., & Chino, Y. M. (2000). Effect of Onset Age of Strabismus on the Binocular Responses of Neurons in the Monkey Visual Cortex. *Investigative Ophthalmology & Visual Science*, *41*(3), 948–954. Retrieved from https://iovs.arvojournals.org/article.aspx?articleid=2199924

Kwon, M., Wiecek, E., Dakin, S. C., & Bex, P. J. (2015). Spatial-frequency dependent binocular imbalance in amblyopia. *Scientific Reports*, *5*(1), 17181. https://doi.org/10.1038/srep17181

Labyt, E., Corsi, M.-C., Fourcault, W., Palacios Laloy, A., Bertrand, F., Lenouvel, F., … Morales, S. (2019). Magnetoencephalography With Optically Pumped He Magnetometers at Ambient Temperature. *IEEE Transactions on Medical Imaging*,

38(1), 90–98. https://doi.org/10.1109/TMI.2018.2856367

Lee, K. M., Lee, S. H., Kim, N. Y., Kim, C. Y., Sohn, J. W., Choi, M. Y., … Hyun Chang, K. (2001). Binocularity and spatial frequency dependence of calcarine activation in two types of amblyopia. *Neuroscience Research*, *40*(2), 147–153. https://doi.org/10.1016/S0168-0102(01)00220-6

Legge, G E. (1984). Binocular contrast summation - I. Detection and discrimination. *Vision Research*, *24*(4), 373–383.

Legge, G. E. (1984). Binocular contrast summation: II. Quadratic summation. *Vision Research*, *24*(4), 385–394.

Lema, S. A., & Blake, R. (1977). Binocular summation in normal and stereoblind humans. *Vision Research*, *17*(6), 691–695. https://doi.org/10.1016/S0042-6989(77)80004-7

Levi, D. M, & Harwerth, R. S. (1977). Spatio-temporal interactions in anisometropic and strabismic amblyopia. *Investigative Ophthalmology & Visual Science*, *16*(1), 90–95.

Levi, D. M, Harwerth, R. S., & Smith, E. L. (1980). Binocular interactions in normal and anomalous Binocular vision. *Vision Res*, *51*(7), 754–770. https://doi.org/10.1016/j.visres.2010.10.009

Levitt, J. B., Schumer, R. A., Sherman, S. M., Spear, P. D., & Movshon, J. A. (2001). Visual Response Properties of Neurons in the LGN of Normally Reared and Visually Deprived Macaque Monkeys. *Journal of Neurophysiology*, *85*(5), 2111–2129. https://doi.org/10.1152/jn.2001.85.5.2111

Li, R. W., Ngo, C., Nguyen, J., & Levi, D. M. (2011). Video-game play induces plasticity in the visual system of adults with amblyopia. *PLoS Biology*, *9*(8). https://doi.org/10.1371/journal.pbio.1001135

Li, X., Dumoulin, S. O., Mansouri, B., & Hess, R. F. (2007). Cortical deficits in human amblyopia: Their regional distribution and their relationship to the contrast detection deficit. *Investigative Ophthalmology and Visual Science*, *48*(4), 1575–1591. https://doi.org/10.1167/iovs.06-1021

Logothetis, N. K., Pauls, J., Augath, M., Trinath, T., & Oeltermann, A. (2001).

Neurophysiological investigation of the basis of the fMRI signal.

Lopez-Gordo, M., Sanchez-Morillo, D., & Valle, F. (2014). Dry EEG Electrodes. *Sensors*, *14*(7), 12847–12870. https://doi.org/10.3390/s140712847

Mansouri, B., Thompson, B., & Hess, R. F. (2008). Measurement of suprathreshold binocular interactions in amblyopia. *Vision Research*, *48*(28), 2775–2784. https://doi.org/10.1016/j.visres.2008.09.002

Medina, J. M., & Mullen, K. T. (2007). Colour-luminance interactions in binocular summation. *Vision Research*, *47*(8), 1120–1128. https://doi.org/10.1016/j.visres.2007.01.015

Meese, T. S., Georgeson, M., & Baker, D. H. (2006). Binocular contrast vision at and above threshold. *Journal of Vision*, *6*(11), 1224–1243. https://doi.org/10.1167/6.11.7

Meese, T. S., & Hess, R. F. (2004). Low spatial frequencies are suppressively masked across spatial scale, orientation, field position, and eye of origin. *Journal of Vision*, *4*(10), 843–859. https://doi.org/10.1167/4.10.2

Meese, T. S., & Hess, R. F. (2005). Interocular suppression is gated by interocular feature matching. *Vision Research*, *45*(1), 9–15. https://doi.org/10.1016/j.visres.2004.08.004

Mendola, J. D., Conner, I. P., Roy, A., Chan, S. T., Schwartz, T. L., Odom, J. V., & Kwong, K. K. (2005). Voxel-based analysis of MRI detects abnormal visual cortex in children and adults with amblyopia. *Human Brain Mapping*, *25*(2), 222–236. https://doi.org/10.1002/hbm.20109

Mirzajani, A., Sarlaki, E., Kharazi, H. H., & Tavan, M. (2011). Effect of lens-induced myopia on visual cortex activity: A functional MR imaging study. *American Journal of Neuroradiology*, *32*(8), 1426–1429. https://doi.org/10.3174/ajnr.A2551

Mitchell, D. E., Howell, E. R., & Keith, C. G. (1983). The effect of minimal occlusion therapy on binocular visual functions in amblyopia. *Investigative Ophthalmology and Visual Science*, *24*(6), 778–781. https://doi.org/10.1016/0039-6257(84)90258-3

Moradi, F., & Heeger, D. J. (2009). Inter-ocular contrast normalization in human visual cortex. *Journal of Vision*, *9*(3), 13–13. https://doi.org/10.1167/9.3.13

Mori, T., Matsuura, K., Zhang, B., Smith, E. L., & Chino, Y. M. (2002). Effects of the Duration of Early Strabismus on the Binocular Responses of Neurons in the Monkey Visual Cortex (V1). *Investigative Ophthalmology & Visual Science*, *43*(4), 1262–1269. Retrieved from https://iovs.arvojournals.org/article.aspx?articleid=2200193

Movshon, J. A., Eggers, H. M., Gizzi,', M. S., Hendrickson, A. E., Kiorpes, L., & Boothe4, R. G. (1987). *Effects of Early Unilateral Blur on the Macaque's Visual System. Ill. Physiological Observations. The Journal of Neuroscience* (Vol. 7). Retrieved from http://www.jneurosci.org/content/jneuro/7/5/1340.full.pdf

Nestares, O., & Heeger, D. J. (2000). Robust multiresolution alignment of MRI brain volumes. *Magnetic Resonance in Medicine*, *43*(5), 705–715. Retrieved from http://www.ncbi.nlm.nih.gov/pubmed/10800036

Norcia, A. M., Appelbaum, L. G., Ales, J. M., Cottereau, B. R., & Rossion, B. (2015). The steady-state visual evoked potential in vision research: A review. *Journal of Vision*, *15*(6), 4. https://doi.org/10.1167/15.6.4

Ogawa, S., Lee, T. M., Kay, A. R., & Tank, D. W. (1990). Brain magnetic resonance imaging with contrast dependent on blood oxygenation. *Proceedings of the National Academy of Sciences of the United States of America*, *87*(24), 9868–9872. Retrieved from http://www.ncbi.nlm.nih.gov/pubmed/2124706

Oner, A., Coskun, M., Everekliogluu, C., & Dogan, H. (2004). Pattern VEP is a useful technique in monitoring the effectiveness of occlusion therapy in amblyopic eyes under occlusion therapy. *Documenta Ophthalmologica. Advances in Ophthalmology*, *109*(3), 223–227. Retrieved from http://www.ncbi.nlm.nih.gov/pubmed/15957607

Orban, G. A., Van Essen, D., & Vanduffel, W. (2004). Comparative mapping of higher visual areas in monkeys and humans. *TRENDS in Cognitive Sciences*, *8*(7), 315–324. https://doi.org/10.1016/j.tics.2004.05.009

Pardhan, S., & Gilchrist, J. (1992). Binocular contrast summation and inhibition in amblyopia. The influence of the interocular difference on binocular contrast sensitivity. *Documenta Ophthalmologica. Advances in Ophthalmology*, *82*(3), 239–248.

https://doi.org/10.1007/BF00160771

Pelli, D. G. (1997). The VideoToolbox software for visual psychophysics: transforming numbers into movies. *Spatial Vision*, *10*(4), 437–442. Retrieved from http://www.ncbi.nlm.nih.gov/pubmed/9176953

Polat, U., Ma-Naim, T., Belkin, M., & Sagi, D. (2004). Improving vision in adult amblyopia by perceptual learning. *Proceedings of the National Academy of Sciences of the United States of America*, *101*(17), 6692–6697. https://doi.org/10.1073/pnas.0401200101

Rahi, J. S., Logan, S., Borja, M. C., Timms, C., Russell-Eggitt, I., & Taylor, D. (2002). Prediction of improved vision in the amblyopic eye after visual loss in the non-amblyopic eye. *Lancet*, *360*(9333), 621–622. https://doi.org/10.1016/S0140-6736(02)09775-1

Richard, B., Chadnova, E., & Baker, D. H. (2018). Binocular vision adaptively suppresses delayed monocular signals. *NeuroImage*, *172*, 753–765. https://doi.org/10.1016/J.NEUROIMAGE.2018.02.021

Robson, S. E., Brookes, M. J., Hall, E. L., Palaniyappan, L., Kumar, J., Skelton, M., … Morris, P. G. (2016). Abnormal visuomotor processing in schizophrenia. *NeuroImage: Clinical*, *12*, 869–878. https://doi.org/10.1016/J.NICL.2015.08.005

Roelfsema, P. R., König, P., Engel, A. K., Sireteanu, R., & Singer, W. (1994). Reduced Synchronization in the Visual Cortex of Cats with Strabismic Amblyopia. *European Journal of Neuroscience*, *6*(11), 1645–1655. https://doi.org/10.1111/j.1460-9568.1994.tb00556.x

Ruff, H. A., & Lawson, K. R. (1990). Development of Sustained, Focused Attention in Young Children During Free Play. *Developmental Psychology*, *26*(1), 85–93. https://doi.org/10.1037/0012-1649.26.1.85

Schafer, J. L., & Yucel, R. M. (2002). Computational Strategies for Multivariate Linear Mixed-Effects Models With Missing Values. *Journal of Computational and Graphical Statistics*, *11*(2), 437–457. https://doi.org/10.1198/106186002760180608

Scheiman, M. M. M., Hertle, R. R. W., Beck, R. R. W., Edwards, A. A. R., Birch, E., Cotter,

S. S. A., … Pediatric Eye Disease Investigator Group. (2005). Randomized trial of treatment of amblyopia in children aged 7 to 17 years. *Archives of Ophthalmology*, *123*(4), 437–447. https://doi.org/10.1001/archopht.123.4.437

Schröder, J. H., Fries, P., Roelfsema, P. R., Singer, W., & Engel, A. K. (2002). Ocular dominance in extrastriate cortex of strabismic amblyopic cats. *Vision Research*, *42*(1), 29–39. https://doi.org/10.1016/S0042-6989(01)00263-2

Scott, W. E., & Dickey, C. F. (1988). Stability of visual acuity in amblyopic patients after visual maturity. *Graefe's Archive for Clinical and Experimental Ophthalmology = Albrecht von Graefes Archiv Fur Klinische Und Experimentelle Ophthalmologie*, *226*(2), 154–157. https://doi.org/10.1007/bf02173306

Searle, A., Norman, P., Harrad, R., & Vedhara, K. (2002). Psychosocial and clinical determinants of compliance with occlusion therapy for amblyopic children. *Eye*, *16*, 150–155. https://doi.org/10.1038/sj/eye/6700086

Sengpiel, F., & Blakemore, C. (1996). The neural basis of suppression and amblyopia in strabismus. *Eye (London, England)*, *10 (Pt 2)*, 250–258. https://doi.org/10.1038/eye.1996.54

Shah, V. K., & Wakai, R. T. (2013). A compact, high performance atomic magnetometer for biomedical applications. *Physics in Medicine and Biology*, *58*(22), 8153–8161. https://doi.org/10.1088/0031-9155/58/22/8153

Shooner, C., Hallum, L. E., Kumbhani, R. D., Ziemba, C. M., Garcia-Marin, V., Kelly, J. G., … Kiorpes, L. (2015). Population representation of visual information in areas V1 and V2 of amblyopic macaques. *Vision Research*, *114*, 56–67. https://doi.org/10.1016/j.visres.2015.01.012

Singh, S. P. (2014). Magnetoencephalography: Basic principles. *Annals of Indian Academy of Neurology*, *17*(Suppl 1), S107-12. https://doi.org/10.4103/0972-2327.128676

Sirawaj Itthipuripat, X., Sprague, T. C., & Serences, J. T. (2019). Functional MRI and EEG Index Complementary Attentional Modulations. https://doi.org/10.1523/JNEUROSCI.2519-18.2019

Smith, E L, Harwerth, R. S., & Crawford, M. L. (1985). Spatial contrast sensitivity deficits in monkeys produced by optically induced anisometropia. *Investigative Ophthalmology & Visual Science*, *26*(3), 330–342. Retrieved from https://iovs.arvojournals.org/article.aspx?articleid=2177029

Smith, Earl L., Chino, Y. M., Ni, J., Cheng, H., Crawford, M. L. J., & Harwerth, R. S. (1997). Residual Binocular Interactions in the Striate Cortex of Monkeys Reared With Abnormal Binocular Vision. *Journal of Neurophysiology*, *78*(3), 1353–1362. https://doi.org/10.1152/jn.1997.78.3.1353

Smith, S. M., Jenkinson, M., Woolrich, M. W., Beckmann, C. F., Behrens, T. E. J., Johansen-Berg, H., … Matthews, P. M. (2004). Advances in functional and structural MR image analysis and implementation as FSL. *NeuroImage*, *23*, S208–S219. https://doi.org/10.1016/j.neuroimage.2004.07.051

Sokol, S., & Moskowitz, A. (1981). Effect of retinal blur on the peak latency of the pattern evoked potential. *Vision Research*, *21*(8), 1279–1286. https://doi.org/10.1016/0042-6989(81)90232-7

Spiegel, D. P., Byblow, W. D., Hess, R. F., & Thompson, B. (2013). Anodal Transcranial Direct Current Stimulation Transiently Improves Contrast Sensitivity and Normalizes Visual Cortex Activation in Individuals With Amblyopia. *Neurorehabilitation and Neural Repair*, *27*(8), 760–769. https://doi.org/10.1177/1545968313491006

Srinivasan, R., Nunez, P. L., Tucker, D. M., Silberstein, R. B., & Cadusch, P. J. (1996). Spatial sampling and filtering of EEG with spline laplacians to estimate cortical potentials. *Brain Topography*, *8*(4), 355–366. Retrieved from http://www.ncbi.nlm.nih.gov/pubmed/8813415

Tailor, V., Bossi, M., Greenwood, J. A., & Dahlmann-Noor, A. (2016). Childhood amblyopia: current management and new trends. *British Medical Bulletin*, *119*(1), 75–86. https://doi.org/10.1093/bmb/ldw030

Talelli, P., Greenwood, R. J., & Rothwell, J. C. (2007). Exploring Theta Burst Stimulation as an intervention to improve motor recovery in chronic stroke. *Clinical Neurophysiology*,

118(2), 333–342. https://doi.org/10.1016/j.clinph.2006.10.014

Tao, X. X., Zhang, B., Shen, G., Wensveen, J., Smith, X. E. L., Nishimoto, S., … Chino, Y. M. (2014). Early Monocular Defocus Disrupts the Normal Development of Receptive-Field Structure in V2 Neurons of Macaque Monkeys, *34*(41), 13840–13854. https://doi.org/10.1523/JNEUROSCI.1992-14.2014

Taylor, K., & Elliott, S. (2014). Interventions for strabismic amblyopia. *The Cochrane Database of Systematic Reviews*, *7*(7). https://doi.org/10.1002/14651858.CD006461.pub4

Teplan, M. (2002). Fundamentals of EEG measurement. *Measurement science review* (Vol. 2). Retrieved from http://www.edumed.org.br/cursos/neurociencia/MethodsEEGMeasurement.pdf

Thompson, B., Mansouri, B., Koski, L., & Hess, R. F. (2008). Brain Plasticity in the Adult: Modulation of Function in Amblyopia with rTMS. *Current Biology*, *18*(14), 1067–1071. https://doi.org/10.1016/j.cub.2008.06.052

Tierney, T. M., Holmes, N., Mellor, S., López, J. D., Roberts, G., Hill, R. M., … Barnes, G. R. (2019). Optically pumped magnetometers: From quantum origins to multi-channel magnetoencephalography. *NeuroImage*, *199*, 598–608. https://doi.org/10.1016/J.NEUROIMAGE.2019.05.063

To, L., Thompson, B., Blum, J. R., Maehara, G., Hess, R. F., & Cooperstock, J. R. (2011). A game platform for treatment of amblyopia. *IEEE Transactions on Neural Systems and Rehabilitation Engineering*, *19*(3), 280–289. https://doi.org/10.1109/TNSRE.2011.2115255

Tommila, V., & Tarkkanen, A. (1981). Incidence of loss of vision in the healthy eye in amblyopia. *The British Journal of Ophthalmology*, *65*(8), 575–577. Retrieved from http://www.ncbi.nlm.nih.gov/pubmed/7295619

Vaegan, & Taylor, D. (1979). Critical period for deprivation amblyopia in children. *Transactions of the Ophthalmological Societies of the United Kingdom*, *99*(3), 432–439. Retrieved from http://www.ncbi.nlm.nih.gov/pubmed/298827

Valberg, A., & Fosse, P. (2002). Binocular contrast inhibition in subjects with age-related macular degeneration. *Journal of the Optical Society of America. A, Optics, Image Science, and Vision*, *19*(1), 223–228. https://doi.org/10.1364/JOSAA.19.000223

Wandell, B A, Chial, S., & Backus, B. T. (2000). Visualization and measurement of the cortical surface. *Journal of Cognitive Neuroscience*, *12*(5), 739–752. Retrieved from http://www.ncbi.nlm.nih.gov/pubmed/11054917

Wandell, Brian A., & Winawer, J. (2011). Imaging retinotopic maps in the human brain. *Vision Research*, *51*(7), 718–737. https://doi.org/10.1016/J.VISRES.2010.08.004

Welbourne, L. E., Morland, A. B., & Wade, A. R. (2018). NeuroImage Population receptive field (pRF) measurements of chromatic responses in human visual cortex using fMRI. *NeuroImage*, *167*(November 2017), 84–94. https://doi.org/10.1016/j.neuroimage.2017.11.022

Wiesel, T. N., & Hubel, D. H. (1963). Single-cell responses in striate cortex of kittens deprived of vision in one eye. *Journal of Neurophysiology*, *26*, 1003–1017. https://doi.org/10.1152/jn.1963.26.6.1003

Wong, A. M. F. (2012). New concepts concerning the neural mechanisms of amblyopia and their clinical implications. *Can J Ophthalmol*, *47*(5), 399–409. https://doi.org/10.1016/j.jcjo.2012.05.002

Zhou, J., McNeal, S., Babu, R. J., Baker, D. H., Bobier, W. R., & Hess, R. F. (2014). Time course of dichoptic masking in normals and suppression in amblyopes. *Investigative Ophthalmology and Visual Science*, *55*(7), 4098–4104. https://doi.org/10.1167/iovs.14-13969

Zuiderbaan, W., Harvey, B. M., & Dumoulin, S. O. (2012). Modeling center-surround configurations in population receptive fields using fMRI. *Journal of Vision*, *12*(3), 10–10. https://doi.org/10.1167/12.3.10